Modelling and CFD Simulation of a Fluidized Bed Process for the Capture of CO_2 from Fossil Fuel Combustion Sources

Mazaher Molaei Chalchooghi

The Centre of Numerical Modelling and Process Analysis, the University of Greenwich, London

A thesis submitted in partial fulfilment of the requirements of the University of Greenwich for the degree of Doctorate of Philosophy

August 2013

Abstract

Fossil fuels provide the main source of energy for power generation in existing power plants. A mitigation option to reduce carbon dioxide (CO_2) emission from existing power plants with fossil fuel combustion is the sequestration of carbon dioxide and storage in geological formations, in the ocean or for use in industrial processes. CO_2 capture from combustion exhaust gases by mineral carbonation using a fluidised bed is studied in this project. CFD modelling has been used to study the efficiency of CO_2 capture in a fluidized bed reactor containing a solid sorbent Calcium Oxide (CaO). This present work seeks to maximize CO_2 conversion by a systematic modification of the flow domain. In particular, it is intended to use a convergent-divergent geometry to control the velocity of particles in the reaction domain thereby keeping the particles in the domain as long as possible. This is expected to improve the performance of the system as more time is allowed for any remaining CO_2 to react with CaO and then be removed in the calcination stage. Further the effect of other key parameters such as particle size, CO_2 concentration of flue gas and mass loading of solid sorbent have also been investigated.

A Lagrangian/Eulerian scheme has been developed for this purpose, which uses a particle tracking model to describe CaO particle trajectories and mass, momentum and energy exchange with the carrier gas, entering the reactor in a typical flue gas composition. A steady-state condition is assumed, with each trajectory representing a parcel of particles of a given mass and diameter. The number of particles entering the fluidised bed is kept constant, and the fluidization velocity is chosen so that particles remain in the reactor. As the carbonation progresses, heavier well-reacted particles are collected at the bottom of the reactor. In the case of a non-uniform size distribution, fine particles would escape from the top of the reactor; in order to keep such particles within the domain the geometry was modified to increase the residence time of particles and to obtain maximum conversion. CO_2 reduction of the order of 90% was achieved in a single pass, with a mass loading of 2.5 times of equivalent solid sorbent to CO_2 in gas.

Acknowledgement

I would like to express my gratitude to my supervisors *Professor Koulis Pericleous* and *Dr. Mayur Patel* for their kind support and guidance during my research. I'm also grateful to *Dr. Georgi Djambazov* for his kind assistance and advices in code development and mesh generation with Mb3.

Financial support of the University of Greenwich towards this research project is hereby acknowledged.

I would like to give my special thanks to my family for their support and encouragement.

NOMENCLATURE

A: Frontal area of particle [m^2]

a, $\acute{a}$: Decay constant in lean region of fluidized bed reactor [-],see Eq. 3.25 and 3.27

a, b: Stoichiometric coefficients for carbonation reaction

b: Constant parameter in carbonation equation [min], see Eq. 3.11

Bi: Biot number [-]

C: Concentration of CO_2, [kmol/m^3]

C_D: Drag coefficient [-]

$C_{\mathrm{b,CO2}}$: Concentration of $\mathrm{CO_2}$ in bubble phase [mole/m^3]

$C_{\mathrm{e,CO2}}$: Equilibrium Concentration of $\mathrm{CO_2}$ [mole/m^3]

$C_{CO_{2_d}}$: Concentration of CO_2 leaving the dense region [mole/m^3]

$C_{CO_{2_{ex}}}$: Concentration of CO_2 at reactor exit [mole/m^3]

c_p: Heat capacity [J/K]

C_μ, C_{1e}, C_{2e}: Turbulence constant parameter [-], see Eq. 4.13

D: Effective product layer diffusivity, [m^2/s]

D_0: Pre-exponential factor, [m^2/s]

d_b: Effective bubble diameter [m]

D_{CO_2}: Effective gas diffusivity of CO_2 in air [m^2/s], see Eq. 3.23

D_p: Apparent product layer diffusion [m^2/s]

d_p: Particle diameter [m]

E_a: Activation Energy [kJ/mole]

f: Constant parameter in carbonation equation [-], see Eq. 3.11

f_a: Fraction of active CaO in carbonator [-], see Eq. 3.13 and 3.14

F_D: Drag force [N]

F_G: Gravity force [N]

F_p: Pressure gradient force [N]

G: Turbulent generation [m^2/s^2], see Eq. 4.15

g_i: Gravity acceleration [m/s^2]

h: Enthalpy [J]

h: Convective heat transfer [$\frac{W}{m^2K}$], se Eq. 4.72

k: Heat conductivity [W/(m.K)]

k: Kinetic energy [m^2/s^2], see Eq. 4.10

K_{ij}: Gas interchange coefficient between regions i and j [s^{-1}]

k_g: Mass transfer coefficient of CO_2 toward the particles [m/s], see Eq. 3.22

K_r: Overall carbonation rate constant [s^{-1}]

K_{ri}: Carbonation reaction constant [s^{-1}], see Eq. 3.22

k_s: Rate constant for surface reaction, [m^4/kmols]

k_{s_0}: Pre-exponential factor in Eq. 7, [m^4/kmols]

L: Height of the reactor [m]

L_0: Initial total length of pore system, [m/m3]

m_p: Mass of particle [kg]

M_{CO2}: Molecule mass of CO_2 [kg/kmole]

M_{CaO}: Molecule mass of CaO [kg/kmole]

M_{Caco_3}: Molecule mass of $Caco_3$ [kg/kmole]

$m_{p,0}$: Initial mass of particle [kg]

N_p: Number of particle trajectories in the system [-]

P: Pressure drop [Pascal]

p_e: number of steps per element [-], see Eq. 4.48

R: Gas constant [$m^3PaK^{-1}mol^{-1}$]

Re: Reynolds number [-]

Re_{mf}: Reynolds number for particles in particulate phase [-], Eq. 3.23

s: Skin friction factor [-], see Eq. 4.17

s_0: Initial surface area of particle [$\frac{m^2}{m^3}$], see Eq. 3.21

$\bar{S}_h$: Energy source term [J.kg/(m^3.s)]

$\bar{S}_m$: Mass source term [kg/(m^3.s)], see Eq. 4.1

$\bar{S}_u$: Momentum source term [kg/(m^2.s^2)], see Eq. 4.2

Sc: Schmidt number [-]

Sh: Sherwood number [-]

t: Time [sec]

T: Temperature [K]

u: Gas velocity [m/s]

u_0: Superficial gas velocity [m/s]

u_b: Bubble rise velocity [m/s]

u_{mf}: Minimum fluidization velocity [m/s]

u_{pi}: Particle velocity at *i*th direction [m/s]

$u_{p_{old}}$: Particle velocity at previous time-step [m/s]

$\bar{u}_\iota$: Average gas velocity at particle position [m/s]

$\tilde{u}$: Fluctuation velocity [m/s]

$\vec{u}$: Gas vector velocity [m/s]

$\bar{u}$: Gas mean velocity [m/s]

V_P: Volume of a particle [m^3]

V_{slip}: slip velocity [m/s]

X: Conversion of CaO particle to $CaCO_3$ [-], see Eq. 3.110

X_{bn}: Carbonation conversion achieved after n cycles [-], see Eq. 3.12

X_N: Maximum carbonation conversion achieved after N cycles [-], see Eq. 3.11

x_p: Particle current location inside the domain at x-direction [m]

$x_{p\ old}$: Particle previous location inside the domain at x-direction [m]

X_r: Constant parameter in carbonation equation [-], see Eq. 3.12

X_u: Particle ultimate conversion [-], see Eq. 3.9

Z: Ratio volume fraction after and before reaction [-]

z_d: Length of dense region [m]

z_l: Length of lean region [m]

Greek letters:

β: Thermal expansion coefficient [1/K], see Eq. 4.17

γ_i: Volume of solid in phase i [-]

Γ: Turbulent diffusivity [m^2/s]

Δt: Time step [sec]

ΔX_i: Particle (*i*th trajectory) conversion at current time-step [-]

ΔH_r: Heat of reaction [kJ/kmole]

δ: Bubble volume fraction [-]

ε: Void fraction [-]

ε_m: Void fraction at minimum fluidization point [-]

ε_{mf}: Void fraction at minimum fluidization

ϵ: Turbulence dissipation rate [m2/s^3]

η: Conversion efficiency of the fluidised bed [-], see Eq. 3.24 and 3.25

η_{be}: Contact efficiency between bubble and emulsion phases [-]

μ: Gas viscosity [kg/(m^2s)]

μ_{eff}: Ffective laminar viscosity [kg/(m^2s)]

υ_{lam}: Kinematic viscosity [m^2/s]

υ_t: Eddy viscosity [Pa.s]

ξ: Random Gaussian number [-]

ρ: Density [kg/m^3)

σ: Bed fraction in bubbles

σ_k: Turbulence constant parameter, see Eq. 4.14

σ_e: Turbulence constant parameter, see Eq. 4.14

τ: Shear stress [Pa]

τ_e: Eddy life time [s]

τ_c: Crossing time [s]

ψ: Particle sphericity [-]

Contents

List of Tables

List of Figures

Chapter1

Introduction

1.1 Motivation

Increasing greenhouse gases in the atmosphere has been a serious problem in recent years. This phenomenon leads to climate change, global warming and consequently imperils human health. Global mean temperature has been raised $0.8^{o}C$ over the past century which signifies a serious issue [1]. Carbon dioxide, methane, nitrous oxides and fluorinated gases are the major components of greenhouse gases associated with human activities. Over the last two centuries, there has been a dramatic increase in CO_2 emission and for about 75% of it resulting from fossil fuel combustion [2]. As a large number of power plants in the world use coal combustion for energy production, they are the greatest source of CO_2 emission, constituting some 54% of all stationary sources [3, 4].

Based on the international energy agency (IEA) report, it has globally been agreed to mitigate about 20% of global emissions by 2050 through the Carbon Capture and Storage (CCS). The largest part of this contribution with 55% is associated to power generation [5]. As fossil fuel burning will remain a major means of energy production in the near to medium future, then CCS remains a viable option to play down on the adverse environmental effects of CO_2 emission. About 35% of UK CO_2 emissions come from energy intensive industries industry. It seems sequestrating CO_2 from power plants would be essential not only for the next generation of power stations but also for all existing power plants due to the high volumes of CO_2 emission from these industries [6].

In order to reduce CO_2 emission to the atmosphere from energy production there are two solutions. The first solution is the use of energy from renewable sources such as wind, solar, hydro energy to mention a few. But compared to fossil fuel they are expensive and have certain limitations which include the absence of sunlight in the night, low wind condition at some geographical locations etcetera. Further, there are limitations in generating capacity of these types of energy sources. The second option involves the continued use of fossil fuel plants with an incorporated cost effective carbon capture and sequestration facility. Although the first solution seems to be more environmentally friendly, those sources of energy cannot meet the high demand of energy in this century. Hence the use of fossil fuels seems unavoidable and this necessitates an accelerated development of practical industrial scale CCS technologies. Carbon capture and storage from the main stations of CO_2 emissions, such as power plants with coal combustion is one of the issues which receives much attention from stakeholders in process industries and government agencies [7].

There are three different configurations of CCS systems: pre-combustion, oxy-fuel combustion and post-combustion [6]. The advantage of CCS is that it can reduce the emission up to 90% depending on the technology, but the disadvantage is the higher energy consumption particularly at the stage of carbon capture [5]. Among these configurations, post-combustion has been widely touted in the literature [8-13] due to its ability to provide CO_2 capture in an existing plant without any significant modifications to the energy production system. It is easier to establish the capture technology as a retrofit alternative in existing power plants.

The development of an efficient carbon capture facility of the post-combustion type is still an emerging technology. Many techniques have been previously employed; one feasible option is the use of absorption processes based on chemical solvents (e.g. Mono-Ethanol-Amine (MEA)). But absorption processes require gas pre-treatment and energy penalties which place a lot of burden on this technique thereby making it unsuitable for industrial scale applications [2, 14].Aside absorption processes, carbon capture can also be achieved using an adsorption process commonly called 'carbonation with CaO' Based on the lower energy penalty of carbonation with CaO, the Carbonate Looping process is feasible and economically appealing for existing power plants to acquire CCS technology. The energy penalty of this process is much lower than the other CO_2 capture schemes that are currently under investigation (e.g., MEA scrubbing) [15].

1-2 Carbon capture with solid sorbents

Capturing CO_2 with solid particles in a post-combustion manner is a promising technology which is still under development. A lot of researchers have investigated the theoretical capture efficiency of different solid sorbent materials [16-24]. Among various solid sorbents, CaO is the best candidate due to its worldwide availability and the low cost of the raw material [25, 26]. In this process, solid particles of CaO react with CO_2 at 650^o C in a fluidized bed reactor (Carbonation) then the reacted particles are transferred to another fluidized bed reactor to regenerate the CaO (at 950^o C) in a process called calcination. For the carbonation process, the high operating temperature gives high conversion rate of reaction; hence it is an advantage. Conversely, the high operating temperatures associated with the calcination process means higher energy expense [16, 27], although the process can be modified to reduce the energy expense by heat integration system which combines maximum heat recovery and minimal heat consumption. A major drawback with CaO carbonation technique is that each regeneration cycle tends to reduce the capturing capacity of the solid sorbent. Regeneration of reacted particles has been studied in many previous works [27-30].

Many researchers [16, 31, 32] have focused on the effect of carbonation/calcinations cycles in ultimate maximum carbonation capacity of solid sorbent. They recognized that carbonation capacity decays with cycles and after 10 cycles it falls to less than 50% of the original capture capacity. Sintering (blockage of tiny pores of a particle during the reaction) is the main reason of decay in capture capacity of CaO sorbent in carbonation/calcinations cycles. Many previous works have been dedicated to investigating the possibility to reduce regenerative degradation of particles; most of which revealed that the use of very fine particles can suppress sintering effect thereby improving the performance of the solid sorbents [33]. In other words, CO_2 can be completely removed from reacted CaO particles during the calcinations and the structure of CaO will not be changed during the regeneration. Deformation of nano-structure of CaO particles results in the decay of solid performance during the regeneration. Calcium Titanate (CaTiCO3) is used as an additive to improve the energy performance of particles [34]. Different precursors are also being utilized to improve the decay of capture capacity but investigations are still ongoing to ascertain whether all related costs are comparable with those of natural calcination process **[**30, 35, 36**].**

The main challenge in CCS is developing a cost effective technology to capture CO_2 with minimum energy consumption. Thus, a good understanding and exploration of CO_2 Capture with solid sorbents is essential. In order to design an energy efficient carbonator reactor it is required to have a deep understanding from hydrodynamic of such reactor. In this present study, the possibility to employ fluidized bed for efficient carbon capture is investigated. It is envisaged that a fluidized bed will maximize CO_2 conversion and also show the effect of key parameters on reactor performance

1-3 CO_2 Capture by fluidized bed reactors

In the case of massive combustion flue gases emanating from a power plant, a high flow contact facility needs to separate CO_2 from exhaust gases. The flow rate of a typical coal fired 1,000MW power plant is about $300Nm^3/s$ [10]. In view of the fact that fluidized bed reactors can provide high degrees of gas-solid contact, an appropriate fluidized bed reactor would be the suitable option to capture Carbon Dioxide from combustion flue gases with solid sorbents. Considering the advantages of fluidized bed reactors which provide efficient gas-solid contact [37], extensive knowledge of gas-solid interaction is required in order to investigate the possibility of providing the right operating condition which could maximize overall processing efficiency. CFD modelling is a powerful tool for this purpose to explore the behaviour of fluidized bed reactor. CO_2 could be captured by CaO with high efficiency, but the CO_2 capture capacity of Calcium Oxide decays with the increasing of carbonation/calcinations due to sintering of particles and thus a loss of surface area and reactivity [38]. CO_2 capture using a fluidized bed reactor can be achieved with high efficiencies (>80%) for a range of reasonable operating conditions by a lab-scale high-velocity fluidized bed carbonator in a continuous carbonation/calcinations system. The CO_2 capture efficiency can be improved by increasing the ultimate conversion of solid sorbent before leaving the reactor [39].

In spite of the increasing number of published works regarding the sorbent performance, reactivation and effect of carbonation/calcinations cycles on efficiency of carbon capture [16-19], there is no comprehensive study on the subject of the application of fluidized bed reactors in carbon capture considering the gas-solid behaviour in a continuous process. Modelling and simulation of a fluidized bed reactor in carbon capture can predict the particles actual residence time and ultimate conversion for any given size of particles as well as the rate of solid sorbent needed to achieve a specific capture efficiency in a carbonator. The results would be essential to design and improve the efficiency of the carbonation system which could become an established and high quality industrial technique. The results will also be useful to guide the design of a continuous pilot-scale for more investigations including validation of the various assumptions in any model and to produce results at an operating scale of interest.

1.4 Research objectives

This project aims to investigate the feasibility of a carbon capture technology which will utilise a fluidized bed reactor with solid sorbent (CaO) in a continuous process, suitable for use in large single source CO_2 producers, including coal/gas/oil power stations. Mainly, the reactor hydrodynamics, heat and mass transfer, particles trajectory and residence time, geometry and particle effect on reactor efficiency has been the concentrated of this research. The multi-physics CFD code, ″PHYSICA″, developed in university of

Greenwich, has been used to study gas-solid multiphase flow to estimate process efficiency as a function of effective parameters. Chemical reaction data and experimental information have been collected from the literature.

Although the effect of carbonation/calcinations has been studied widely, but maximizing the particle conversion in carbonator reactor has not been considered. For this propose, different reactor shapes has been examined to ascertain the particles' behaviour considering the CO_2 removal efficiency at identical gas/solid ratio for all type of the reactors. The effect of particle size has also been studied in this work. While it is common theoretical knowledge that small particles can offer higher conversion rate in comparison with large particles, the hydrodynamics of fluidization in combination with chemical reaction needs to be investigated to ascertain the behaviour of each size of particles in carbonation process.

1.5 Thesis outline

Chapter 2 presents an overview of CO_2 Capture and storage. Different CCS technologies based on the available literatures has been investigated. In this chapter CO_2 capture with solid sorbents of CaO and fundamentals of fluidized bed reactors were highlighted.

Chapter 3 presents carbonation kinetics and 1-D model of a carbonator reactor. Carbonation chemical reaction model has been investigated using Kunii-Levenspiel (KL) 1-D model.

Chapter 4 provides information about gas-solid fluidization and modelling strategies used in this research. Particle tracking and chemical reaction of CO_2 with solid CaO particles, during the particles residence inside the reactor has been modelled to illustrate the carbonation in fluidized bed reactors. Eulerian-Lagrangian framework had been used to model the gas hydrodynamics and particles' motion.

Chapter 5 presents the numerical solution, boundary conditions and the results obtained from the simulation in a 2-D and 3-D Cartesian system. Effect of some key parameters on carbonation process has also been investigated and presented. The results predict the possibility of reasonable CO_2 capture capacity in a fluidized bed reactor.

Chapter 6 proves the simulation results of 2-D Cartesian in 3-D cylindrical system and also provides some key findings. A high efficiency of CO_2 Capture in a fluidized bed reactor (~ 90%) has been achieved that can be used in the design of fluidized bed reactors to be implemented in industrial field.

Chapter 7 provides the conclusions and suggestions for future works.

Chapter 2

Research Background and Theoretical Study

2.1 Introduction

The need to mitigate CO_2 emission from industrial sources is critical towards achieving moderate global warming and climate change in fossil fuel based power plants [40]. The whole process of capturing and storage of CO_2 from industrial sources is capital intensive, with the bulk of the cost being on the capture rather than transport and storage. It is proposed to capture almost 90% of CO_2 from industrial flue gases to achieve the intergovernmental agreement goals in mitigation of greenhouse gases in the future [2]. To meet this goal using current CCS technologies requires up to 40% of extra fuel consumption in comparison with a plant with no capture facility. Furthermore, the general efficiency of those plants will reduce by 10-15% (e.g., from 55% to 45%) with a corresponding increase in cost of energy by 20-70% depending on type of a power plant, capture technology and availability of raw materials. It is therefore expedient to improve energy input required for CO_2 capture, and this can be a very challenging task. Energy integration and recycling of the heat of capture process is currently under development as a candidate to reducing energy input requirement of CCS facilities particularly in particularly in mineral carbonation with CaO sorbent at high temperature [41- 43].

Carbon capture and storage (CCS) is a process to sequestrate CO_2 from the combustion of fossil fuels or other industrial processes that release carbon dioxide to the atmosphere. The captured CO_2 must be transported for long term storage, well away from the atmosphere. Different alternatives for storage can be used based on the availability and storage cost. In comparison with capturing process the cost of storage is not really significant [44]. Typical CCS in power plants with about 85% of capture efficiency will cost about \$30 for 90/tCO_2 depending on the technology, CO_2 purity and site. This cost includes capture in range of \$20 (for 80/t$CO_{2)}$, transport \$1(for 10/t$CO_{2)}$ per 100km; storage and monitoring \$2 (for 5/tCO_2) [5].

Available technologies can potentially capture up to 95% of the CO_2 from combustion exhaust gases of power plants. For secure storage, the expectation is that a power plant with CCS could reduce CO_2 emissions to the atmosphere by approximately 80–90% per net kWh compared to a plant without CCS [IPCC Special Report 2005].

2.2 CO_2 Capture

The aim of CO_2 capture is to avoid CO_2 from combustion exhaust gases from being emitted into the atmosphere. The captured CO_2 is compressed and transported to deep ocean or depleted well for storage. Industries with fossil fuel combustion such as conventional coal-fired power plants are the major producers of CO_2.

Carbon capture technologies dates back to the 70's when they were originally utilised to purify natural gas in an amine-based chemical absorption process, but with increasing CO_2 emissions in last decades, this technology has been adopted in controlling CO_2 emission from power plants [45, 46]. Continuing to use fossil fuels in energy intensive industries requires capturing carbon dioxide to mitigate emission of carbon dioxide to the atmosphere. So far, different concepts of carbon capture have been investigated by researchers, but due to the high penalty rate of carbon capture systems a further study of CCS technologies is necessary to scale up existing capture technologies to industrial plants while keeping energy requirement as low as possible. Among different capture technologies (amine based chemical solvents, membrane, condensation at high pressure and chemical adsorption with solid materials), amine based capture systems are used more widely in industrial scale mainly for natural gas purification.

There are three main methods used in CO_2 capture: Pre-Combustion, oxy-fuel combustion and post-combustion. Post-combustion is much more remarkable among these three methods, because it can easily be retrofitted to existing plants which originally does not have CCS facility.

2.2.1 Pre-Combustion

In this process, carbon can be removed from the fuel before combustion takes place (Figure 2.1). The fuel is converted to hydrogen and CO_2 where H_2 will play the role of a fuel in the combustion process. The mixture of CO_2/H_2 (around 40% CO_2) is first subjected to a hydrate process where the concentration of CO_2 reaches 85% at the end of the process. This process does not need costly equipment and it is referred to Integrated Gasification Combined Cycle (IGCC) [47,48]. Pre-combustion capture is mainly applicable to IGCC (Integrated Gasification Combined Cycle) power plants

Pre-combustion employs membrane, sorbents or solvents to separate carbon dioxide from the gas mixture. Separation using chemical solvents (mainly Amine based) such as MDEA or physical solvents like Rectisol or Selexol has been used for many years in gasification plants [8, 11, 49, 50, 51]. The drawback of this method is that it requires very high energy for regeneration, usually in the order of 1-2MJ/kg CO_2 which has an adverse impact on the power plant efficiency [52-55]. Membrane based pre-combustion technique has also been considered for carbon capture [56-58]. CO_2 selective membranes such as non-porous polymeric membranes and H_2-selective membranes such as metallic, porous inorganic and polymeric membranes have been previously investigated to their relative feasibility for carbon capture [59]. Separation by membranes is attractive, particularly in the cases where membranes are used in conjunction with a chemical solvent for which they act as a selective contactor with CO_2 (combination of filtration and chemical absorption), but there are also many problems with the development of this technique which include: impact of dust, steam, physical degradation of membranes [60].

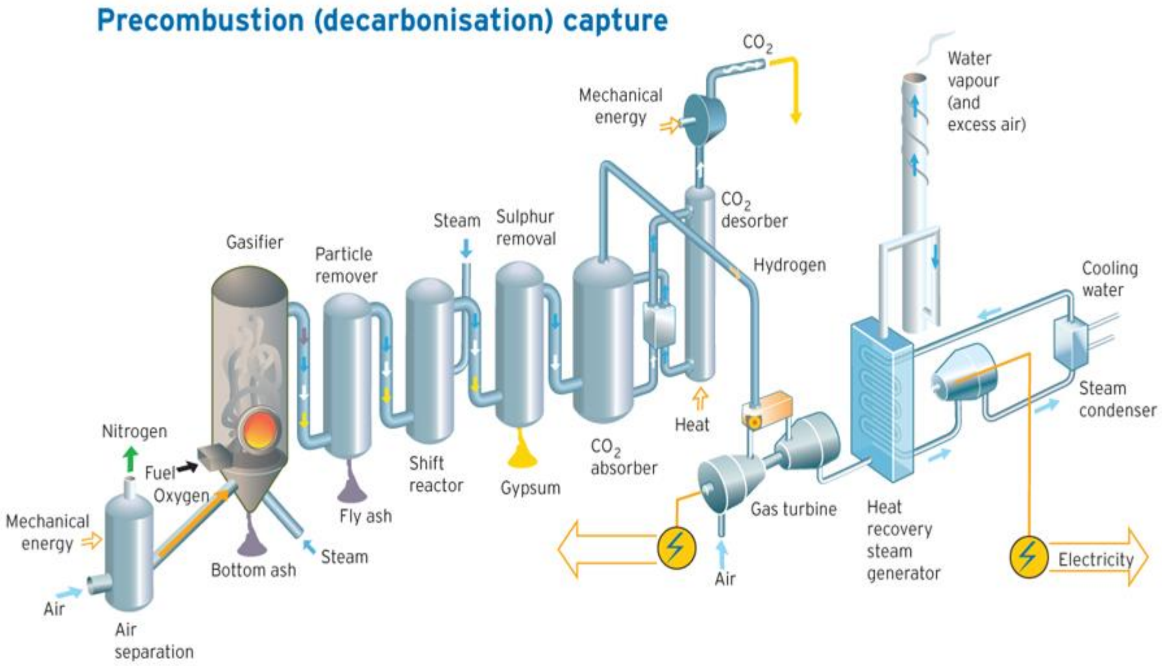

Figure 2-1: A schematic diagram of a pre-combustion process [61]

This process has been mentioned for completeness and will not be considered further in this thesis.

2.2.2 Oxy-Fuel Combustion

Oxy-fuel combustion is a technique that uses an air separation unit (ASU) to produce an oxygen rich stream in place of air for combustion (Figure 2.2). The combustion is accomplished in the absence of the large amounts of nitrogen which air would have brought in if enriched oxygen was not used, causing the process to produce only CO_2 and H_2O. CO_2 separation is accomplished by condensing water from the flue gas and therefore requires only a modest amount of energy. However, a relatively large amount of energy (7–10% of the total system input) is needed for the oxygen production. In this process the flue gas stream rich in H_2O and CO_2 (around 80%) ideally facilitates a relatively simple

CO_2 separation process by condensing out the H_2O [62-64]. As above, this process has been mentioned for completeness and will not be considered further in this thesis.

Oxy-fuel combustion was first proposed for CO_2 capture in the power industry by Abraham et al., [65]. Further investigations have been carried out to develop this method to a feasible option in competition with other carbon capture techniques [66-72].

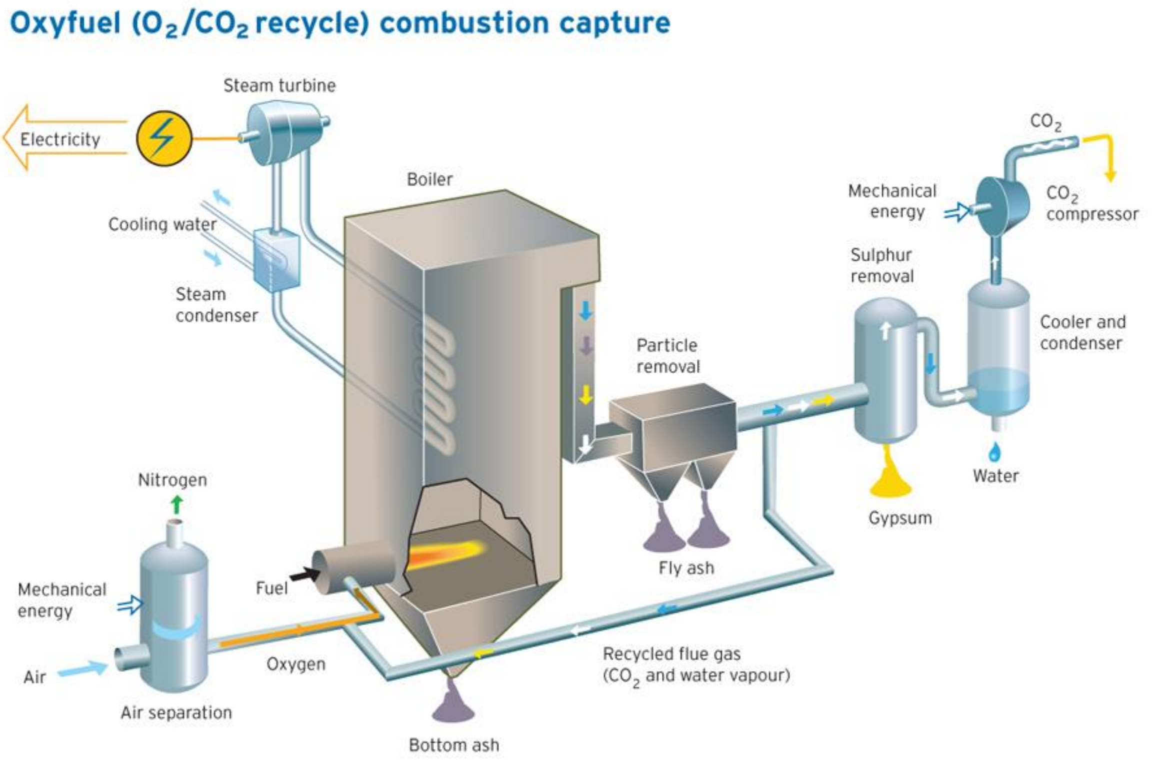

Figure 2-2: A schematic diagram of an Oxy-Fuel process [61]

Oxy-combustion is an alternative to post-combustion CO_2 capture, for new and existing conventional PC-fired power plants that offers the potential for near 100% capture of CO_2. Retrofitting an existing pulverized-coal-fired power plant to oxy-fuel operation requires a number of new process units such as air separation facility to provide the combustion process with almost pure oxygen, ducts and fans for external recirculation of flue gas to the burners in order to control flame temperatures, and a CO_2 processing facility producing a near-pure CO_2 stream for storage. The retrofit to oxy-fuel operation will reduce the plant electrical efficiency by about 10 percent points depending on the initial efficiency. The principal advantage of oxy-combustion is that it increases very significantly the partial pressure of CO_2 in the exhaust gases from combustion, because it avoids the dilution of exhaust gases with nitrogen in air [60].This method is also still under development and needs to achieve a certain cost estimates considering all effective parameters in a large scale implementation [73].

2.2.3 Post combustion

Post combustion employs a process technology of CO_2 removal from combustion off-gases with some kind of materials selective to carbon dioxide separation. In this process CO_2 is captured from flue gases after combustion (Figure 2.3). The process has attracted a lot of researches in an effort to achieve a reasonable method for CO_2 sequestration [4, 13, 17, 64, 74, 75]. Due to the worldwide availability and low price of limestone, lots of researches in post combustion field has focused on mineral carbonation [76-81]. Different methods has been considered over past decades to find a proper solution of CO_2 capture technology to apply for existing power plants to mitigate the rate of carbon dioxide emission to the atmosphere. Each method has some advantages and of course some disadvantages which makes it difficult to come up with a highly efficient technology applicable in a large scale.

Post-combustion CO_2 capture is primarily applicable to conventional coal-fired, oil-fired or gas-fired power plants, but could also be applicable to IGCC and natural gas combined cycle (NGCC) flue gas capture. It is also applicable to any large volume flue emission containing CO_2 from industrial plants: cement-making, steel-making, etc.

The post-combustion approach utilizes solvents, solid sorbents or membrane-based systems to capture CO_2 from combustion flue gas. Post-combustion solvent-based CO_2 capture involves chemical or physical sorption of CO_2 from flue gas into a liquid carrier.

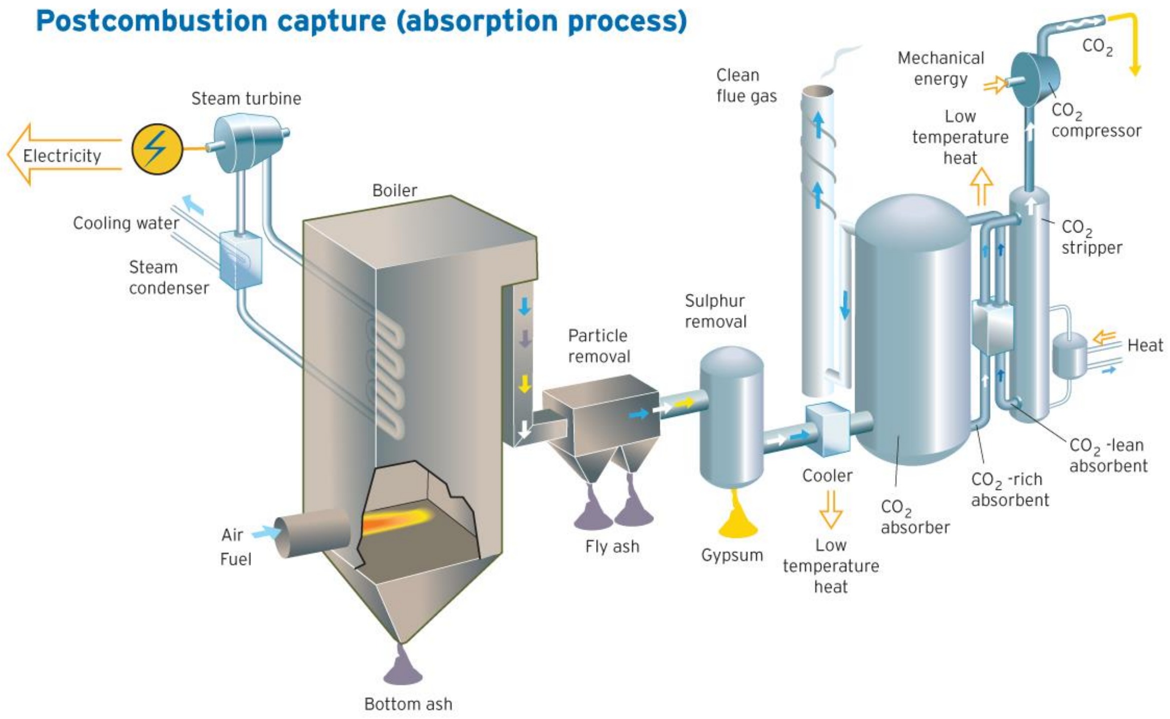

Figure 2-3: Schematic of a post-combustion CO2 capture system in a power plant [61]

Scrubbing with aqueous amine solutions (MEA, MDEA, DEA) is a well-known technology as a chemical absorption system in carbon sequestration [82]. Although this method can produce a relatively pure CO_2 which can be used for other purposes, it needs intensive energy to regenerate the amine solvent [83]. Post-combustion membrane-based CO_2 capture uses permeable or semi-permeable materials that allow for the selective transport and separation of CO_2 from flue gas. [84].

Post-combustion capture with CaO solid sorbent is a potential method for carbon capture from combustion flue gases at high-temperatures. In this method, the energy penalty is about 2.75% lower than that of other carbon capture technologies [15].

2.3-1 Solvent scrubbing

One of those methods considered over past decades is solvent scrubbing in which combustion exhaust gases is cooled down followed by gas-liquid contact to absorb CO_2 by solvent (Figure 2.4). The solvent is conducted to another vessel to release pure CO_2 by heating up to produce carbon dioxide up to 99% of purity. One of the most common solvents in this method is Mono-Ethanol-Amine (MEA), which has been successfully applied on an industrial scale. Due to a high energy requirement of this method, it is not really energy effective practically [85]. In industrial scale, it needs a higher rate of sorbent that makes a set of huge equipments with concern to corrosion of equipments associated with the solvent [86, 87, 88]. The efficiency penalty regarding the use of MEA method in a power plant is estimated as 10-12 percentage points of power output [2].

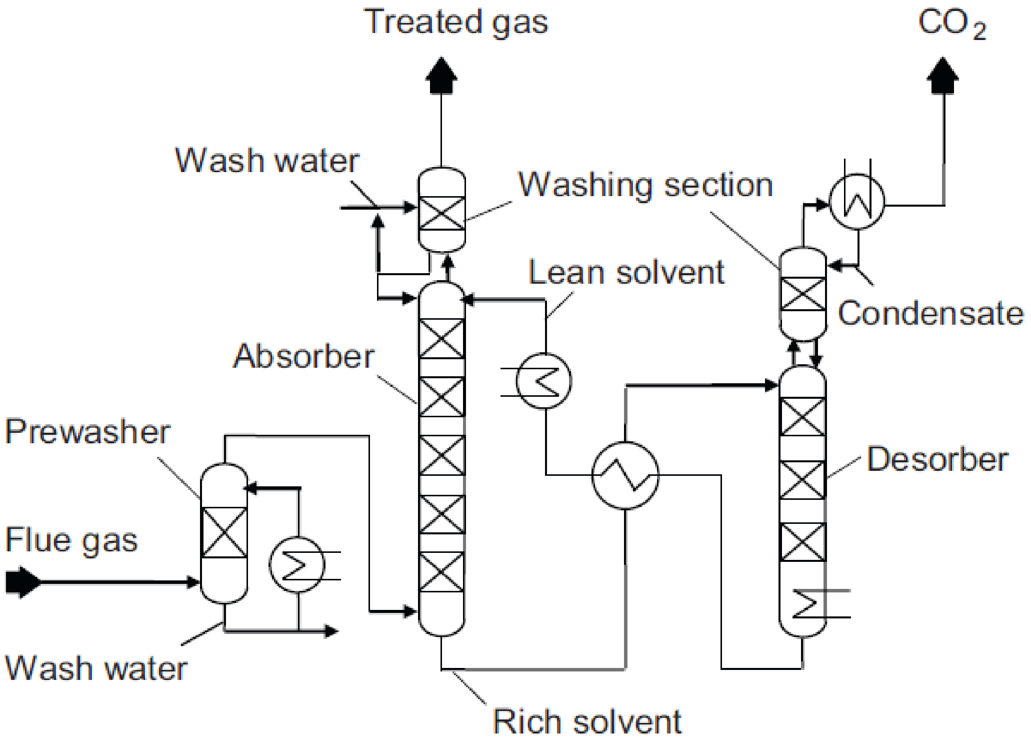

Figure 2-4: Schematic diagram of absorption/desorption process for CO_2 capture via post combustion system [89].

2.3.2 Membrane separation

In this method, combustion off-gases are separated through permeable tailored materials, with pressure difference between two sides of the membrane that makes separation possible based on the molecule size of the gas mixture. Different types of membranes such as ceramic, polymeric and metallic substances can be used in CO_2 separation from a gas mixture. This process is limited to small scales of CO_2 separation, due to the higher expenses of membrane materials as well as the life time of the membrane [90].

Their potential is generally viewed positively for high-pressure applications, such as IGCC, but not as promising for low-pressure combustion flue gas without further process enhancements. Energy consumption is a significant problem for gas-separation membrane processes [84].

2.3.3 Solid sorbent

Carbon capture with solid sorbents has been considered by many researchers in recent years [16, 18, 19, 23, 24]. Most solid sorbents for carbon capture are in the early developmental stages and are currently being tested on the laboratory scale. Solid sorbents such as Li-based, Ca-based and Mg-based systems are under development as a feasible option to implement in industrial scale. Among different type of solid sorbents, Ca-based sorbents are more easily accessible in large volumes due to the availability of raw material worldwide as well as the low cost of those substances.

In this process limestone ($CaCO_3$) is crushed and converted in to a fine powder. Once the fine particles are heated up to 950^oC then CO_2 is realised and active CaO generated is used in carbonation reaction. In this method CaO is carbonated to $CaCO_3$ in contact with flue gas at about 650^oC and afterwards $CaCO_3$ regenerated in Calciner to CaO and pure CO_2 at 900^oC that can be compressed the carbon dioxide to geological storage. The carbonation reaction can take place also at low temperatures but the overall efficiency of carbonation-calcination at high temperature is higher than low temperature absorption or absorption systems. In addition, a pure CO_2 stream is produced in a carbonation-calcination process

[28, 19]. A fundamental investigation and search on this route of carbon capture with CaO was conducted by Shimizu et al., [17]. Capture capacity of CaO in different cycles of carbonation/calcinations has been studied in the literature [27, 16, 32]. Carbonate looping for CO_2 capture is an efficient post combustion process for existing power plants. It can react sufficiently fast with carbon dioxide only up to a certain level of conversion, marked by the formation of a product layer [19] of calcium carbonate on all free surfaces of calcium oxide (including interior surfaces) which is called sintering of particles. Although carbonation with CaO takes place at high temperature in comparison with other alternatives of CCS, reuse of heat extracted from a carbonation loop to generate super-critical steam can increase the energy efficiency of the power plant and consequently minimise the penalty of the this (Q_4 in Figure 2.5).

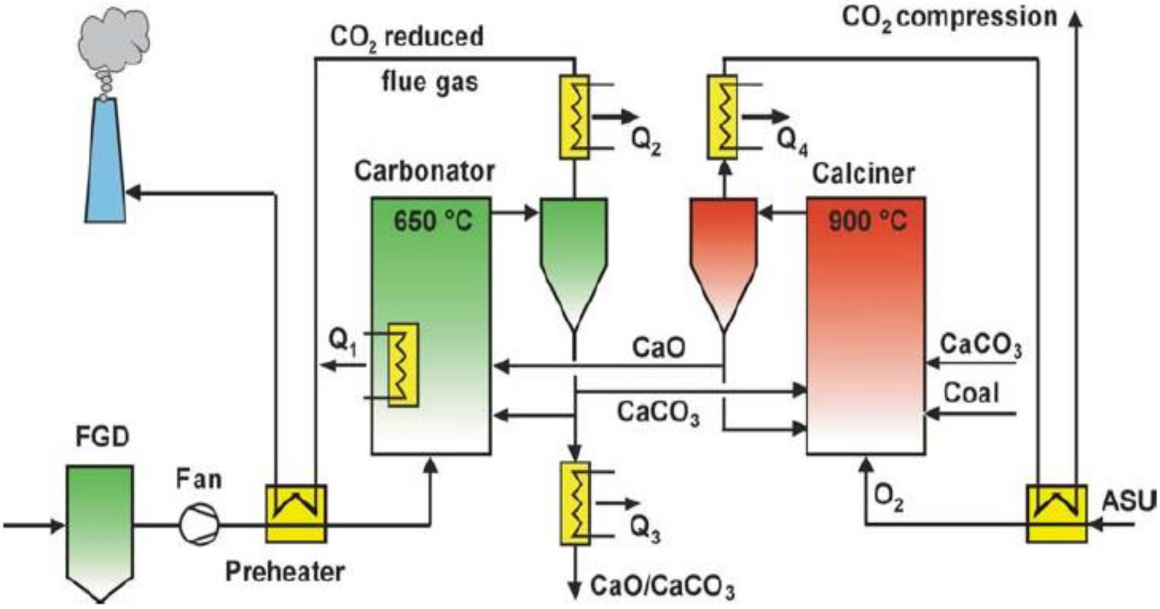

Figure 2-5: Process scheme of a carbonate looping plant [11]

Due to the high cost of this technique in terms of energy consumption and separation cost, cost effective methods with acceptable energy consumption are under development. Separation of CO_2 with solid sorbents in a fluidized bed reactor is one of the best alternatives so far to overcome these limitations, but it is still under investigations to find a solution with optimum operating conditions applicable to an industrial scale.

2.3.3.1 Carbonation with solid sorbents at low temperature

In low temperature capture with solid sorbent, solid substances (mainly amine based) are used to separate carbon dioxide from combustion off-gases. The drawback of this method is that the reaction rate is low which makes it unsuitable for industrial scale application. Consequently, a large quantity of solid sorbent would be required which invariably would mean an increased size of associated equipments. This method is still under research to reduce the rate of solid sorbent circulation and also the size of equipments with acceleration of carbonation reaction [91, 92]. Accelerated carbonation technology has been made possible by using industrial wastes including cement kiln dust, clinical waste, fly ash and paper sludge, steel wastewater sludge and sewage sludge incinerator ash [93]. Among all of these substances, cement dust and paper incinerator ash has higher reactivity in comparison with others; this is due to the higher content of calcium in these materials.

2.3.3.2 Accelerated carbonation at low temperature

Accelerated carbonation of cement-based inorganic waste materials at room temperature is also considered as an alternative in carbon capture technology. In this scheme, a combination of contaminated soil and industrial inorganic waste materials containing calcium or silicon salts are treated to sequestrate carbon dioxide and stabilize waste materials that can be used in construction materials with higher strength [94, 95]. This is one of the novel methods that is under development to employ it at large industrial scales. The drawback of this method is the low reaction rate of carbonation at ambient temperature. Investigations on municipal solid waste incineration fly ashes shows 12% conversion [91] after 180mins, meaning that it needs a higher ratio of solid materials.

Based on the achievements of CARBON8 research group, in cooperation with Greenwich University, Cement dusts and paper incineration ashes were the most reactive in natural carbonation process at ambient temperature [93]. They also indicated that increasing the temperature above the ambient temperature doesn’t increase the rate of the carbonation reaction because the reaction is inherently exothermic. The significant advantage of this method is the low energy consumption of carbonation step. On the other hand there is no need of extra heating to treat raw materials prior to the carbonation reaction. Although this process takes place at low temperature, the reaction rate is lower in comparison with high temperature carbonation process. Low carbonation reaction rate of this kind of material increases the amount of required raw material for a certain degree of removal, and hence a larger volume of equipment, higher rates of transportation and also high energy demand associated with equipments such as mixers and conveyers.

2.3.3.3 Carbonation with solid sorbents at high temperature

In this process carbonation reaction takes place at high temperature (concerning CaO carbonation at 650^{oC}) to give a higher reaction rate (70-80% ultimate conversion) reducing the amount of solid sorbent required and as a result requires smaller size of equipment in comparison to low temperature carbon capture at lower reaction rate [96]. MgO and CaO are two eligible and accessible raw materials for carbonation process, because calcium and magnesium are the only common elements that form stable carbonate minerals. It should be noted that steel slag is also the other common element, which may be considered, and it may be efficient to use in situ in steel-making plants. There are many sources in nature for calcium and magnesium silicate matrix ($MgO:xSiO_2$ and $CaO:xSiO_2$) in the form of rock.

Maintaining high temperatures in carbonation reactor is the solution to speed up the reaction rate, therefore very fast reaction takes place at 650^o(C) in carbonator [33]. In a chemical looping system (carbonation/calcination), further energy is required usually in the range 650 to 950^oC to regenerate CaO from $CaCO_3$ and this is the main energy consuming state of the carbon capture with mineral carbonation [97]. The main challenge is to bring down the capture cost which is mainly regarded to energy consumption cost during the carbon capture process.

Minimizing the energy penalty of this method is under research to obtain a cost effective solution. One method that is presently being adopted to improve the applicability of this technology is the utilization of energy released during carbonation in steam generation thereby recycling the supplied energy to the process to use in steam generation will make this method a promising[98, 99].

2.4 Source of calcium oxide

Although calcium and magnesium oxide (CaO and MgO) cannot be found in the nature in a vast amount, but it is accessible in a form of silicate matrix of rock in a large amount [100]. Limestone is not pure calcium carbonate, some of other impurities presents in the natural sources. These impurities and also ash in the regenerator can react to form other calcium compounds (e.g. Ca_2SiO_4, $2CaO.Fe_2O_3$, $CaO.Al_2O_3$). These compounds affect the carbonation process by reducing the capacity of the sorbent [3].

2.5 CO_2 storage

Captured CO_2 must be compressed and transported to sequestrate permanently under Deep Ocean or reservoir oil. In comparison with CO_2 capture process the cost of CO_2 storage is much lower. Based on the availability and economical matter different options can be considered in CO_2 storage.

CO_2 can be injected as a liquid or supercritical fluid to the depths below about 800–1000m of underground for permanent sequestration. Depleted oil and gas reservoirs, possibly coal formations, and particularly saline formations can be used for storage of CO_2.

Captured CO_2 can also be transported via pipelines or ships to an ocean storage site, where it is injected directly into the deep ocean at depths greater than 1,000 m. As a CO_2 abatement option, ocean storage is still in the research phase. However, there have been small-scale field experiments and 25 years of theoretical, laboratory and modelling studies [2].

2.6 Costs of CO_2 capture

The cost of the CO_2 capture is based on the technology in capturing process. Generally the technology must capture approximately 80-90% of emitted CO_2 from combustion exhaust gases. In order to reduce the transportation cost CO_2 is compressed after purification for transport and storage. In general, the factors such as plant size, location, efficiency, fuel type, fuel cost, capacity factor and capital and operating cost will affect the total CO_2 capture cost. The estimated cost of CO_2 capture increases the cost of electricity production by 35–70% for natural gas combined cycle (NGCC), and 40–85% for a supercritical pulverized power plant (PC). Table 2.1 shows that the main cost of the CO_2 capture and storage is related to the storage step. Although there is considerable uncertainty about the cost reductions through the technology development, the literature suggests that, provided R&D efforts are sustained, improvements to commercial technologies can reduce current CO_2 capture costs by at least 20–30% over approximately the next ten years, while new technologies under development could achieve more substantial cost reductions.

Using CaO sorbent with 86.0% of CO_2 capture can be achieved with 15.7 €/ (ton CO_2) of penalty [25]. Due to the high capital cost of the carbon capture plants it is economically hard to use CCS technology in power plants with fossil fuel combustion and particularly for the medium and small plants [52]. Plant equipment cost (per power output) decreases with increasing in plant capacity [13].

Table 2.1: 2002 Cost ranges for the components of a CCS system as applied to a given type of power plant or industrial source [2].

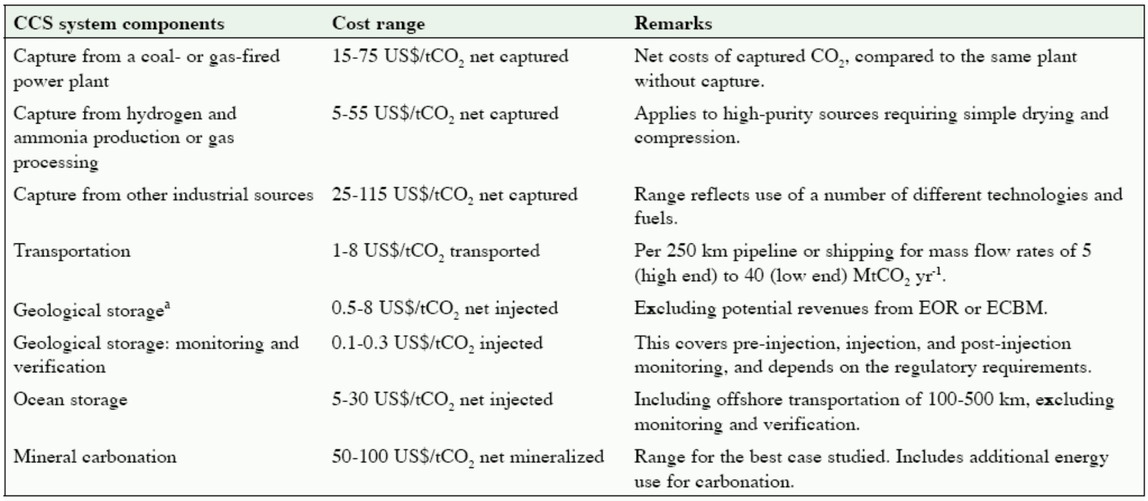

CCS system components	Cost range	Remarks
Capture from a coal- or gas-fired power plant	15-75 US$/t$CO_2$ net captured	Net costs of captured CO_2, compared to the same plant without capture.
Capture from hydrogen and ammonia production or gas processing	5-55 US$/t$CO_2$ net captured	Applies to high-purity sources requiring simple drying and compression.
Capture from other industrial sources	25-115 US$/t$CO_2$ net captured	Range reflects use of a number of different technologies and fuels.
Transportation	1-8 US$/t$CO_2$ transported	Per 250 km pipeline or shipping for mass flow rates of 5 (high end) to 40 (low end) MtCO_2 yr^{-1}.
Geological storage[a]	0.5-8 US$/t$CO_2$ net injected	Excluding potential revenues from EOR or ECBM.
Geological storage: monitoring and verification	0.1-0.3 US$/t$CO_2$ injected	This covers pre-injection, injection, and post-injection monitoring, and depends on the regulatory requirements.
Ocean storage	5-30 US$/t$CO_2$ net injected	Including offshore transportation of 100-500 km, excluding monitoring and verification.
Mineral carbonation	50-100 US$/t$CO_2$ net mineralized	Range for the best case studied. Includes additional energy use for carbonation.

It seems investigating a capture cost is a complicated subject and based on a plant's situation and all other parameters that affecting the capital and operating costs. Therefore for every individual power plant, parametric investigations over the total capture cost are essential to implement an economically reasonable CCS technology.

2.7 Introduction to fluidized bed reactors

Fluidized beds have been widely utilized in many different applications including combustion, gasification and catalytic cracking. Many research studies have been done dealing with the development and application of mathematical models to find out the fluid and particle behaviour in fluidized bed reactors [37, 101-105].

In a circulating fluidized bed (CFB), particles are separated from the fluid using cyclones and are recycled back to the bed. The part of the system where the carryover of solids transpires is normally referred to as the riser. The different types of fluidized beds are discussed in the section 2.8.

Using a circulating fluidized bed reactor to sequestrate CO_2 from flue gases seems to be a promising approach but with a lot of challenges to be overcome. Literature sources [98, 21] show that using CFB for CO_2 capture is still under development. It is still necessary to find out the proper operating conditions as well as the proper new design to fulfil the energy efficient process which is economically applicable to the industrial scale. At present, it is not economically viable at an industrial field due to the higher energy consumption during this process which reduces the total efficiency of the plant. A new design needs to overcome this problem with a minimum waste of energy in the process.

2.8 Fluidization

A fluid travelling upwards through a packed bed of solid particles sustains a pressure drop due to fluid drag. When the fluid drag force is equal to the bed weight the particles will start to move up and this is the fluidization point (Figure 2.6).

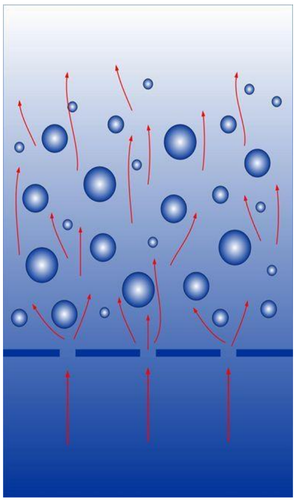

Figure 2-6: Schematics fluidization of solid particles

The associated gas velocity at the fluidization point is called the minimum fluidization velocity (V_{mf}). If the fluid velocity is increased, the pressure drop does not significantly increase further, but the bed may be expanded. This can be expressed mathematically [37]:

$$\Delta P = \left(\rho_p - \rho_g\right)(1 - \varepsilon_m)gL \tag{2.1}$$

Where ΔP is the pressure drop, ρ_p and ρ_g are the density of the particle and gas respectively. ε_m is the porosity at minimum fluidization, and L is the height of the bed. The Ergun equation can be used to calculate the pressure drop in packed beds [106]:

$$\frac{\Delta P}{L} = \frac{150\mu u}{d_p^2}\frac{(1-\varepsilon)^2}{\varepsilon^3} - \frac{1.75\rho_g u^2}{d_p^2}\frac{(1-\varepsilon)}{\varepsilon^3} \tag{2.2}$$

Where u is the superficial velocity (volume flow rate divided by cross-sectional area), μ is the viscosity. d_p is the particle diameter and ε is the void fraction of packed bed.

2.9 Fluid particle interaction

Interaction between fluid and particles can be represented primarily by the drag force (F_d). A drag force acting on a spherical particle can be expressed as follows:

$$F_D = \frac{1}{2}\rho_g C_D A\left|u_p - u\right|\left(u_p - u\right) \tag{2.3}$$

Where u_p and u indicate solid and gas velocities respectively. A is the frontal area of the particle and C_D is the drag coefficient. Because in particle tracking the initial static bed does not affect the trajectories therefore the most important parameter associated with static bed at fluidization point, called minimum fluidization velocity does not appear in equations of the model.

Inside the fluidized bed reactor different regimes form as particles are fluidized. These regimes represent the probability of particles' presence at each part of the reactor based on the particles velocity. When the flow of a gas passing through a bed of particles is increased continually, a few vibrate, but still within the same height as the bed at rest. This is called a fixed bed (Figure 2.7-A). With increasing gas velocity, in a point which the drag force associated to upward moving gas equals to the weight of the particles, and the voidage of the bed increases slightly: this is the start-point of fluidization and is called minimum fluidization (Figure 2.7-B) with a corresponding minimum fluidization velocity, u_{mf}. Further increasing the gas velocity, bubbles are started to be formed in fluidization region. At this point, a bubbling fluidized bed occurs as shown in Figure 2.7-C.

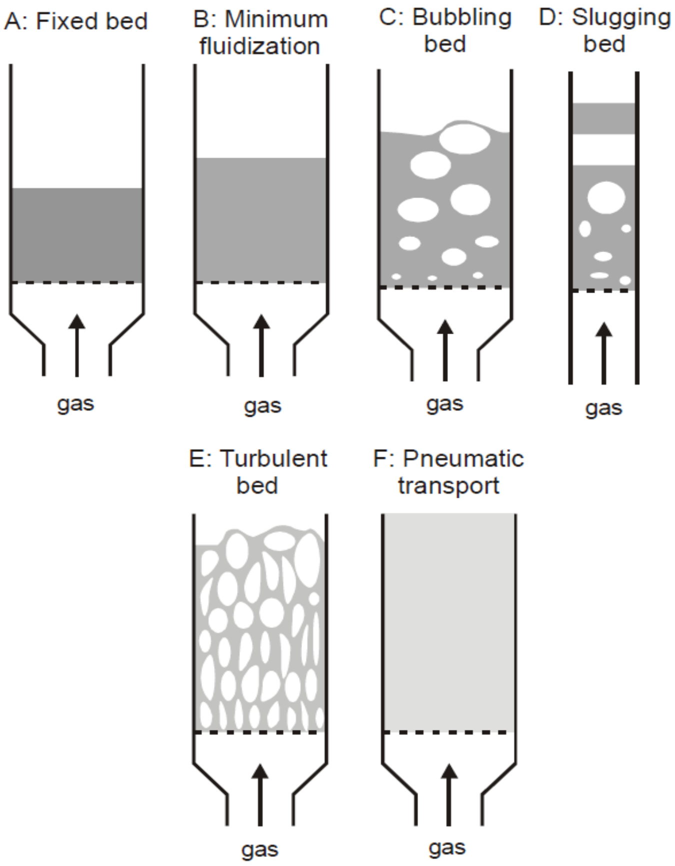

Figure 2-7: Schematic representation of fluidized beds in different regimes [107]

As the velocity is increased further still, the bubbles in a bubbling fluidized bed will coalesce and grow as they rise. If the ratio of the height to the diameter of the bed is high enough, the size of bubbles may become almost the same as diameter of the bed. This is called slugging (Figure 2.7-D). If the particles are fluidized at a high enough gas flow rate, the velocity exceeds the terminal velocity of the particles. The upper surface of the bed disappears and turbulent motion of solid clusters appears. Beds under these conditions are called turbulent beds as shown in Figure 2.7-E. With further increases of gas velocity, eventually the fluidized bed becomes an entrained bed in which we have disperse, dilute or lean phase fluidized bed, which amounts to pneumatic transport of solids.

2.10 Modelling approaches

The subject of modelling in multiphase flows is vast and consists of various matters associated with features of the phases. There are three main approaches to describe the behaviour of multiphase flows; volume of fluid (VOF), Eulerian-Lagrangian (EL) and Eulerian-Eulerian (EE). Based to the flow characteristics and presence of thermodynamic phases such as gas-liquid, gas-solid, gas-liquid-solid, liquid-liquid, liquid-solid, one of the above modelling approaches can be employed to solve the problem. In this work a gas-solid system in Eulerian-Lagrangian framework has been implemented to a fluidized bed reactor. Broadly, flow regimes are classified as dispersed flows, mixed flows and separated flows [108]. In dispersed flows all the phases except one exist as dispersed (discontinuous) particles flowing through the continuous fluid. Examples of this flow regime include bubbles in liquid, solid particles in gas or liquid and liquid droplets in gas or other immiscible liquid. In separated flows, none of the phases exist in discontinuous particle form. All the phases flow in a semi-continuous mode with interfaces between the different phases. Examples of this flow regime include film flow, annular flow and jet flow. In mixed flow regimes, dispersed particles as well as semi-continuous interfaces exist together. Examples of this regime include droplet annular flow (where liquid flows in the form of an annular film over the pipe as well as suspended droplets in the gas core), bubbly annular flow (where some gas bubbles flow through the annular liquid film) and slug flow. Separated or mixed flow regimes may exist in trickle bed reactors. However, in most of the other reactors, dispersed flow regimes exist. In other gas-solid reactors (fluidized reactors), gas is the continuous phase and solid particles are suspended within this continuous phase. For relatively small gas flow rates, the reactor may contain a dense bed of fluidized solid particles. The bed may be homogeneously fluidized or gas may pass through the bed in the form of large bubbles. Further increase in gas flow rate decreases the bed density and the gas-solid contacting pattern may change from dense bed to turbulent bed, then to fast-fluidized mode and ultimately to pneumatic conveying mode. In all these flow regimes the relative importance of gas-particle, particle-particle and particle-wall interaction is different. It is, therefore, necessary to identify these regimes to select an appropriate mathematical model [109].

In the VOF approach, the motion of all phases is modelled by formulating local, instantaneous conservation equations for mass, momentum and energy. This approach is naturally limited to modelling the motion of only a few dispersed phase particles. For simulations of dispersed multiphase flows in large equipment, this approach is not suitable, as it requires huge computational resources to resolve flow processes around each dispersed phase particle. VOF-based models can be very useful as learning tools and can provide valuable information to develop appropriate closure models for Eulerian-Lagrangian and Eulerian-Eulerian approaches.

In the Eulerian-Lagrangian approach, explicit motion of the interface is not modelled. This means small-scale fluid motions around individual dispersed phase particles are not considered. Their influence is modelled indirectly while considering the motion of dispersed phase particles. In this approach, motion of the continuous phase is modelled using an Eulerian framework. The motions of dispersed phase particles (trajectories) are explicitly simulated in a Lagrangian framework. Averaging over a large number of trajectories is then carried out to derive the required information for the modelling of the continuous phase. In this approach, particle-level processes such as reactions, heat and mass transfer etc. can be simulated in adequate details. In the case of turbulent flows, it is necessary to simulate a very large number of particle trajectories to obtain meaningful averages. Therefore by increasing the number of particles in a certain domain the particle-particle interaction becomes significant which needs to be included more equations in numerical solution and computational resources become stretched. The approach is, therefore, suitable for simulating dispersed multiphase flows containing a low (<10%) volume fraction of the dispersed phases. For denser dispersed phase flows, it may be necessary to use an Eulerian-Eulerian approach.

The Eulerian-Eulerian approach models the flow of all phases in an Eulerian framework based on the interpenetrating continuum assumption. In this approach, trajectory simulations and averaging are not carried out at a computational level but are implicitly achieved at a conceptual level. The discrete character of the underlying process is, therefore, averaged out to provide a model involving a continuum associated with the dispersed phase particles. This approach is the most difficult one to understand conceptually, requiring extensive modelling efforts. Various averaging issues will have to be addressed while formulating the governing equations in this approach. If modelled successfully, this approach can be applied to multiphase flow processes containing large volume fractions of dispersed phase. It may, therefore, be extended to modelling and simulation of complex industrial multiphase reactors consisting of a large number of dispersed particles.

chapter 3

Carbonation Kinetic and 1-D Modelling of a Carbonator

3.1 Carbonation/Calcination Process

Carbonation reaction takes place in a carbonation reactor and regenerated in a calcinations reactor for the recirculation of CaO particles. A rapid chemical reaction takes place initially which then slows down to saturation. The product layer is governed by diffusion of the particle in the second stage, controlling the rate of reaction. Hydration of CaO by steam ($Ca(OH)_2$) is seen to be more effective than dry carbonation but it requires an additional reactor, a steam generation system and a larger temperature range. CO_2 capture capacity with solid particles have been studied by several researchers to determine the rate of decay in conversion rate over several cycles [16,17,28,75,81,110].

Several advantages of carbonation with CaO including selective and rapid reaction with CO_2, vast amount of limestone ($CaCO_3$) sources in worldwide, permanent storage of CO_2 on solid (after a few carbonation/calcination cycles those solids must be removed from the system to the environment) and exothermic carbonation reaction, make it a promising technology to establish at large industrial scale to mitigate CO_2 emission to the atmosphere. The drawback of this substance in carbon capture is regarded to decay of capture capacity with number of cycles in carbonation/calcinations process. Repeated carbonation/calcination cycles reduce the capture capacity of solid substances that cannot give the same efficiency of fresh materials. This phenomenon has been studied over past decade with investigation of carbonation/calcination efficiency with effect of cycles [16, 32].

This drawback is related to the changes on particle structure due to the carbonation reaction which makes the formation of product layer on the surface and pores of the solid sorbent that controls the reaction by dropping the diffusion rate to the solid. The carbonation rate decreases when multiple cycles are used because the available pores over the solid sorbent decreases due to changing of particle structure during the carbonation/calcinations cycles. Salvador et al., [27] shows that after 13 cycles the capacity of sorbent reduced from 80% in first cycle to 30% in cycle 13 and no change after the cycle 13.

In order to overcome to overcome to reactivation of the sorbent Na_2CO_3 and NaCl were used as additives to the process [27, 111]. It is perceived that use of NaCl is more effective than Na_2CO_3 for reactivation, in which use of NaCl improves the capacity of the last cycle from 30% to 40%, but this introduced a drop of about 50% in capture capacity of the initial cycles (after cycle 1). Nevertheless, it should be considered that the low performance of modified sorbents during a few cycles is less important than the high performance for long-term behaviour of the sorbent. It has also been reported that that the type of limestone is not such an important factor in carbonation-calcinations process. The following equation has been suggested for the decay of the capture capacity [16,27]:

$$X_N = f_m^N(1 - f_w) + f_w \tag{3.1}$$

Where X_N is the maximum carbonation conversion achieved after N cycles, f_m=0.77 and f_w=0.17.

CaO sorbent chemically absorbs CO_2 as in the following reaction,

$$CaO + CO_2 \rightarrow CaCO_3 \qquad\qquad \Delta H^o_{r\,298} = -178\ kJ/mole$$

M_{CaO}=56.08, M_{CO2}=44.01, M_{CaCO3}=100.09

According to the above reaction formulation, theoretically 1kg CaO can absorb 0.785kg of CO_2. Investigations show that under real operating conditions, only 0.628kg of maximum CO_2 capture can be achieved, because the ultimate conversion approaches 80% (and not 100%) as reported in literatures [110]. This value of ultimate conversion decreases by number of cycles in a carbonatioan/calcination system. This means that the amount of the maximum capture will decay rapidly with number of cycles. After 13 cycles it will decline to around 30% [27, 16]. Because of this decay in carbonation, there is a big challenge to find alternative ways to minimise this decay in the capture process.

At atmospheric pressure, the maximum temperatures at which CO_2 concentration below 1 vol% and 5 vol% can be maintained are 642 ^{o}C and 718 ^{o}C, respectively [111, 112]. This means that when temperature is increased beyond the maximum (and the above range of CO_2 concentration), decomposition or reverse reaction occurs which drops the stability of the captured CO_2 on solid sorbent and goes on to reduce the efficiency of the carbonation process significantly. In order to operate in high conversion rate of the reaction and also avoid any reverse reaction operating temperature in carbonator must be set slightly lower than the associated maximum temperature and literatures suggested the 650^{o}C.

In calcination, the operating temperature would absolutely higher than that maximum temperature as we need for inverse reaction of carbonation and based on the experimental data it is higher than 900^{o}C [16, 75]. It is clear that both carbonation and calcination reactions take place at high temperature and require a supply of large amounts of the energy for this operating condition. Increasing contact time between the gaseous and solid streams and consequently maximizing the ultimate conversion of solid sorbent before leaving the reactor would be essential to increase the efficiency of the process.

Carbonation /calcination looping with fluidized bed reactor is a promising technology to achieve almost 80% of CO_2 capture on an industrial scale [39, 98], but it still needs more exploration on gas-solid contact to design a proper energy efficient equipment with a suitable operating condition to make it commercially applicable in the industry. Scaling up of solid sorbent technology in carbon capture with circulating fluidized bed reactor is under examination in pilot scales [113].

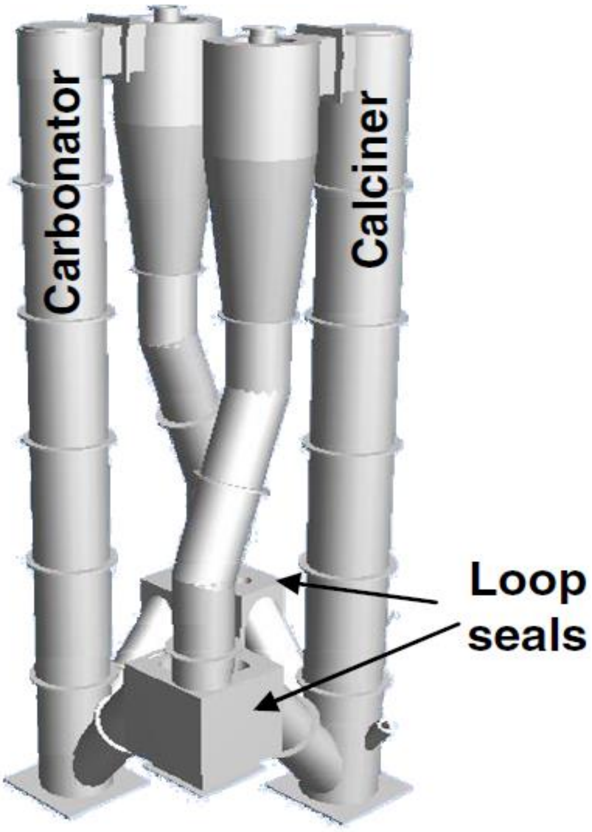

Figure 3-1: diagram of a Carbonation/Calcination looping for carbon capture system [113].

A carbonation/calcination looping system for a pilot plant [Figure 3.1] of 1MWth is supposed to treat flue gases of 1400kg/h in a carbonator with 15m of height. It has been reported that a promising post-combustion with solid sorbent at high temperature has the potential of 70-80% of CO_2 capture with 30% improvement in energy penalties and capture cost against the oxy-fired systems [113].

To obtain a suitable operating condition and dimensions of the carbonator, CFD simulation is a powerful tool to study gas-solid behaviour, effective parameters on reaction and residence time of solid sorbent inside the carbonator. The analysis of CFD simulation results can support to establish a suitable CCS system at existing or new power plants to mitigate the global warming and climate change with low CO_2 emission to the atmosphere. Obtaining the knowledge of particle behaviour inside the reactor, including particle's residence time, the rate of added mass on particle, the possibility of the attrition effect on particles and ultimate conversion all are essential. Mathematical modelling and simulation is vital in accumulating the necessary information.

3.2 Carbonation Kinetics

Carbonation reaction of CaO with CO_2 takes place in atmospheric pressure and ambient temperature slowly on geological time scale. In order to speed up the reaction rate, the reaction temperature needs to be increased to about 650^{o}C. Although the carbonation process is exothermic ($\Delta H^{o}_{r\,298} = -178\, kJ/mole$) inherently, but the activation energy of 30kJ/mol (with 100% pure CO_2) must be supplied to complete the reaction [3]. The released heat during the reaction is comparable with burning of fossil fuel in combustion process of power plant’s heat generation.

$$C + O_2 \rightarrow CO_2 \qquad \Delta H_r = -394\, kJ/mole \tag{3.2}$$

The heat of reaction can be considered in heat integration of a power plant with CCS technology to increase the energy efficiency with conducting this heat to generate superheated steam.

Gas-solid CO_2- CaO reaction is governed by two different rates of regimes. Initially it is a rapidly chemical controlled carbonation reaction followed by second slow rate of reaction controlled by diffusion. At the second stage, due to the sintering of outer surface of particles, diffusion of CO_2 is limited and it cannot reach to the non-reacted portions of particles. Based on the literature, the ultimate conversion of carbonation reaction can be in the range of 70-90% of an ideal complete reaction [96, 114]. Un-reacted shrinking core model of Kunii-Levenspiel [115] considered to describe the gas-solid reaction model [110].

$$\frac{t}{\tau} = 1 - (1 - X)^{1/3} \tag{3.3}$$

$$\frac{t}{\tau} = 1 - 3(1 - X)^{2/3} + 2(1 - X) \qquad (3.4)$$

Where X is conversion of CaO, t is time and τ represents the time for complete conversion of CaO. The Eq. (3.3) describes a chemical controlled reaction regime and Eq. (3.4) expresses the diffusion controlled reaction flowing by the first rapid reaction regime. In previous models, the structure of particles are not considered, therefore the effect of blockage in surface of particles and changing the reaction regime cannot be seen, because those models are only the function of time.

Bhatia and Perlmutter [114] suggested a random pore model to take into account the effect of particle's pores in reaction calculation:

$$\frac{1}{\Psi}\left[\sqrt{1 - \Psi ln(1 - X)} - 1\right] = \acute{k}t \qquad (3.5)$$

$$\frac{1}{\Psi}\left[\sqrt{1 - \Psi ln(1 - X)} - 1\right] = \sqrt{\acute{\acute{k}}t} \qquad (3.6)$$

Where $\acute{k}$ and $\acute{\acute{k}}$ stand for constants of the models proportionally for reaction controlled and diffusion controlled regimes and Ψ represents the structural parameter as a function of surface area, porosity and the initial total length pore system per unit volume.

In spite of the fact that this model can prescribe the carbonation reaction considering particle's structure, but it is complicated to take into account the material characteristics such as initial total length of pore system. Lee [110] developed a simple model that can predict the progress of reaction by the flowing equation:

$$\frac{dX}{dt} = k\left(1 - \frac{X}{X_u}\right)^n \qquad (3.7)$$

Where k is the constant of carbonation conversion, X_u is ultimate conversion in which the reaction rate goes to zero and n is a parameter of the model. Allocating *2* for the parameter of model $(n = 2)$, and integrating over the equation (Eq. 3.7) resulted the following equation:

$$X = \frac{X_u t}{\frac{X_u}{k} + t} \tag{3.8}$$

Where k is a constant parameter and depends on temperature. To obtain a linear format of the reaction model, it has been assumed that at t=b reaction progressing to the half of ultimate conversion ($X=X_u/2$). Considering the equation (3.8) with this assumption gives:

$$X_u = kb \tag{3.9}$$

Where *b* is the equation parameter is sensitive to temperature. Rewriting the equation (3.8) in a linear format results the following equation representing the carbonation conversion as a function of time reaction features:

$$\frac{1}{X} = \frac{1}{k}\left(\frac{1}{t}\right) + \frac{1}{kb} \tag{3.10}$$

Table (3.1) shows the kinetic parameters fitted to the equation (3.10) at two different reaction rate regimes. Two set of data, by Bhatia and Perlmutter [114] with symbol *a* and by Gupta and Fun [96] associated with symbol *b*, are employed to obtain those constants at different operating temperatures.

The data obtained by Bhatia and Perlmutter [114] are associated with average particle size of 81 μm (-170+200 mesh) and surface area of 15.6m^2/g. Activation energy in the literature was reported 72.2 and 189.3 kJ/mol respectively for chemical reaction controlled and diffusion control regime [114]. Data reported by Gupta and Fan [96] is regarded to particles with 12.8m^2/g in surface area and activation energy of 72.7 and 102.5 *kJ/mol* in chemical and diffusion controlled regimes respectively.

Table 3.1: kinetic parameters for the linear reaction model [110]

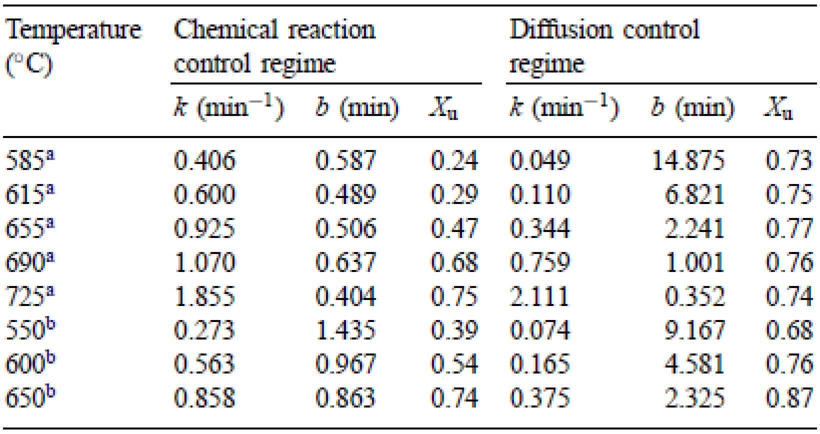

Temperature (°C)	Chemical reaction control regime			Diffusion control regime		
	k (min^{-1})	b (min)	X_u	k (min^{-1})	b (min)	X_u
585[a]	0.406	0.587	0.24	0.049	14.875	0.73
615[a]	0.600	0.489	0.29	0.110	6.821	0.75
655[a]	0.925	0.506	0.47	0.344	2.241	0.77
690[a]	1.070	0.637	0.68	0.759	1.001	0.76
725[a]	1.855	0.404	0.75	2.111	0.352	0.74
550[b]	0.273	1.435	0.39	0.074	9.167	0.68
600[b]	0.563	0.967	0.54	0.165	4.581	0.76
650[b]	0.858	0.863	0.74	0.375	2.325	0.87

Carbonation/calcination cycles leads to the reduction of the maximum capture capacity of solid sorbents. This issue has been studied by Abanades [16] and the following equation has been suggested to predict the maximum achievable conversion rate in carbonation process after N cycles.

$$X_N = f^{N+1} + b \tag{3.11}$$

Where X_N represents the carbonation conversion after N cycles, f and b are constant and obtained from experimental data fitting (f=0.872, b=0.174). This correlation is approximately independent (with correlation coefficient of 0.982) from temperature, CO_2 partial pressure and particles size. The experimental operating temperature is in the range of 873-1139K for different set of data used to obtain this equation representing the decay of capture efficiency.

Figure (3.2) shows a profile of carbonation conversion in a set of cycles, in which there is a significant reduction of ultimate conversion associated with cycles. It seems the rate of decay in capture efficiency in earlier cycles is much more significant, while after 15 cycles it follows slowly.

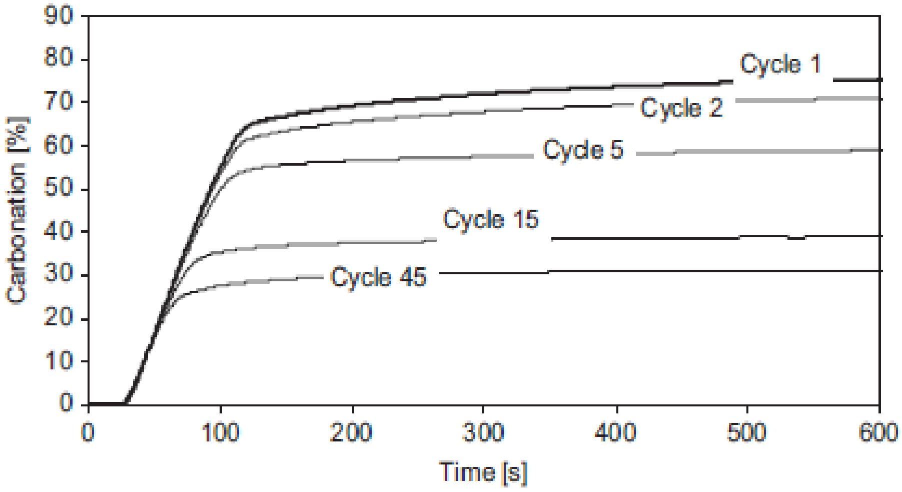

Figure 3-2: Effect of cycles in carbonation ultimate conversion [32]

Abanades et al., [29] suggested the following alternative formulation to express the effect of cycles in carbonation/calcinations.

$$X_{bn} = \left(\frac{1}{1-X_r} + kN\right)^{-1} + X_r \qquad (3.12)$$

Where *k=0.52*, X_r*=0.075* which are obtained with experimental data fitted to Eq. (3.12).

F. Zeman [116] used steam hydration techniques to abate the rate of decay in the carbonation cycles. The hydration process can help to reduce the effect of sintering by changing the molar properties of the sorbent particles. In this technique, steam is used to form a hydrate before proceeding to the carbonation step as in the following reaction:

$$CaO_{(s)} + H_2O_{(g)} \xrightarrow{\Delta H=-105\frac{kJ}{mol}} Ca(OH)_{2(s)}$$

$$Ca(OH)_{2(s)} + CO_{2(g)} \xrightarrow{\Delta H=-69\frac{kJ}{mol}} CaCO_{3(s)} + H_2O_{(g)}$$

Hydrating the lime takes place at around 300°C. Fitting the experimental data obtained by steam hydration yields the values of the constants in equation (3.12) as follows [116];

$k=0.505, X_r=0.48$

A FORTRAN program was employed to solve models associated to different methods of carbonation process to show the effect of hydration effect on cycles [27, 29, 116]. The results of the program presented are in Figure 3.3 which shows the conversion of CaO over a number of cycles. It shows apparent advantage of hydration against the dry base. After 20 cycles both dry base carbonations were limited to less than 20% whilst the hydration technique can improve this to more than 50%.

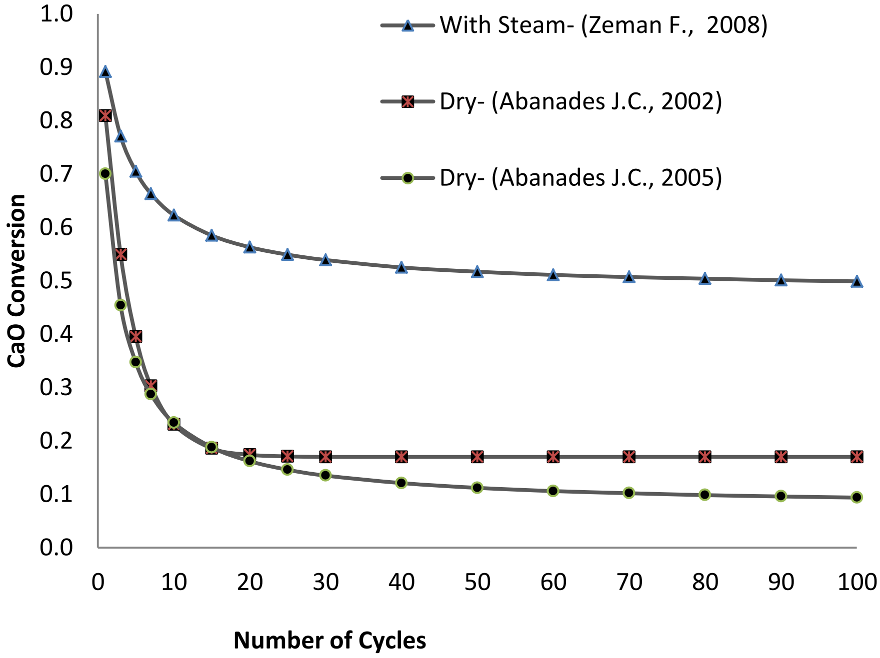

Figure 3-3: Comparison between two different formulations (dry based and hydrated) in the conversion of CaO after a number of cycles.

It seems that the hydration process is more efficient than the dry base, but of course requires additional energy and extra facilities. It needs to be investigated economically in a continuous process. It is understandable that using dry base requires more frequent feeding of fresh materials in comparison with the hydration method and this matter should be considered in comparison of these two methods. Alternative materials to CaO exist, and are being addressed in accelerated carbonation research [94], where carbonation takes place at ambient temperature.

3.3 A 1-D Model for Carbonator

The schematic diagram for mass balance over a circulating fluidized bed reactor for CO_2 separation from flue gases by chemical adsorption process is given in figure 3.4.

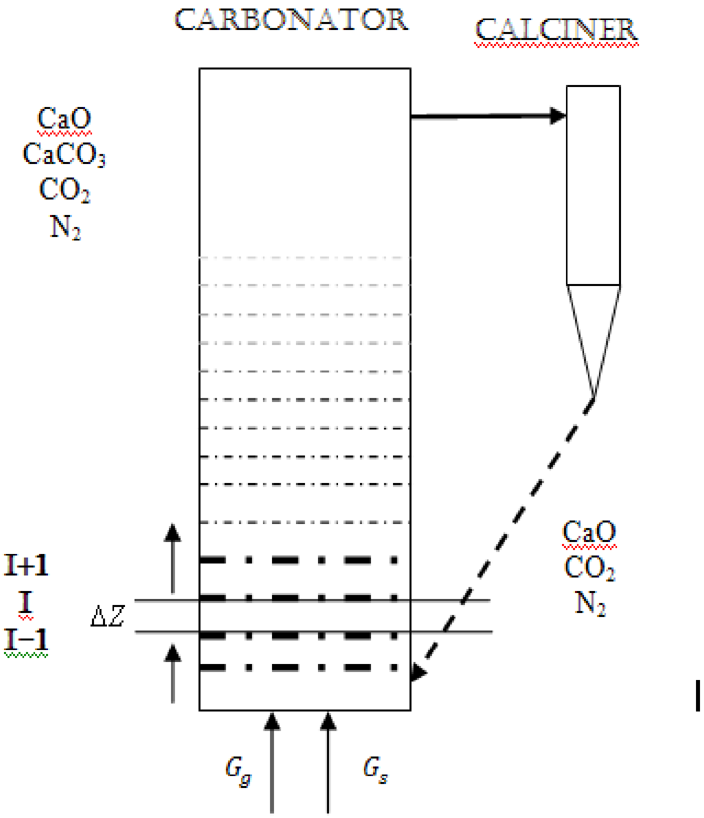

Figure 3-4: Material balance in a circulating fluidized bed reactor for carbonation of CaO.

In a circulating fluidized bed reactor, there are two solid inflows which they can be combined to give a total solid mass flow rate with an average active CaO (x_{bn}) for solid inflow. Therefore the solid and gas flow goes in to the system through the bottom of the reactor continuously. In an actual fluidized bed reactor, due to the solid distribution the reactor is divided in to dense and lean regions. The dense region which is in the lower section of the reactor contains higher volume fraction of solids in comparison with lean region which is considerably dilute in solid concentration.

Mass balance in dense region can be categorized in two different phases: bubble phase and emulsion phase [107].

[mass of CO_2 in to the control volume]- [mass of CO_2 out from control volume] = [reaction in control volume]

The result of two terms on the left hand side represents the variation of CO_2 concentration inside the control volume and the term on the right hand side refers to the CO_2 consumption in control volume due to the reaction. By separating the above mass balance for emulsion and bubble, it can be written as following:

[Variation of CO_2 concentration in emulsion phase of the control volume]= [reaction in emulsion] + [transfer from emulsion to the bubble phase]

[Variation of CO_2 concentration in bubble phase of the control volume]= [reaction in bubble] + [transfer from bubble to the emulsion phase]

Where the arithmetical summation of transfer terms in two above expressions would be zero, thus the overall summation of those mass balances would be same as the general mass balance in control volume.

Variation of CO_2 concentration in gas flow at *z*-direction (see Figure (3.9)) can be expressed by following equation for bubbling phase in dense region [107]:

$$-\delta u_b^* \frac{dC_{\mathrm{b,CO2}}}{dz} = \delta \gamma_b f_a K_r \left(C_{\mathrm{b,CO2}} - C_{\mathrm{eq,CO2}}\right) + \delta K_{be} \left(C_{\mathrm{b,CO2}} - C_{\mathrm{e,CO2}}\right) \tag{3.13}$$

and CO_2 mass balance in emulsion phase at dense region can be expressed by [107]:

$$\begin{aligned} -(1-\delta) u_{mf} \frac{dC_{\mathrm{b,CO2}}}{dz} &= (1-\delta)\left(1-u_{mf}\right) f_a K_r \left(C_{\mathrm{b,CO2}} - C_{\mathrm{eq,CO2}}\right) \\ &\quad - \delta K_{be} \left(C_{\mathrm{b,CO2}} - C_{\mathrm{e,CO2}}\right) \end{aligned} \tag{3.14}$$

where K_{be}, the overall interchange coefficient between emulsion and bubble phase can be expressed as following [107]:

$$K_{be} = 4.5\frac{u_{mf}}{d_b} \tag{3.15}$$

Where d_b is spherical equivalent diameter of the bubble and is estimated from the following correlation [117]:

$$d_b = 0.54\left(u_0 - u_{mf}\right)^{\frac{2}{5}}\left(z + 4\sqrt{A_0}\right)^{\frac{4}{5}} g^{-\frac{1}{5}} \tag{3.16}$$

The velocity of bubble is calculated using the following estimation [118]:

$$u_b = \left(u_0 - u_{mf}\right) + 0.711\sqrt{g d_b} \tag{3.17}$$

The minimum fluidization velocity is determined by [107]:

$$u_{mf} = \frac{\left(\psi d_p\right)^2}{150\mu}\left[g\left(\rho_p - \rho_g\right)\right]\frac{\varepsilon_{mf}^3}{1 - \varepsilon_{mf}} \tag{3.18}$$

where ψ is particle sphericity, d_p is particle diameter and μ is gas laminar viscosity, ρ_g and ρ_s are gas and solid density respectively. ε_{mf} is the void fraction at minimum fluidization point can be calculated by following expression [118]:

$$\varepsilon_{mf} = 0.586\psi^{-0.72}\left(\frac{\mu^2}{\rho_g\left(g\left(\rho_p - \rho_g\right)\right)^2 d_p^3}\right)^{0.029}\left(\frac{\rho_g}{\rho_p}\right)^{0.021} \tag{3.19}$$

The fraction of bubbles in the bed is estimated through the following expression by Kunii and Levenspiel [107] which is subjected to use at $u_b \cong 5\frac{u_{mf}}{\varepsilon_{mf}}$:

$$\delta = \frac{u_0 - u_{mf}}{u_b} \tag{3.20}$$

The chemical reaction rate is determined by following expression [28]:

$$K_{ri} = k_s \frac{X_{bn} s_0 \rho_{CaO}}{M_{CaO}} (1 - X)^2 \tag{3.21}$$

Where $s_0 = 1.7 \times 10^7 \frac{m^2}{m^3}$ is the initial surface area of particles per unit volume of solid CaO and $k_s = 5.95 \times 10^{-10} \frac{m^4}{s\,mol}$ [28]. X_{bn} is CaO active fraction of solid particles inflowing to the carbonator.

The overall chemical reaction rate is determined by following expression [107]:

$$\frac{1}{K_r} = \frac{d_p}{k_g} + \frac{1}{K_{ri}} \tag{3.22}$$

where k_g is the mass transfer coefficient of CO_2 toward the particles in emulsion phase and can be obtained from Sherwood number [119].

$$Sh = \frac{D_{CO_2}}{k_g d_p} = 2\varepsilon_{mf} + 0.95 Re_{mf}^{0.5} Sc^{0.3} \tag{3.23}$$

where D_{CO_2} stands for effective gas diffusivity of CO_2 in air, Sc is the Schmidt number and Re_{mf} is Reynolds number at particulate phase.

The model equations were incorporated in a Fortran program and then solved to determine carbonation behaviour. Figure 3.5 represents the effect of active CaO fraction (*fa*) in CO_2 removal at dense region only. The CO_2 conversion turns slower with decreasing the *fa* in carbonator. It also indicates that sensitivity of CO_2 conversion to CaO active fraction is higher at lower values of *fa* factor while at higher values of *fa* there is no effect on CO_2

conversion with changing on CaO fraction values. This figure also shows a good agreement between the results of the present work and those by Abanades et al., [28].

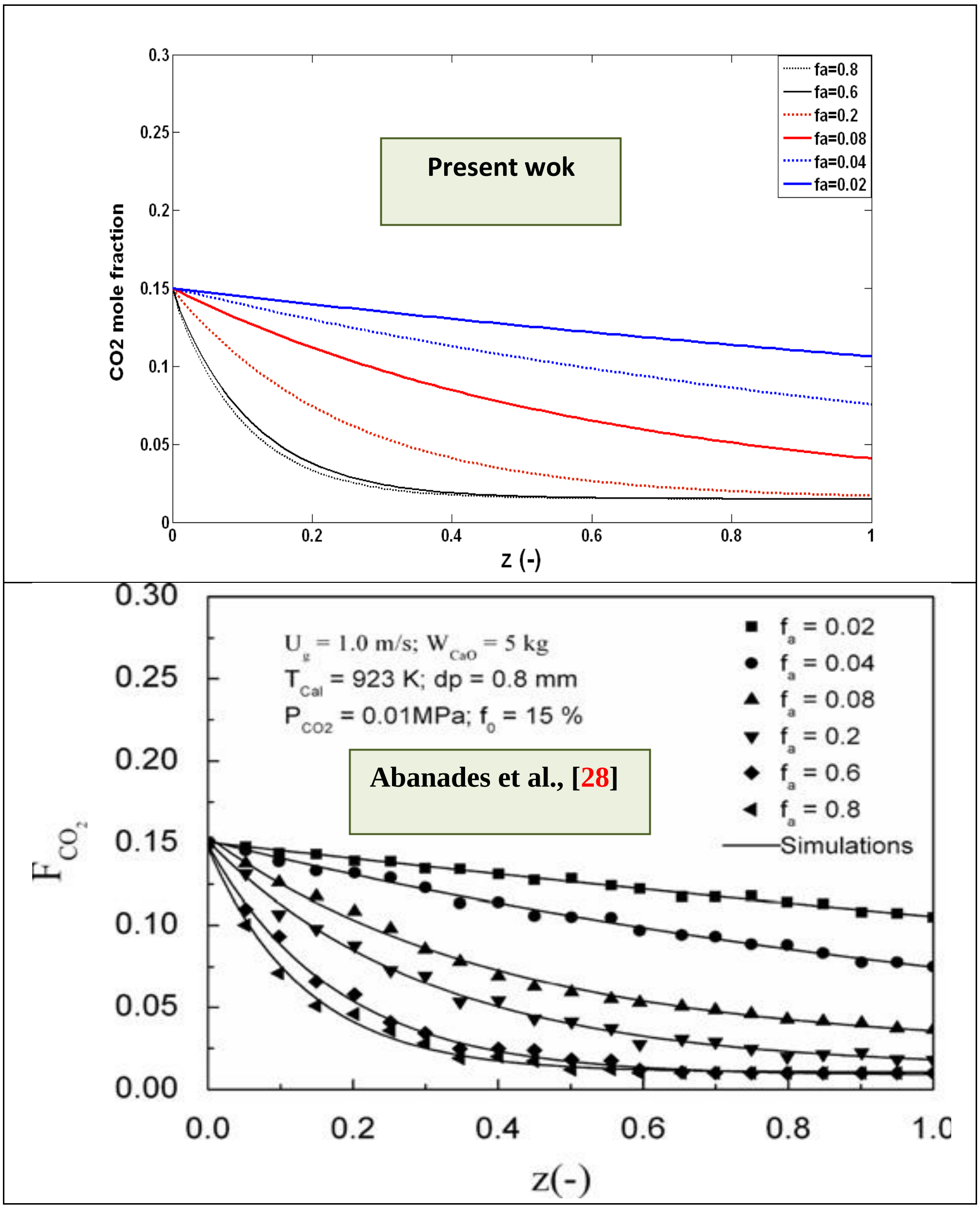

Figure 3-5: CO_2 conversion in dense region at different values of CaO active fraction (top: present work, bottom: Abanades et al., [28])

It can be figure out from the results that a carbonator reactor which operates with the entire fresh CaO (no cycle) is as good as a reactor which has lower circulation rate and higher make up flow to keep *fa* value within the range of fast carbonation reaction stage. In other words with increasing the solid circulation rate and using lower make-up (fresh CaO) flow, the required solid circulation exponentially increases to achieve a certain CO_2 removal efficiency because the lower active solid fraction (*fa)* values turns down the reaction rate to diffusion controlled stage which considerably slower than the fast carbonation stage.

The previous 1-D model for dense region of a reactor needs to be linked to a model for lean region to predict CO_2 concentration along the entire height of the reactor forward to the exit. The KL model [107] for lean region has been adapted to carbonation reactor to investigate CO_2 along the entire bed. Following molar balance of CO_2 in upward gas flow can be written as:

$$-\bar{u}\frac{dC_{CO_2}}{dz} = \left(1-\varepsilon_f\right)\eta K_r C_{CO_2} \tag{3.24}$$

Considering the gas-solid contact efficiency that increases in lean region exponentially and becomes unity at reactor exit, the following expression can represents the lean bed efficiency along the reactor height above the dense region up to the reactor exit [107].

$$\frac{1-\eta}{1-\eta_{be}} = e^{-\acute{a}z} \tag{3.25}$$

where $\acute{a}$ is the equation parameter with constant value of $6.62m^{-1}$, η_{be} is the efficiency of contact at bed surface, which can be expressed by following equation for fast reactions [107]:

$$\eta_{be} = \frac{\gamma_b \delta}{1-\varepsilon_f} \tag{3.26}$$

where ε_f is the void fraction at lean region.

Integrating over the equation and applying the boundary conditions of $C_{CO_2} = C_{CO_{2d}}$ @ $z = z_d$ and $C_{CO_2} = C_{CO_{2ex}}$@ $z = z_l$ can be written as:

$$\ln \frac{C_{CO_{2ex}}}{C_{CO_{2d}}} = \frac{\left(1-\varepsilon_f\right)_{be} K_r}{u_0 a}\left[\left(1-e^{-az_l}\right) - \frac{1-\eta_{be}}{1+\frac{\acute{a}}{a}}\left(1-e^{(a+\acute{a})z_l}\right)\right] \tag{3.27}$$

Where a is the equation parameter and is a function of particle diameter (d_p) and gas inlet velocity (u_0). The value of a can be obtained from the graph which has been generated from various experimental works [107, 120], z_l is the length of the lean region.

3.4 Validation of the Model

Both of the models for dense region and lean region are solved in a sequence where the output of the dense region used as the lean region input. Table 3.2 shows the parameters which are applied to solve the model.

Table 3.2: parameter of prediction of CO_2 capture by a lab scale carbonation reactor [121]

d_{dense} (m)	d_{lean} (m)	d_p (mm)	Z_{dense} (m)	Z_{lean} (m)	Inlet gas flow (m^3/h)	CO2 volume fraction	Particle density (kg/m^3)
0.1	0.04	0.35	1.0	4.0	14.13	0.15	1,580

Figure 3.6 shows the results of the adapted KL model and comparison by F. Fang et al., [121]. It indicates a good agreement between these two models at dense and lean region which both are adapted based on the KL model. The main difference of these two models is related to the acceleration zone and also lean region are different expressions have been used. But the results indicate no significant difference in leans region, the only difference is about the acceleration zone which has not been considered in this work and the results

also confirm that even without taking into account of the acceleration zone reasonable results can be obtained.

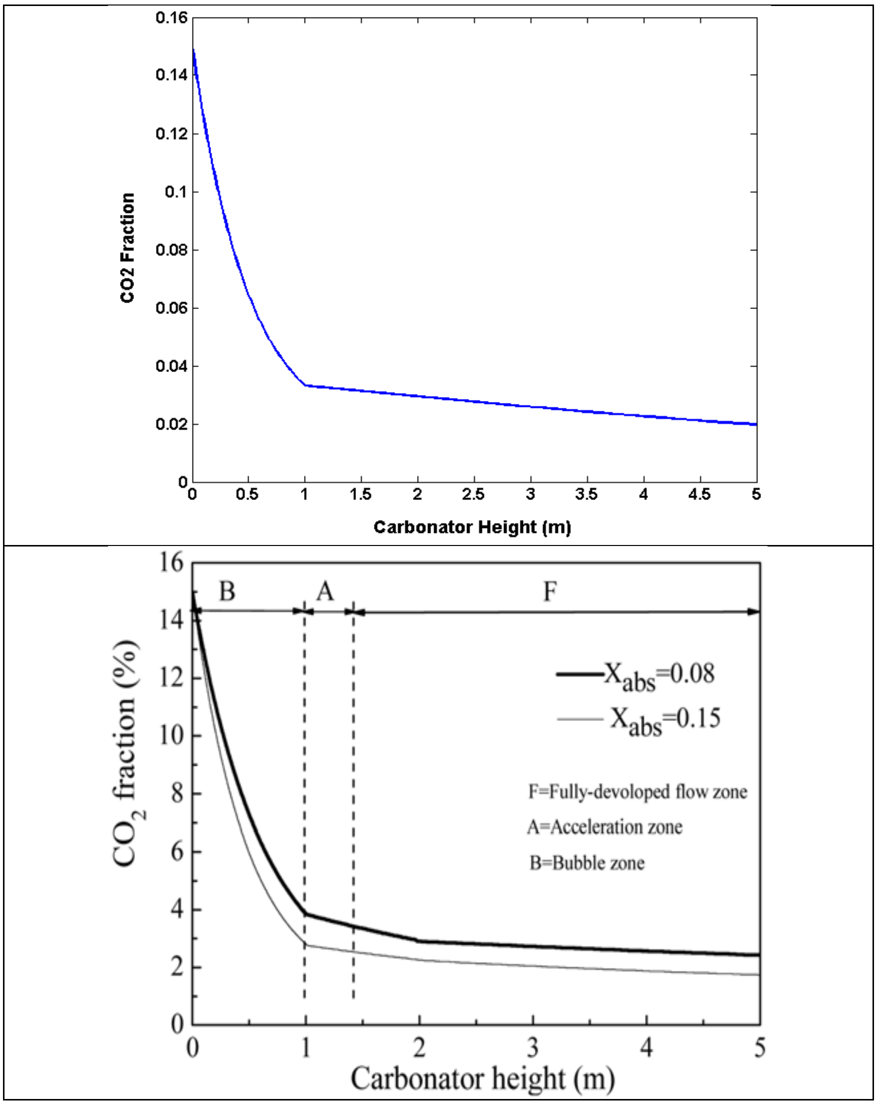

Figure 3-6: Predictive CO_2 mole fraction along the bed height in a continuous system of carbonation reactor, (left: this work with X_{abs}=0.15, right: by F. Fang et al., [121]) .

Figure 3.7 shows CO_2 mole fraction on dense and lean region. It indicates that by increasing the height of dense region the CO_2 concentration decays faster, because the overall reaction rate at dense is higher due to the existence of higher volume of solid particles exposed to the gas phase.

An important issue to use a 1-D model in fluidized bed reactors is about the hydrodynamic parameters which are not identified to use in 1-D model. A1-D model is useful when there are some key parameters as input data to set into the model such as height of the dense region. In order to explore more in carbonation reactor and increase the functionality of the 1-D model, CFD simulation of a fast fluidized bed reactor has been carried out in following chapters. CFD simulation can predict the key parameters such as the bed void fraction and dense region height which are essential to be identified to use in 1-D model for further investigations.

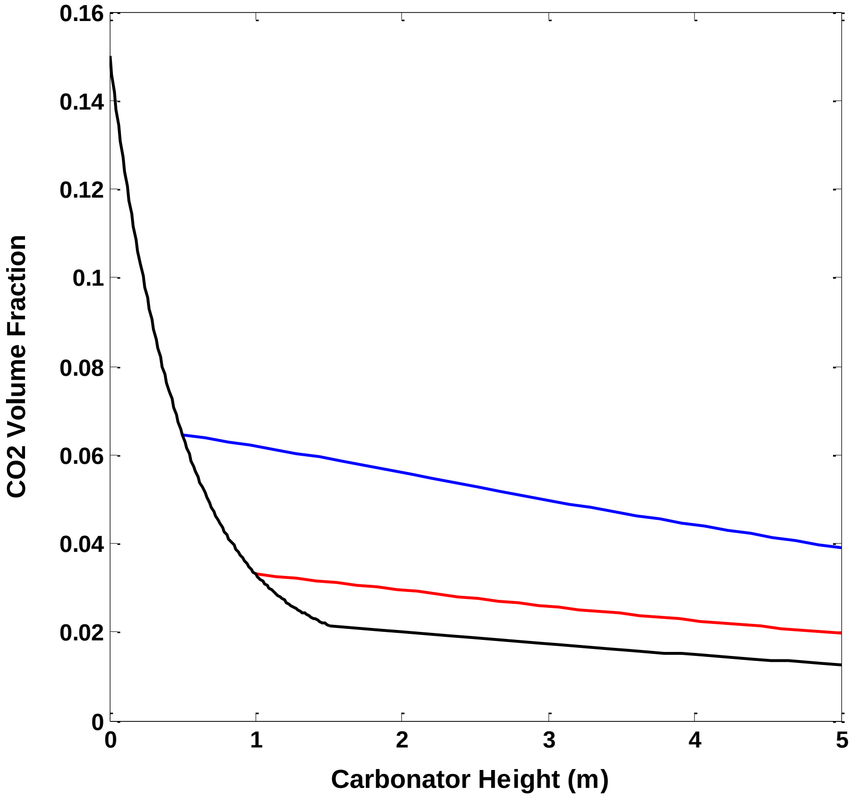

Figure 3-7: Effect of dense region height (z_d) on ultimate CO_2 removal yield (black, red and blue lines proportionally corresponds to z_d=1.5, 1.0 and 0.5).

3-5 Conclusion

In this chapter the kinetic of carbonation reaction of CaO with CO_2 has been presented. The effect of cycles on particle’s capability in CO_2 adsorption is investigated based on the models from the literature. A 1-D model of a fluidized bed reactor has been utilized to the carbonator which can predict CO_2 removal efficiency in a carbonator. It can also predict the required reactor height to achieve a particular degree of CO_2 capture.

This model requires some hydrodynamic parameters such as bed volume fraction which needs use CFD simulation or experimental work. In chapter 6 CFD simulation results provided the reuired input data to the 1-D which can predict the CO_2 concentration along the reactor height. The drawback of this model is the input data which are not known without experimental work or simulation, but it can give good estimation of concentration profiles if there is a set of available input data for a certain operating condition. Once a set of data are set to this model, the effect of parameters such as CO_2 concentration and gas velocity can be predicted by 1-D model without repeating the experimental work or computationally expensive simulation.

chapter 4

Modelling Description of a Gas-Solid Fluidized Bed Reactor for Carbon Capture

4.1 Introduction

In this work we focus on CO_2 capture in a fluidized bed reactor (carbonation reactor) with solid sorbents without the regeneration reactor. Calcination or regeneration can be considered in future research, using the same techniques developed in this research for the carbonation reactor. In this research we proposed to investigate the maximum feasible CO_2 capture in a single fast fluidized bed reactor as well as effective parameter are investigated. Modelling of a fluidized bed reactor with gas-solid contact has been modelled and solved numerically with CFD technique. An Eulerian-Lagrangian approach is utilized to model the hydrodynamics of a fast fluidized bed reactor. The dispersed phase is modelled by direct modelling in a particle-tracking framework using the motion equations of particles based on the Newtonian second-law considering the mass, momentum and heat exchange with continuous phase.

4.2 Gas-Solid Multiphase Flow Model Description

In this work, Particle Source in Cell (PSICell) method is used to model the solid particles hydrodynamic inside the reactor [122]. In this method steady state time averaged conservation equations is used for continuous phase and particle trajectories are tracked individually using Newton's second law of motion. Interaction between particles and continuous phase is taken into account with source terms of mass, momentum and energy in conservation equations. The source terms are calculated at every cell that particles go through and are updated in continuous phase calculations.

4.3 Hydrodynamic model and governing equations

The calculation of the gas-phase hydrodynamics is presented at this section [123]. It is based on the numerical solution of the following set of partial differential equations that can be seen as a generalized form of the Navier-Stokes equations for a gas interacting with a solid phase as originally derived by Anderson and Jackson [124]. Gas-solid multiphase flow in a Eulerian-Lagrangian framework employs general Navier-Stokes equations for gas phase and considering the mass, momentum and heat transfer in source term of those equations. The steady state time-averaged conservation equations solved using finite volume discretization:

$$\frac{\partial \rho}{\partial t} + div(\rho \vec{u}) = \bar{S}_m \tag{4.1}$$

Where ρ is density of gas phase and $\vec{u}$ represents the velocity of gas phase and $\bar{S}_m$ stands for mass exchange between solid particles and gas phase in a given control volume.

The momentum conservation equations can be expressed by following equation [125]:

$$\frac{\partial}{\partial t}(\rho \vec{u}_i) + div(\rho \bar{u} \vec{u}_i) = -\frac{\partial P}{\partial x_i} + div\left(\mu_{eff} \, \mathrm{grad} \, \vec{u}_i\right) + \bar{S}_{u_i} \tag{4.2}$$

Where u_i and P represent the instantaneous velocity at x_i direction and pressure of gas phase, respectively. μ_{eff} is an effective laminar viscosity of the gas phase and $\bar{S}_{u_i}$ stands for momentum exchange of gas-solid interaction.

Enthalpy has been employed in scalar model to describe heat transfer by following expression:

$$\frac{\partial}{\partial t}(\rho h) + div(\rho \bar{u} h) = div \left[k \, \mathrm{grad} \, \frac{h}{c_p} \right] + \bar{S}_h$$

(4.3)

Where h represents the instantaneous enthalpy. k is heat conductivity, c_p is heat capacity and $\bar{S}_h$ stands for energy source term. It is assumed that these values consist of a time averaged component and a fluctuating term:

$$u_i = \bar{u}_i + \acute{u}_i \quad p = \bar{p} + \acute{p} \quad h = \bar{h} + \eta \tag{4.4}$$

Substitution of the equalities of (4.4) into the conservation equations, (4.2) and (4.3), and dropping the over-lines signifying the *time-averaged values*, produces for the continuity equation:

$$\frac{\partial \rho}{\partial t} + div(\rho\bar{u}) = \bar{S}_m$$

(4.5)

The momentum conservation equations become:

$$\frac{\partial}{\partial t}(\rho\vec{u}_i) + div(\rho\bar{u}\bar{u}_i) = -\frac{\partial p}{\partial x_i} + div\left(\mu_{eff}\ \mathrm{grad}\ \bar{u}_i\right) - \frac{\partial}{\partial x_j}\left(\rho\overline{\acute{u}_i\acute{u}_j}\right) + \bar{S}_{u_i} \tag{4.6}$$

and the scalar equation of enthalpy transforms into:

$$\frac{\partial}{\partial t}(\rho h) + div(\rho\bar{u}h) = div\left[\ k\ \mathrm{grad}\ \frac{h}{c_p}\right] - \frac{\partial}{\partial x_j}\left(\rho\overline{\acute{u}_i\eta}\right) + \bar{S}_h \tag{4.7}$$

The above equations are the governing equations for the mean flow quantities. No approximations have been made in their derivation. The non-linearity of the equations (4.2) and (4.3) has produced terms in equations (4.6) and (4.7) which are the correlations between fluctuating velocities, $\rho\overline{\acute{u}_i\acute{u}_j}$, and between velocity and enthalpy $\rho\overline{\acute{u}_i\eta}$. The correlations represent the transport of momentum and heat due to turbulent motion. The term $\rho\overline{\acute{u}_i\eta}$is the transport of x_i momentum in the x_j direction and it acts as a stress on the fluid so it is termed the turbulent or Reynolds stress; $\rho\overline{\acute{u}_i\eta}$ is the transport of enthalpy in the $x_i$direction and is termed the turbulent heat flux. For a fully turbulent flow the turbulent stresses and fluxes are much greater than the laminar diffusion terms. The equations (4.6) and (4.7) can be solved for the mean values of the velocity, pressure and enthalpy once the correlation terms have been determined. Transport equations for these correlations exist but they contain turbulence correlations of higher orders. This means that closure of these equations can not be obtained, as conservation equations for any order of correlation contain terms involving higher order correlations. Thus an alternative approach is required to evaluate the correlations.

Turbulence occurs at high Reynolds numbers and is the cause of an eddying motion, with a large range of eddy sizes, in the fluid. The movement of a fluid is turbulent if it is rotational, diffusive, intermittent, highly disordered and dissipative. The largest eddies, which are associated with the low frequency fluctuations, are determined by the boundary conditions of the flow and their size is of the same order as that of the flow domain. The smaller eddies are determined by the viscous effects. The transport of momentum and heat is mainly affected by the large scale turbulent motion and this is the major contributor to the correlation terms. As a consequence it is the large scale motion which needs to be simulated in the turbulence model in order to determine the correlation terms and hence the velocities and the enthalpy fields.

The larger scale eddies interact with the flow extracting kinetic energy from the average motion and setting up the large scale turbulent motion. Eddies act as vortex elements which stretch each other. In this way the energy is transmitted to smaller scale eddies. The process carries on until the viscous forces dissipate the energy. The rate at which energy, from the mean flow, is transformed into turbulent motion is determined from the large scale motion. The energy transformed is the only energy available to the smaller scale motion and hence the only energy to be dissipated. Thus the rate of dissipation of energy is also determined by the large scale motion despite dissipation being effected by viscous actions and taking part in the small eddies. The larger the Reynolds number, i.e. the smaller the viscous effects, the smaller the dissipative eddies are relative to the large scale motion.

Boussinesq introduced the eddy viscosity concept which assumes that the turbulent stresses are proportional to the mean velocity gradients in a similar manner to viscous stresses in laminar flows [126]. This is expressed as

$$-\overline{\acute{u}_i\acute{u}_j} = v_t\left(\frac{\partial u_i}{\partial x_j}+\frac{\partial u_j}{\partial x_i}\right)-\frac{2}{3}k\delta_{ij} \tag{4.8}$$

Where v_t is defined as the turbulent or eddy viscosity. The turbulent viscosity is not a fluid property but is a value dependent on the turbulence and so may vary from place to place within the fluid. This does not overcome the difficulties of solving a turbulent problem but it does reduce the problem to one of determining the value of v_t. The term in (4.8) which includes the Kronecker delta is necessary because the sum of the normal stresses must be equal to twice the kinetic energy. Without this term the normal stresses are given by

$$\bar{\acute{u}}_1^2 = -2v_t\frac{\partial u_1}{\partial x_1} \qquad \bar{\acute{u}}_2^2 = -2v_t\frac{\partial u_2}{\partial x_2} \qquad \bar{\acute{u}}_3^2 = -2v_t\frac{\partial u_3}{\partial x_3} \tag{4.9}$$

the sum of which is zero by the continuity equation. The formula for the kinetic energy of the fluctuating motion is given by

$$k = \frac{1}{2}\left(\bar{\acute{u}}_1^2+\bar{\acute{u}}_1^2+\bar{\acute{u}}_1^2\right) \tag{4.10}$$

The Kronecker delta term assures that the sum of the normal stresses is equal to the required $2k$. The normal stresses act in a direction perpendicular to faces in the same manner as pressure forces and as k is a scalar the second part of (4.8) constitutes a pressure. In the elimination of the correlation term in the momentum equation the second part is absorbed into the pressure gradient term. Thus the appearance of k in equation (4.8) does not force its calculation in order to solve the momentum equation only the determination of the turbulent viscosity is required.

Alike to the turbulent momentum transport the turbulent heat transport is assumed to be proportional to the gradient of the enthalpy:

$$-\overline{\acute{u}_\iota \eta} = \Gamma \frac{\partial h}{\partial x_i} \tag{4.11}$$

where Γ is the turbulent diffusivity of heat. In the same way as the eddy viscosity is not a fluid property Γ depends not on the fluid but on the state of turbulence. The Reynolds analogy between heat and momentum transport implies that the turbulent diffusivity is related to υ_t by

$$\Gamma = \frac{\upsilon_t}{\sigma_t} \tag{4.12}$$

where σ_t is the turbulent Prandtl number. It has been shown experimentally that the Prandtl number does not vary to any great extent across a flow or between flows. The value of σ_t is a function of buoyancy [127] but in what follows the value of 1.0 will be given to it.

A number of turbulent models exist from the zero equation models, such as those based on the assumption of constant eddy viscosity or those involving deriving equations for the mixing length, all the way through to the higher order models which employ more than two equations. The lower order models offer the advantages of being computationally cheap whilst giving adequate answers for a number of problems. The greater the number of equations used the more the potential that the scheme will produce an adequate solution to a general problem. One of the most widely used methods is the $k - \varepsilon$ model.

4.4 Standard $k - \epsilon$ turbulence Model

At high Reynolds numbers the rate of dissipation of kinetic energy is equal to the viscosity multiplied by the fluctuating vorticity. An exact transport equation for the fluctuating vorticity, and thus the dissipation rate, can be derived from the Navier Stokes equation. The $k - \epsilon$ model consists of the turbulent kinetic energy equation

$$\frac{\partial}{\partial t}(\rho \vec{u}_i) + \mathrm{div}(\rho \vec{u} k) + \mathrm{div}\left(\left[\mu + \frac{\rho v_t}{\sigma_e}\right] \mathrm{grad}\; k\right) + \rho v_t G + G_b - \rho\epsilon \tag{4.13}$$

and the dissipation rate equation

$$\frac{\partial}{\partial t}(\rho \vec{u}_i) + \mathrm{div}(\rho \vec{u} \epsilon) + \mathrm{div}\left(\left[\mu + \frac{\rho v_t}{\sigma_k}\right] \mathrm{grad}\; \epsilon\right) + C_{1e} \rho v_t G \frac{\epsilon}{k} + C_3 \frac{\epsilon}{k} G_b -$$

$$C_{2e} \rho \frac{\epsilon^2}{k} \tag{4.14}$$

Where G represents the turbulent generation rate which is equal to:

$$G = 2\left(\left[\frac{\partial u}{\partial x}\right]^2 + \left[\frac{\partial v}{\partial y}\right]^2 + \left[\frac{\partial w}{\partial z}\right]^2\right) + \left(\frac{\partial u}{\partial y} + \frac{\partial v}{\partial x}\right)^2 + \left(\frac{\partial u}{\partial z} + \frac{\partial w}{\partial x}\right)^2 + \left(\frac{\partial v}{\partial z} + \frac{\partial w}{\partial y}\right)^2 \tag{4.15}$$

and G_b is the generation due to buoyancy and is equal to

$$G_b = -v_t \vec{g}.\nabla\rho/\sigma_T \tag{4.16}$$

With $\vec{g}$ being the gravity vector and σ_T is the turbulent Prandtl number used in the heat equation. If the Boussinesq approximation [128] is being used in the calculation of buoyancy then ρ in the above equation is calculated from

$$\rho = \rho_{ref}\beta\left(T_{ref} - T\right) \tag{4.17}$$

Where β is the thermal expansion coefficient and ρ_{ref} and T_{ref} are the reference density and temperature used in the calculation of the buoyancy source in the flow equations. In the implementation of this model the Kolmogorov - Prandtl expression for the turbulent viscosity is used together with equation (4.11) for the eddy diffusivities.

$$\upsilon_t = C_\mu \frac{k^2}{\epsilon} \tag{4.18}$$

In the above C_μ, σ_k, σ_e, C_{1e} and $C_{2e}$are all taken to be constants and are given respectively the values 0.09, 1.0, 1.3, 1.44 and 1.92 [129].

Handling of the boundary conditions concerned with turbulent flows is the same as for laminar flows except in the case of walls. The $k - \epsilon$ model provides accurate solutions only for fully developed turbulent flows. In near wall region that local Reynolds number of turbulence, $k^2/\upsilon\epsilon$, is so small which the viscous effects become more significant than the turbulent ones. In this viscous sub-layer very sharp gradients occur and to accurate modelling fine mesh would be required in this region. Fortunately it is not necessary to discretise the k and ε conservation equations over this region as there are suitable laws concerning the wall conditions to values of the dependent variables just outside the viscous sub-layer [130]. In the region just outside the sub-layer, such that

$$30 < \frac{yU_\tau}{\upsilon_{lam}} < 100 \tag{4.19}$$

Where y is the perpendicular distance to the wall and U_τ is the resultant friction velocity, the generation of turbulent kinetic energy is balanced by its dissipation. In this region

$$\frac{\tau}{\rho k} = \frac{U_\tau^2}{k} = \sqrt{C_\mu} \tag{4.20}$$

where τ is the wall shear stress. The wall skin friction factor, s, which is defined by

$$s = \frac{2\tau}{\rho u^2} \tag{4.21}$$

where u is the fluid velocity, is determined from the formula:

$$\sqrt{s} = \frac{k}{\ln(E\ Re\sqrt{s})} \tag{4.22}$$

where k, the Kaman constant, is equal to 0.435, E, the wall roughness parameter, usually being set to 9.0, which represents smooth walls, and Re, the local Reynolds number, which is defined by the formula

$$Re = \frac{Vy}{v} \tag{4.23}$$

For a node positioned just outside the viscous sub-layer the effective viscosity is set to the maximum of the laminar dynamic viscosity ρv and sVy. From equation (4.20) the kinetic energy of turbulence at this point is given by

$$k = \frac{\tau}{\rho\sqrt{C_\mu}} = \frac{sV^2}{\sqrt{C_\mu}} \tag{4.24}$$

As previously stated in this region the production of turbulent kinetic energy is equal to its dissipation.

$$\epsilon = U_\tau^2 \frac{\partial V}{\partial y} \tag{4.25}$$

and when s is replaced by its formula (4.21) in equation (4.22) and the equation is differentiated with respect to y then as Ev/U_τ is less than y and using (4.24)

$$\epsilon = \frac{0.1843}{k} \frac{k^{1.5}}{y} \tag{4.26}$$

The source terms in the conservation equations (4.13) and (4.14) include the quantity G which is the rate of generation of turbulent kinetic energy the formula for which is given in equation (4.15). The calculation of G requires the values of the derivatives of the three Cartesian velocity components with respect to the three Cartesian directions. The simplest method for the estimation of any of these is to use the following formulae

$$\int_V \frac{\partial u_i}{\partial x_j} \approx V \frac{\partial u_i}{\partial x_j} \tag{4.27}$$

But using the divergence theorem

$$\int_V \frac{\partial u_i}{\partial x_j} = \sum_F \int_F u_i n_j dS \tag{4.28}$$

By making the usual approximations to the right hand side of (4.28) and equating to (4.27) the following estimate for the derivative's value at P, pointing to centre of control volume, is obtained.

$$\frac{\partial u_i}{\partial x_j} \approx \frac{1}{V} \sum_F A_F n_j (u_i) F \tag{4.29}$$

This formula only requires the estimation of a representative value of u_i on each face of the control volume and so can use the methods discussed previously, for example those included in the section on the cross product diffusion terms. At a wall there is no generation of turbulence so for near wall elements care is required in the calculation of the differentials.

4.5 Gas-solid inter-phase modelling

Fluid drag force acting on each particle has been considered in momentum exchange between gas phase and solid particles. Mass and energy source terms are also employed to take into account of the consequence of reaction taking place between gas and solid particles. At every single time step of particle tracking, the reaction progress has been updated and also source terms associated with reaction are calculated to that cell which particle is belonging to. This development will continue until particle leaves the domain.

4.5.1 Momentum exchange between gas phase and solid particles

Using this approach, trajectories of dispersed phase particles are simulated by solving an equation of motion for each trajectory of particle [Appendix A.1]. Motion of the continuous phase is modelled using a conventional Eulerian framework. The equation of motion of a single rigid sphere in a stagnant fluid was first studied by Stokes [134]. He derived the well-known drag formula based on this study. To examine issues other than the drag force, a good starting point may be the so-called BBO (Basset-Boussinesq-Oseen) equation [135]. Tchen [136] attempted to generalize the BBO equation to the case when the fluid is no longer at rest. Maxey and Riley [137] developed equations of motion for a small rigid particle in a non-uniform flow. The general force balance over a single particle considering the drag fore and gravity can be given as a following equation:

$$m_p \frac{du_{p,i}}{dt} = F_D + F_P + F_G \tag{4.30}$$

where F_D, F_P and F_G are drag force, pressure gradient force and gravity force respectively. The sum of forces due to continuous phase pressure gradient and gravity can be written:

$$F_P + F_G = V_P \nabla P - \rho_P V_P g \tag{4.31}$$

Where p is pressure in the continuous phase and V_P is volume of the particle. The drag force, F_D, can be written:

$$F_D = \frac{\pi}{8} C_D \rho d_P^2 |u - u_P| (u - u_P) \tag{4.32}$$

Where C_D is the drag force and for a single rigid sphere, the drag coefficient is usually approximated by the correlation proposed by Schiller and Naumann [138]:

$$C_D = \begin{cases} Re_p < 1{,}000 & \rightarrow \quad \frac{24}{Re}(1 + 0.15 Re^{0.687}) \\ Re_p \geq 1{,}000 & \rightarrow \quad 0.44 \end{cases} \tag{4.33}$$

The motion of any individual particle is calculated from the Newtonian law:

$$\frac{dx_i}{dt} = u_{p,i} \tag{4.34}$$

$$m_p \frac{du_{P,i}}{dt} = \frac{18\mu}{\rho_P d_P^2} \frac{C_D Re_P}{24} m_P \left(u_i - u_{P,i}\right) + m_p g_i \tag{4.35}$$

Where m_p refers to the mass of the particle and $u_{p,i}$ indicates the velocity of the particle in i direction, $u_{f,i}$ is the gas velocity and C_D is the drag coefficient. The force due to the pressure gradient is neglected, because the magnitude order of that is quite small (dilute fluidized bed reactor operating at atmospheric pressure) comparing the gravity and drag force.

The particle velocities are calculated through the data obtained from the Eulerian gas phase model at particle current location. Solving the particle momentum equation Eq. (4.35) will give the following expressions to update particle velocities and calculate the momentum source terms [131]:

$$u_p = u - \left(u - u_{p_{old}}\right) \frac{1}{\exp(\frac{\Delta t_{old}}{\tau})} + g_j \tau \left(1 - \frac{1}{\exp(\frac{\Delta t_{old}}{\tau})}\right) \tag{4.36-a}$$

$$S_{u,i} = \dot{m} \left[\left(u_{p_{old}} - u_p\right) + g_{\mathrm{j}} \Delta t\right] \tag{4.36-b}$$

Where g_j is the gravity acceleration at direction of j, u_p is particle velocity when leaving the cell, $u_{p_{old}}$ is particle velocity when entered into the cell, $\dot{m}$ is trajectory mass flow rate, Δt is particle residence time in that cell and $S_{u,i}$ is the source term due to the *i*th trajectory. Since the mass flow rate varies (increases) due to the carbonation reaction, it is updated when particle leaves the cell, therefore $\dot{m}$ in equation (4.36-b) is an updated mass flow rate corresponding to the previous cell. The parameter of τ is the particle relaxation time as a rate of the particle acceleration to the relative velocity of the particle and fluid as follow [131]:

$$\tau = \frac{4\rho_p d_p^2}{3\rho\mu C_d Re} \tag{4.37}$$

Where d_P indicates the particle diameter and ρ, μ are the density of particle and fluid respectively. C_d is the drag coefficient and *Re* indicates Reynolds number.

$$C_d = \frac{24}{Re}\left(1 + 0.15Re^{0.687}\right) + \frac{0.42}{1+\frac{42.5\times10^3}{Re^{1.16}}} \tag{4.38}$$

$$Re = \frac{V_{slip} d_P \rho_f}{\mu_f} \tag{4.39}$$

$$V_{slip} = \sqrt{\left(u_p - u\right)^2 + \left(v_p - v\right)^2} \tag{4.40}$$

The stochastic turbulence model [Appendix A.2] is generating fluctuating velocities using Gaussian random numbers and gas turbulent kinetic energy [132].

$$\tilde{u} = \xi * \sqrt{2k/3} \tag{4.41}$$

Where the ξ is the random Gaussian number with mean zero and standard deviation of unity. *k* is gas turbulent kinetic energy calculated from gas flow field at current position of the particle. In this method of turbulence treatment, it is believed that the particle interact with eddy for an interaction time, τ_{int}. The interaction time can by the flowing equation:

$$\tau_{int} = Min(\tau_e, \tau_c) \tag{4.42}$$

Where τ_e stands for eddy life time and τ_c represents crossing time which is the time required for the particle to cross the eddy. The eddy life time can be calculated by following expression [133]:

$$\tau_e = \frac{l_e}{\sqrt{\frac{2}{3}k}} \tag{4.43}$$

where $C_\mu C_d = 0.09$ and the mean values of the normal distribution function is set to zero $\overline{\hat{u}_{p,\iota}} = 0.$ The crossing time can be obtained through the eddy length scale and particle relative velocity as following [130]:

$$\tau_c = \frac{l_e}{|\vec{u} - \vec{u}_p|} \tag{4.44}$$

The lengths scale, as the characteristic dimension of the eddy referring to the dissipation length scale can be obtained by following equation [130]:

$$l_e = \frac{C_\mu^{3/4} k^{3/2}}{\varepsilon} \tag{4.45}$$

If the crossing time is less than the eddy life time the particle would jump to another eddy and the fluctuation values would be updated otherwise the current values would be used to calculate the calculate the particle actual velocity as following:

$$u = \bar{u} + \tilde{u} \tag{4.46}$$

$$v = \bar{v} + \tilde{v} \tag{4.47}$$

In calculation of particle tracking, time step determined by the number of time steps which particle should take in moving across an element and the velocity of the particle. The value of this time step is calculated by the following equation:

$$\Delta t \ = \ \mathrm{MAX}\ (\ \mathrm{MIN\_TIME}, \mathrm{MIN}\ (\frac{2d}{p_e u_p}, \mathrm{MAX\_TIME}\ )\ ) \tag{4.48}$$

$$u_p = \left(\sum_i {u_{p,i}}^2\right)^{1/2} \tag{4.49}$$

Where d is the smallest face to element centroid distance for the element containing the particle, p_e is the number of steps per element (which is set to 15) and u_p is the particle velocity. The position of the particle is updated [Appendix A.3] through the following equation:

$$x_p = x_{p\ old} + \Delta t \frac{u_{p_{old}} + u_p}{2} \tag{4.50}$$

$$y_p = y_{p_{old}} + \Delta t \frac{v_{p_{old}} + v_p}{2} \tag{4.51}$$

$u_{p_{old}}$, $v_{p_{old}}$ and u_P, v_p indicate the previous and current particle velocity in x and y directions. $x_{p_{old}}$ and $y_{p_{old}}$ are the previous particle position and Δt is the time step for particle tracking. Trajectory history of particle are stored and source terms due to the mass transfer, momentum and heat transfer are calculated and stored at each belonging cell to update new flow field in continuous phase for next iterations. This loop will continue until get final convergence based on residual values.

4.5.2 Mass source term

The mass source terms [Appendix A.4] is associated with the reaction taking place between the gas phase and solid particles, based on the following reaction:

$CaO + CO_2 \rightarrow CaCO_3$

In this case, CO_2 from gas phase is reacting with solid CaO particles and $CaCO_3$ solid product remains on particle. The mass source due to the reaction can be described in every cell as follow:

$$S_m = \sum_i^{NP} S_{m,i} \tag{4.52}$$

Where, S_m is a mass source term associated with the reaction in a cell, $S_{m,i}$ is a reaction source terms belonging to a particle *i* that passed over the cell with a possibility of reacting with CO_2 content of that cell and NP is the number of particles passed over the cell. The source term related to a single particle during staying in a cell can be described as follow:

$$S_{m,i} = \frac{1}{\Delta t_i} \Delta X_i m_{p,0} \frac{M_{CO2}}{M_{CaO}} \tag{4.53}$$

Where, Δt_i is the residence time of a particle i in a cell, ΔX_i is the conversion of the particle subjected reacting with CO_2 in that cell, $m_{p,0}$ is the initial mass of the particle, M_{CO2} and M_{CaO} are molecule of weight of CO_2 and CaO, respectively.

The following equations are used to describe the reaction of CO_2 with CaO inside the fluidized bed reactor [*30*]. Equation 4.54a indicates integrated form of the 4.54 for chemical reaction controlled stage. For diffusion controlled stage the equation of 4.54b is used. In this equation, it has been assumed that when the particle conversion approaches to 55% then the mechanism turns into diffusion controlled mechanism, therefore the value of X_{k-D} in Eq. 4.54b is set to 0.55.

$$\frac{dX}{dt} = \frac{k_s S_0 C(1-X)\sqrt{1-\Psi\, ln(1-X)}}{1-\varepsilon\left[1+\frac{\beta Z}{\Psi}\sqrt{1-\Psi\, ln(1-X)}-1\right]} \tag{4.54}$$

$$X = 1 - exp\left(\frac{1-\left(\frac{\tau}{2}\Psi+1\right)^2}{\Psi}\right) \tag{4.54a}$$

$$X = X_{k-D} + \left(1 - exp\,\frac{1}{\Psi} - \frac{\left[\sqrt{1+\beta Z\tau} - \left(1 - \frac{\beta Z}{\Psi}\right)\right]^2 \Psi}{\beta^2 Z^2} \right) \tag{4.54b}$$

$$\tau = \frac{k_s(C_b - C_e)S_0 t}{(1-\varepsilon)} \tag{4.54c}$$

Where X is particle conversion, s_0 is initial surface area of particle, C is CO_2 oncentration, ε is particle porosity, Ψ is particle sphericity and k_s is rate constant for surface reaction is defined as:

$$k_s = k_{s_0} exp\left(\frac{-E_a}{RT}\right) \tag{4.55}$$

Where k_{s_0} is pre-exponential factor and E_a is activation energy. The parameter of β in Eq. 4.54 is expressed as:

$$\beta = \frac{2k_s a\rho(1-\varepsilon)}{M_{CaO} b D_P S_0} \tag{4.56}$$

Where D_p is apparent product layer diffusion and is expressed as:

$$D_p = \frac{bM_{CaO}DC}{a\rho} \tag{4.57}$$

Where a and b are stoichiometric coefficients for carbonation reaction and D is effective product layer diffusivity and is defined as:

$$D = D_0 \exp\left(\frac{-E_{aD}}{RT}\right) \tag{4.58}$$

The parameter of Ψ in Eq. 4.54 is a structural parameter and can be expressed is the following equation:

$$\Psi = \frac{4\pi L_0(1-\varepsilon)}{S_0^2} \tag{4.59}$$

where L_0 refers to the initial total pore of the particle per unit volume.

4.5.3 Energy source term

Heat exchange between gas phase and solid particles is regarded to the reaction of CaO with CO_2 as an exothermic reaction. The source term due to the reaction can be described as follow:

$$S_h = \sum_i^{N_p} S_{h,i} \tag{4.60}$$

Where, S_h is the energy source term in an element, N_p is the number of trajectories goes through the element, $S_{h,i}$ is energy source term in a cell associated with particle i and it can be expressed as follow:

$$S_{h,i} = \int_0^{\Delta t_i} \frac{m_{p,0}}{M_{CaO}} \Delta H_r X_i(t) dt \tag{4.61}$$

Where, ΔH_r is the required heat to react CaO with CO_2. X_i refers to conversion rate of the particles of ith trajectory and Δt_i is residence time of ith trajectory particles inside the element. The heat released from the carbonation reaction is added to the gas phase is a source term. This energy source can be considered as a maintenance heat which results less energy consumption during the carbonation process.

4.6 Particle tracking algorithm

Particle tracking employs hydrodynamic of the domain to predict the actual position of particle at every time step. Perhaps predicting the particle location is the most difficult section. At all stages of tracking the coordinates of the particle position are known, but to the relationship of that point to the mesh. This knowledge is necessary as the properties of the continuum at the particle location are required to determine where the particle will move to next. As a simple scheme, which is computationally expensive test, it can be determined the closest element centroid to the particle but that is not sufficient to accurately identify the element containing the particle [139].

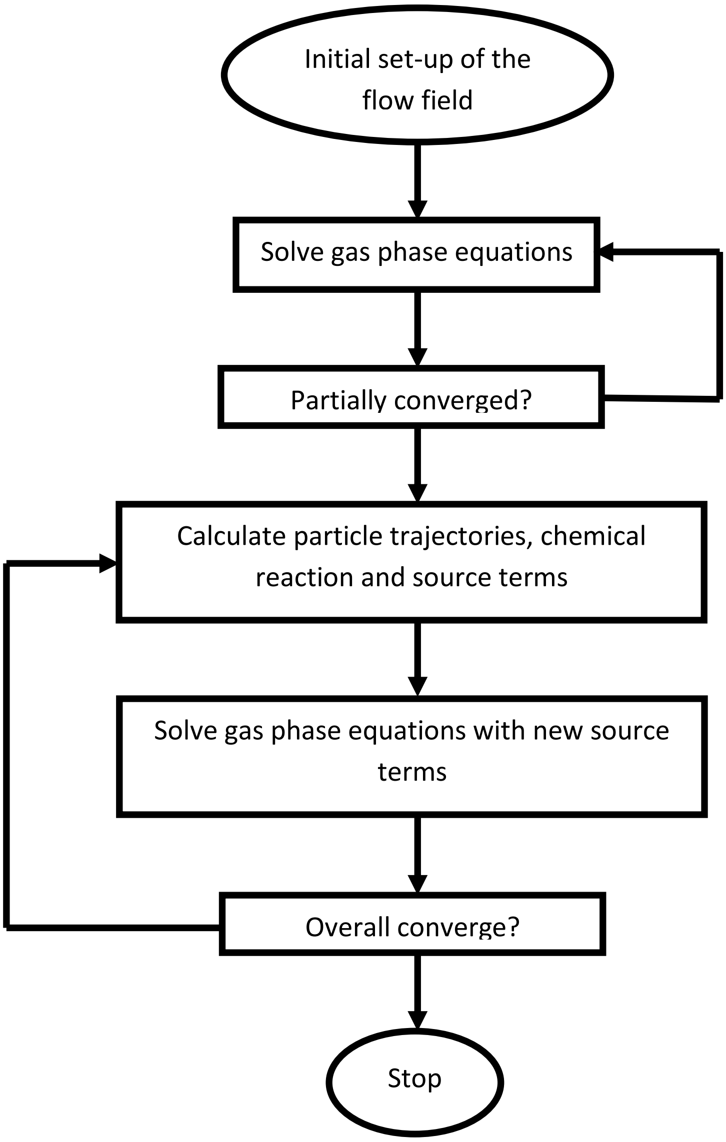

Figure 4-1: Schematic diagram of particle tracking algorithm

In this thesis, subsequent to solving the fluid flow equations for continuous phase with approximately the solution convergence, particle tracking is started. The particles are randomly situated closely to the lower end of the reactor and the new positions of the particles is tracked in a transient way using a specified time step which is between the minimum (1e-5) and maximum (1e-2) defined range for time step. The exact value of time step within an element is calculated by the particle's current velocity and element size

(Eq.4.48). Every track will start from particle’s initial location and continuous until leaving the domain. When the calculation of all trajectories is ended, which the number trajectories depends on the track flow rate of every trajectory and overall inlet flow rate, the stored source terms of mass, monument and heat are considered at next iteration of continuous phase with an appropriate relaxation factors applied to them. This procedure continues until overall convergence take place on continuous phase (Figure 4.1).

4.7.4 Calculation of the shape functions for an element

Having calculated the shape function values for the sub-tetrahedron the question is how do these transfer to the element (see Appendix B). The look up tables for the sub-tetrahedron will tell its corners in terms of the parent element. These corners may be corners of the parent element, centres of the faces of the parent element or the parent element centroid. For a corner of the parent the shape function from the sub-tetrahedron is just added to that of the parent corner. For a corner that corresponds to a face centroid then the sub-tetrahedron shape function value is equally divided amongst the corners of the face. Similarly if the corner is located at the parent element centroid the shape function value is equally divided to each corner of the parent element [139].

4.8 Assumptions in Modelling

In order to explain a phenomenon by computational fluid dynamics (CFD) with an acceptable computational cost, the simplifying statement of model is inevitable. Every modelling in engineering includes some assumptions to simplify the model and reduce the computational cost. In modelling and computational substances, realizing acceptable results with an uncomplicated model is more precious. In this modelling scheme, the effect of attrition of particles due to the impact with wall or collision with other particles is neglected. In heat transfer modelling, temperature distribution inside the particles is neglected and an uniform temperature for entire body of the particle is utilized.

4.8.1 Attrition between the particles is neglected

Investigating the effect of attrition on particle size distribution shows that in a normal operating condition of a circulating fluidized bed reactor there is no significant change on the particles size due to the attrition. Figure 4.2 shows that after 5h only less than 25 of particle size have been reduced due to the attrition [140], although normally in a real case of a circulating fluidized bed reactor the residence time o the particles inside the reactor is from a few seconds to a few minutes therefore the magnitude of operating time for a certain amount of solid particles would be in order of minutes and not the hours. Considering this statement and figure 4.2 the attrition effect on particle size would be negligible. It would be less than 1% change in particle size in a few minutes and it could be valuable in the case of generating active surface area for reaction.

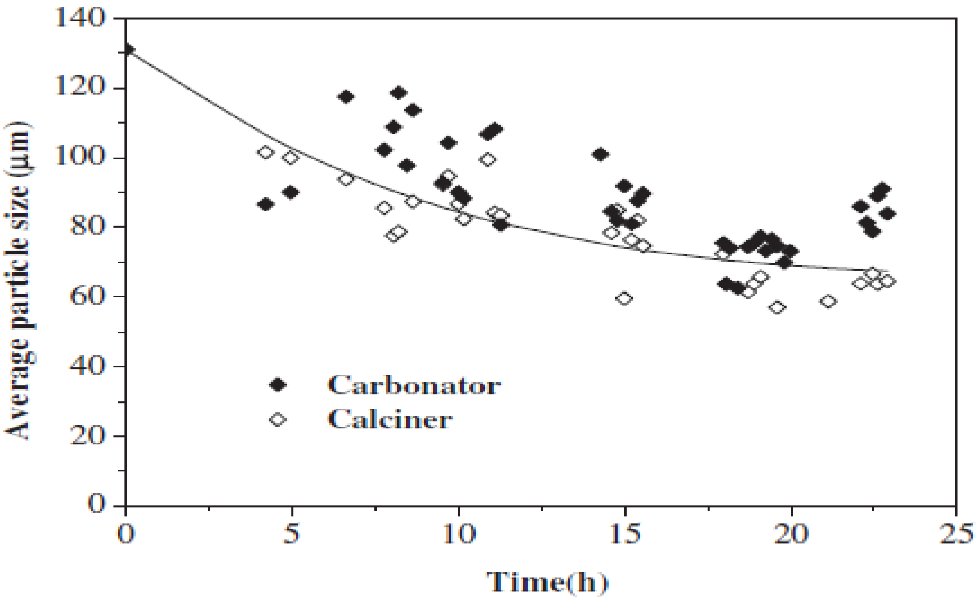

Figure 4-2: Evolution of the average particle size of the solids with accumulated circulation time for the carbonator and the calciner [140].

Hence, the un-reacted core shrinks as the reaction proceeds, but the overall particle size still remains constant. Although the non-reacted shrinking core model does not exactly represent the whole mechanism of gas–solid reactions, but the theory behind this model can be used to take into account of gas-solid reaction behaviour regarding the product formation and particle size.

In carbonation/calcinations, intrinsically, the sizes of particles are not growing by the reaction (Figure 4.3). In this process, since the reaction is taking place on the porosity surface areas and thus particles are getting denser rather than getting bigger. The only change on the particle size is associated to the product layer [30] on the outside side of the particle in maximum 50nm of increasing on particle radius and it’s really negligible in comparison with particles diameter (100µm). Based on the intrinsic of *CaO* particles with high level of porosity the outside surface area of a particle is negligible in comparison with the active surface area belonging to the porosity of particle.

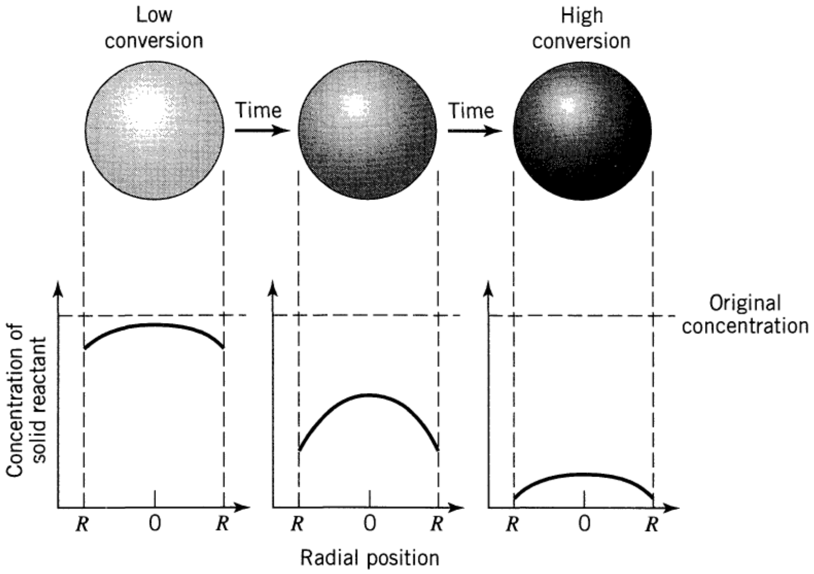

Figure 4-3: According to the progressive-conversion model, reaction proceeds continuously throughout the solid particle [115].

The following calculation shows that there is a big difference between the porosity area and outside surface area (Table 4.1).

As a result, in modelling the porosity and active surface area must be considered to obtain accurate model that can predict the carbonation reaction taking in account the blockage and sintering of the porosity. The sintering of porosity, not only leads to reduce the effective gas diffusivity in outer layers of the particle but also avoids gas to reach the fresh *CaO* even gas flows in some porous zones in internal portions of the particle, far away from the particle's shell.

Table 4-1: Porosity area against the particle surface area.

Parameter	Value	Expression
$\boldsymbol{S_0\left(\frac{m^2}{m^3}\right)}$ **[30]**	4.2×10^{7}	-
$\boldsymbol{d_p\ (m)}$	1×10^{-4}	-
$\boldsymbol{V_p\ (m^3)}$	5.23×10^{-13}	$\frac{\pi}{6}D_p^3$
$\boldsymbol{S_{0,p}\ (m^2)}$	2.19×10^{-5}	S_0V_p
$\boldsymbol{A_p\ (m^2)}$	3.14×10^{-8}	πD_p^2
$\%\boldsymbol{\frac{A_p}{S_{0,p}}=\frac{3.14\times10^{-8}}{2.19\times10^{-5}}\times100=0.143}\%$		

Considering this complicated phenomena, parameters in a comprehensive model can be obtained in using a range of experimental data.

$$S=S_0(1-X)f_s(\varepsilon) \tag{4.69}$$

$$D_e=D_0f_D(\varepsilon) \tag{4.70}$$

$$\varepsilon=\varepsilon_0f_e\left(r,X,P_{CO_2}\right) \tag{4.71}$$

Where *S* refers to the active surface area, *ε* is particle porosity, X is the *CaO* conversion, D_e indicates the effective diffusivity. The functions f_s, f_D and f_e indicate parametric correlations for active surface area, effective diffusivity and porosity respectively.

Partial pressure of CO_2 has significant effect on maximum CaO conversion (Figure 4.4). At low CO_2 partial pressure the ultimate conversion is higher while at higher CO_2 partial pressure the ultimate conversion reduced.

The concept behind this phenomenon is regarded to sintering of porosity in surface of the particle due to the fast reaction rate associated to rapid reaction stage of carbonation which is the function of CO_2 partial pressure.

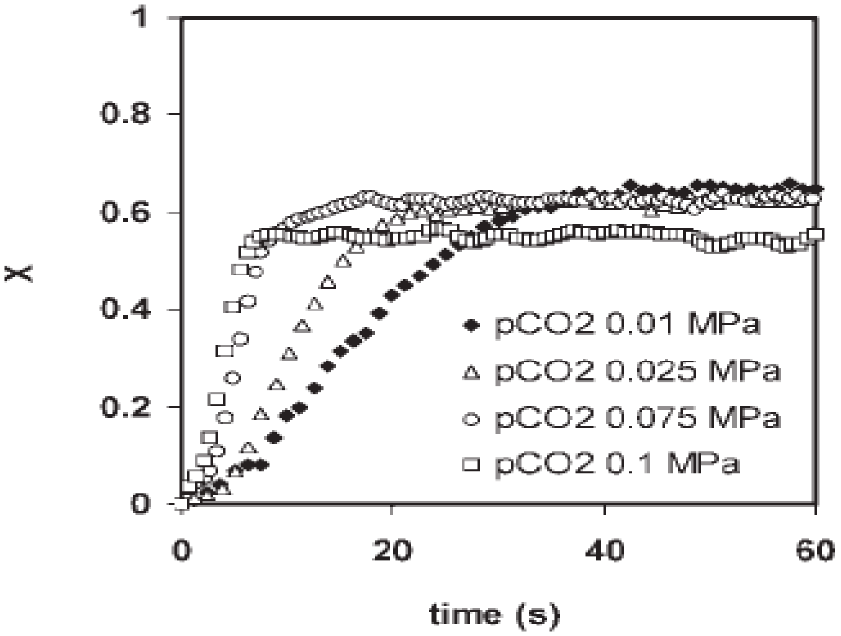

Figure 4-4: Carbonation curves for different CO2 partial pressures at 650^o (C) [30]

Figure 4.5 shows altering the pore volume belonging to porosity of a CaO particle during the carbonation reaction. It shows that in 100sec the majority of pores are blocked, particularly the small pores. The mean particle size regarded to the maximum pore volume is shifted to the larger pores. It means, the fast stage of carbonation reaction ended and the diffusion is controlling the conversion.

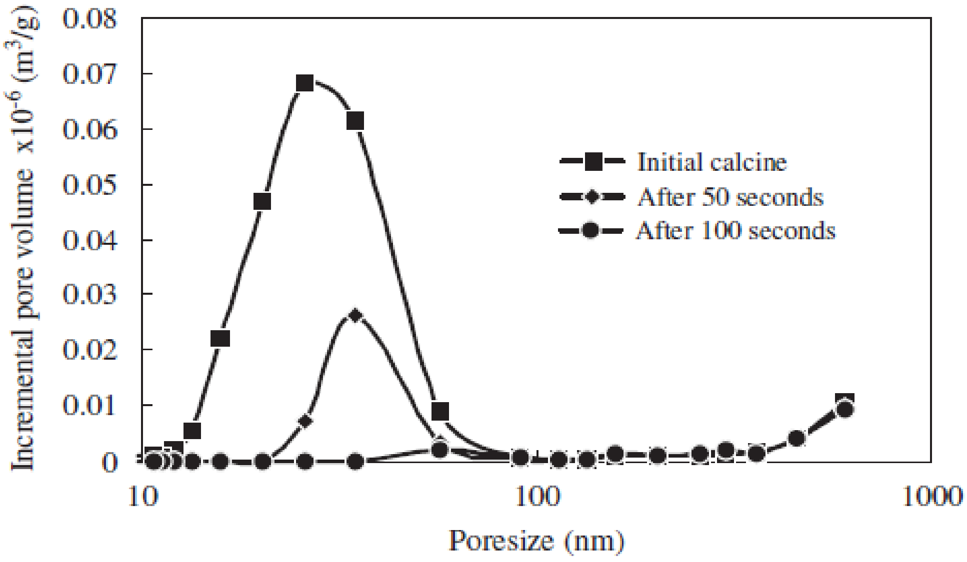

Figure 4-5: Pore size distribution carbonation at 600° (C) and 80 kPa CO_2 partial pressure [141].

The attrition of particles doesn’t confirm a significant change on particle size distribution due to the breakage on collisions. The main parameter in carbon capture is regarded to particle’s porosity; therefore a parametric correlation of porosity during the reaction would be essential in the case of accurate conversion rate prediction while it is very complicated to consider the porosity variation.

4.8.2 Uniform temperature within the particle

Since the Biot number for particles is less than unity therefore a uniform heat transfer can be assumed within the particle. The Biot number can be expressed for every single particle as following:

$$Bi = \frac{h.d_p}{k_s} \tag{4.72}$$

Where h (for air ~ 10.0 $\frac{W}{m^2K}$) is the convection heat transfer coefficient between the particle and the fluid, k_s (for calcium oxide ~ 0.1 $\frac{W}{m.K}$)is the thermal conductivity of the solid and d_p (in this work ~ 10^{-4} m) is the particle diameter. For many gas–solid systems the thermal conductivity of the solid is greater than that of the gas by more than an order of magnitude (e.g. air–coal, air–Ferrous oxide, air–fused silica) and results in a Biot number that is less than 0.1. The small Biot number encountered in many practical gas–solid systems suggests a lumped capacitance model for the particle temperature, where the spatial variation of temperature inside the particle can be neglected.

4.8.3 Particles collision is neglected

In this work, Discrete Particle Modelling used to simulate gas-solid behaviour in a fluidized bed reactor. In the DPM (an Euler-Lagrange model) the gas phase is treated as a continuum and every particle is tracked individually. Although a collision model can be used to account for non-ideal particle-particle or particle-wall interactions however at low solid fraction (<0.01) it can be neglected due to low rate of particles' collision. Elgobashi [142] proposed a regime map to analyse multiphase dispersion flows in aspect of different coupling ways (Figure 4.6). It suggested that for dilute multiphase flows one way coupling can be safely applied in modelling procedure. For dispersed phase with volume fraction between 10^{-6} to 10^{-3} two-way coupling has to be accounted for. In dense phases, four-way coupling is necessary to consider the effect of particles collision as well as particle-fluid interaction. In the present work, due to the low solid volume fraction (<0.001), two-way coupling used in modelling approach.

Theoretically, when particle relaxation time is much more smaller than eddy life time corresponding to that particle ($\tau_{12}^{x} \ll \tau_{12}^{x}$), the particle motion is governed by continuous phase turbulence, but when collision time scale is much more smaller than particle relaxation time scale $\tau_{12}^{x} \gg \tau_{12}^{c}$, particle motion is governed by particle's collision. In dilute multiphase systems particles motion is governed by continuous phase, therefore one-way or two-way coupling for this type of dispersed flows can be safely reasonable in simulation process.

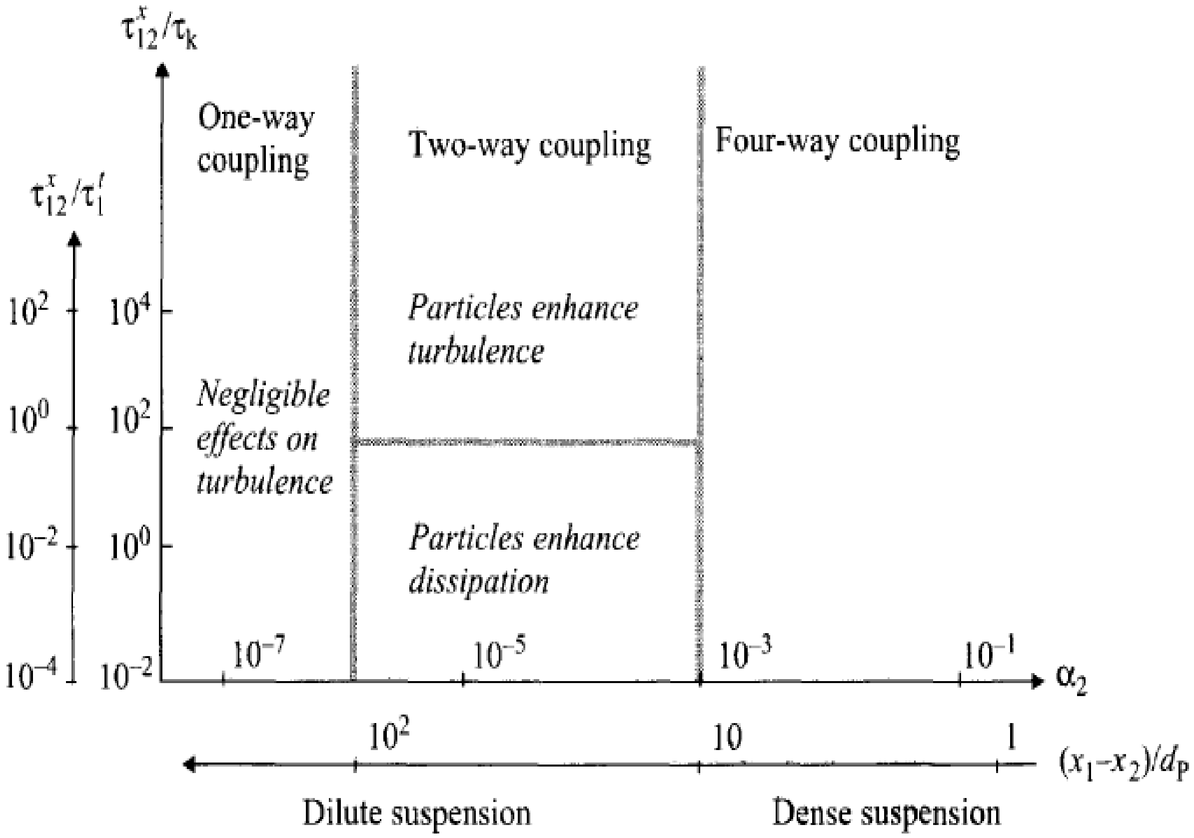

Figure 4-6: Coupling between phases in dispersed multiphase flow [142]

4.9 Numerical solution and discretisation scheme

CFD simulations typically involve the solution of flows with heat transfer, species transport, and chemical reactions. These types of flows are described by the equations of mass, momentum, and energy conservation. The most commonly used approach to discretizing the general transport equations are the finite-difference, finite-volume, and finite-element techniques. These methods discretize the governing equations directly, using a variety of local profile assumptions or approximations, thereby reducing the original partial differential equation into a set of coupled algebraic equations, which must then be solved.

Finite-difference methods approximate the derivatives in the governing differential equation using truncated Taylor series expansions. In the finite element method, the fluid domain under consideration is divided into finite number of sub-domains, known as elements. The equations of equilibrium for the entire structure or body are then obtained by combining the equilibrium equation of each element such that the continuity is ensured at each node.

In the Finite Volume method the domain over which the equation is to be solved is divided into a set of non-overlapping polyhedral control volumes. In each of these control volumes a single node is positioned. This set of nodes form the selected points at which the values of scalar quantities are sought. The Finite Volume method involves integrating the conservation equations over each control volume, as well as over time, and a solution is sought which makes each of these integrals equal to zero. Assumptions are made as to the variation, between nodes, of the quantities involved in the equation. For each control volume this leads to a linear equation involving the unknown values of the scalar quantity at the node in the control volume and the nodes in the neighbouring control volumes.

In this work, finite volume scheme was utilized to discritize the computational domain in numerical solution. Once the continuous phase has been solved with a number of iterations and it has converged partially, then the computed flow field as seen by the particle is utilized to predict the trajectory of every individual particle. With the trajectory of the particle computed, source terms of mass, momentum and energy are utilized to update the flow field. This takes into account the modification of the flow field due to the motion of the particles giving a full fledge two-way coupled process.

A hybrid scheme developed by Spalding [143], which combines central differencing scheme and the upwind scheme, is used in the numerical solution due to its inherent advantages as first suggested by Courant, Isaacson et al., [144].

In the cell centred method the control volumes correspond to the mesh elements and the node is positioned at the centre of the element. Discretisation of all terms in the conservation equation is designed to produce a diagonally dominant matrix. The convection term is the only term that may produce asymmetry in the discretised equation but this asymmetry is compensated for by placing off-diagonal convection contributions into the source vector. Consequently the resulting symmetric, diagonally dominant linear system can be solved by most iterative linear solvers.

Cell centred discretisation scheme was used for the conservation equations. In this method, the nodes associated with the elements of the mesh are positioned at the centre of the element. Unlike the vertex based method that needs transformation of local co-ordinate system into global co-ordinates, Cell centred method doesn’t need the transformation but mesh orthogonality evaluation is required. Since in this simulation there are no highly skewed elements therefore the cell centred method is used with reasonable orthogonal mesh.

The integrated form of one dimensional steady-state conservation equation with diffusion and convection terms can be expressed as:

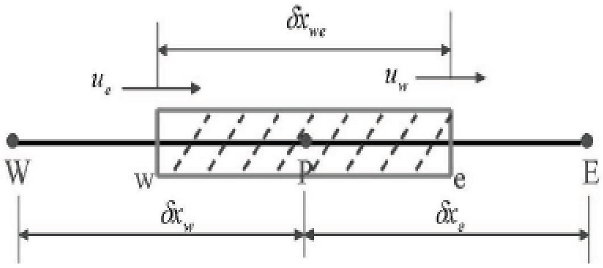

Figure 5-7: Discretisation scheme

$$(\rho u\phi)_e - (\rho u\phi)_w = (\Gamma(\phi_E - \phi_P)/\delta x_e) - (\Gamma(\phi_P - \phi_W)/\delta x_w) \tag{4.73}$$

Where $(\rho u\phi)_w$ is the property entering the west face and $(\rho u\phi)_e$ is the property leaving the east face of the control volume as described in Figure 5.1.

In central differencing scheme the following simple averaging of ϕ-properties is used:

$$\phi_e = \frac{\phi_E + \phi_P}{2} \tag{4.74}$$

$$\phi_w = \frac{\phi_W + \phi_P}{2} \tag{4.75}$$

The above equations can be arranged in terms of the cell centred values as:

$$A_P\phi_P = A_E\phi_E + A_W\phi_W \tag{4.76}$$

The convection and diffusion fluxes are expressed by:

$$F = \rho u \qquad and \quad D = \frac{\Gamma}{\delta x} \tag{4.77}$$

The influence coefficients are described as:

$$a_E = D_e - \frac{F_e}{2} \tag{4.78}$$

$$a_W = D_w + \frac{F_w}{2} \tag{4.79}$$

$$a_P = D_e + \frac{F_e}{2} + D_w - \frac{F_w}{2} = a_E + a_W + (F_e - F_w) \tag{4.80}$$

Disadvantage of the central difference scheme is regarded to the flow direction changes, where some of the coefficients become negative. This issue can result in an unbounded solution.

The upwind scheme uses the value of the nodal upwind value for the property ϕ for the interface value. In this method the coefficient are all positive then it helps to produce a bounded solution. These coefficients are given as:

$$a_E = D_e - \max(F_e, 0) \tag{4.81}$$

$$a_W = D_w - \max(F_w, 0) \tag{4.82}$$

$$a_P = D_w + \max(F_w, 0) + D_w - \max(-F_w, 0) = a_E + a_W + (F_e - F_w) \tag{4.83}$$

The disadvantage of the upwind scheme is that it is susceptible to regarded to the artificial diffusion which causes numerical merging.

In order to avoid these issues associated with central difference and upwind scheme, the hybrid scheme is considered which can resolve these problems to produce more reasonable results. Hybrid scheme uses local Peclet number, which is the ratio of the strength of convection to diffusion, to evaluate flux through each control volume faces. The Peclet number is described as following:

$$Pe = \frac{\rho u}{\Gamma/\delta x} \tag{4.84}$$

When the flow is in the positive direction, the values of ϕ in the domain are influenced more by upstream value, ϕ_W. Similarly for negative flows the value of ϕ is more dependent on ϕ_E which again is the upstream value. As P increases in either the positive or a negative manner the value of ϕ within the domain becomes more strongly influenced by the relevant upstream value of ϕ. If |P| increases then $\frac{d\phi}{dx}$ tends to 0.0 at the centre of the region indicating that diffusion is nearly absent. The upwind scheme always uses a linear relationship between ϕ and x and hence at large |P| values it overestimates the influence of diffusion term [145].

The hybrid scheme turns to the central difference scheme at Peclet number within the range of $-2 < Pe < 2$ while the outside of this range the upwind scheme is used and the diffusion is set to zero. The influence coefficients are expressed as following:

$$a_W = \max\left(-F_e, D_e - \frac{F_e}{2}, 0\right) \qquad when \quad -2 < Pe < 2 \tag{4.85}$$

$$a_E = D_w + \max\left(-F_w, D_w + \frac{F_e}{2}, 0\right) \qquad when \quad 2 \leq Pe \tag{4.86}$$

$$a_P = a_E + a_W + \max(F_e - F_w) \qquad when \quad -2 \geq Pe \tag{4.87}$$

chapter5

Simulation Results in 2-D

5.1 Introduction

A CFD model of a fluidized bed reactor operating at steady-state condition, with time-average values associated with two ways coupling has been implemented using multi-physics PHYSICA code developed in university of Greenwich. PHYSICA code has the general platform of fluid flow, heat transfer and turbulence equations [139] which can be modified for different applications by implementing appropriate subroutines.

5.2 Geometry and mesh generation

MB3 Mesh Builder, developed by *G.Djambazov* [146] was used to generate the mesh for numerical solution. MB3 is a FORTRAN based program which implements a Meta tool for building meshes for PHYSICA. The mesh is built out of blocks (or parts). The blocks are joined at matching faces with the option of first rotating them and moving them into place. The matching cell faces are specified by the user in the corresponding block definitions at obvious interfaces of the geometry (like machine parts coming together, certain narrow links, etc.) and will most often be on a planar or cylindrical surface with regular mesh, so that different blocks can be built with different tools from the list above.

In this section of simulation, a 2-D geometry in Cartesian system is considered which has dimensions of 8.0m in height and 0.1m in width [Figure 5.2]. This is the typical size of a fluidized bed riser as well as experimental works from literatures particularly for carbon capture with CaO [147, 120]. The geometry (consists of 4,800 cells) is divided into 12 elements in radial direction, and 400 elements along the reactor lengths.

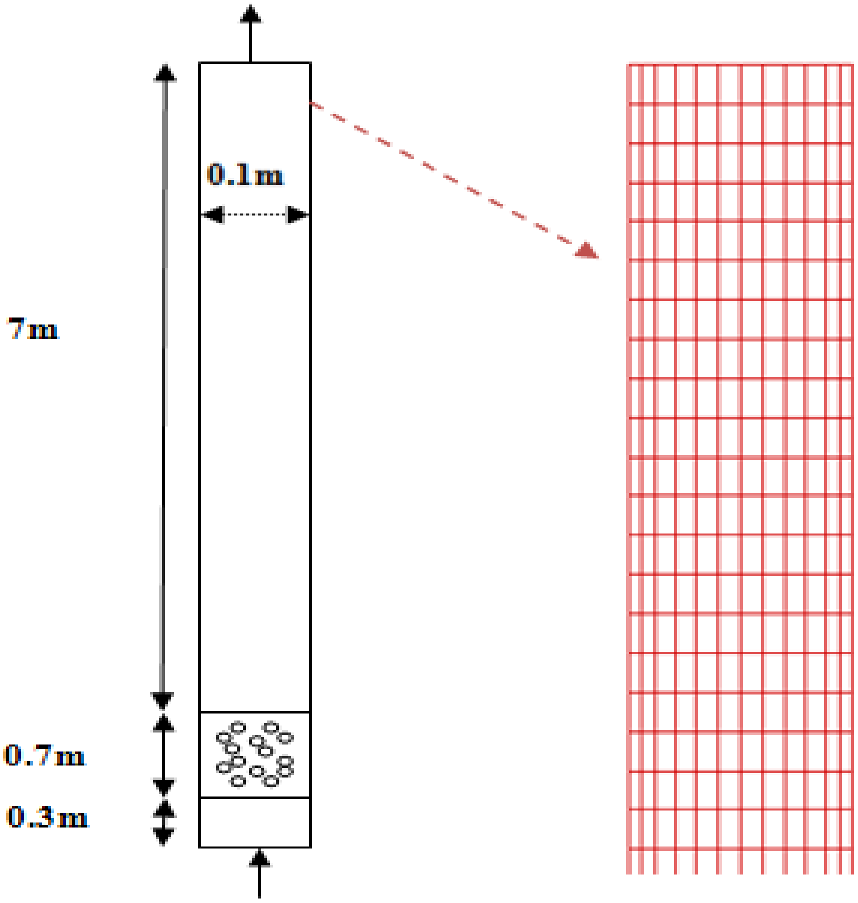

Figure 5-1: Simulation geometry

Mesh refinement independency has successfully been implemented to achieve an appropriate mesh enhancement for numerical solution. Although the calculation is carried out in 2-D, one cell is used in the third dimension to express the quantities of mass and volume flow rates which are required in calculation. The geometry size of the third dimension (z-direction) is adjusted based on the gas to solid flow rate and it is specified as 4*mm*. This value is also reasonable comparing with the mesh size in x-direction which is about 8*mm*. Since the particle tracking takes place in a steady-state system (particles are fed into the reactor continuously) therefore the features of static bed height (and bed porosity) and minimum fluidization velocity do not appear in these calculations.

Table 5.1 Boundary conditions

Description	**Value**
Particles	
Particle density($kg.m^{-3}$)	**3340**
Particle diameter(μm)	**$100 - 200$**
Particles sphericity	**1.0**
Fluxes	
Gs: Solid mass flux ($kg.m^{-2}.s^{-1}$)	**0.064-1.0**
Gg: Gas inlet mass flux ($kg.m^{-2}.s^{-1}$)	**0.84-1.3**
Initial Parameters	
CO_2 mole fraction [30]	**0.1**
Gas initial temperature(°C)	**650**
Geometry	
Reactor width (m)	**0.1-0.15**
Height of the reactor (m)	**8.0**
Operating Conditions	
Carbonator Temperature (°C)	**650-660**
Gas inlet velocity (m/s)	**2.15-3.8**
Outlet pressure (kPa)	**101.03**

5.3 Results and discussion

Figure 5.3 presents the solid fraction inside the reactor as a function of reactor height. It shows a high solid fraction (dense zone) at down-side of the reactor and a low solid fraction at upper part (lean zone). The dense zone is formed between 1.0m to 3m above the reactor inlet. Above this region the solid fraction decreases gradually forward to the reactor exit. The Figure 5-3 also shows that the reacted particles are leaving the reactor from the wall region at bottom of the reactor (green colour near the wall at reactor inlet in the bottom). Because the particles with higher residence time get heavier, therefore the gravity force against the drag force becomes dominant and those particles drop down and collected from the bottom of the reactor. The simulation predicted a sharp reduction of CO_2 concentration at dense region. Above this region the reduction rate became slower due to the lower solid fraction in the lean region. . It also indicates annulus shape of solid distribution inside the reactor. The maximum solid fraction is located somewhere between centre and wall of the reactor which is compatible with solid distribution patterns in dilute fluidized bed reactors (Figure 5.3 right-bottom).

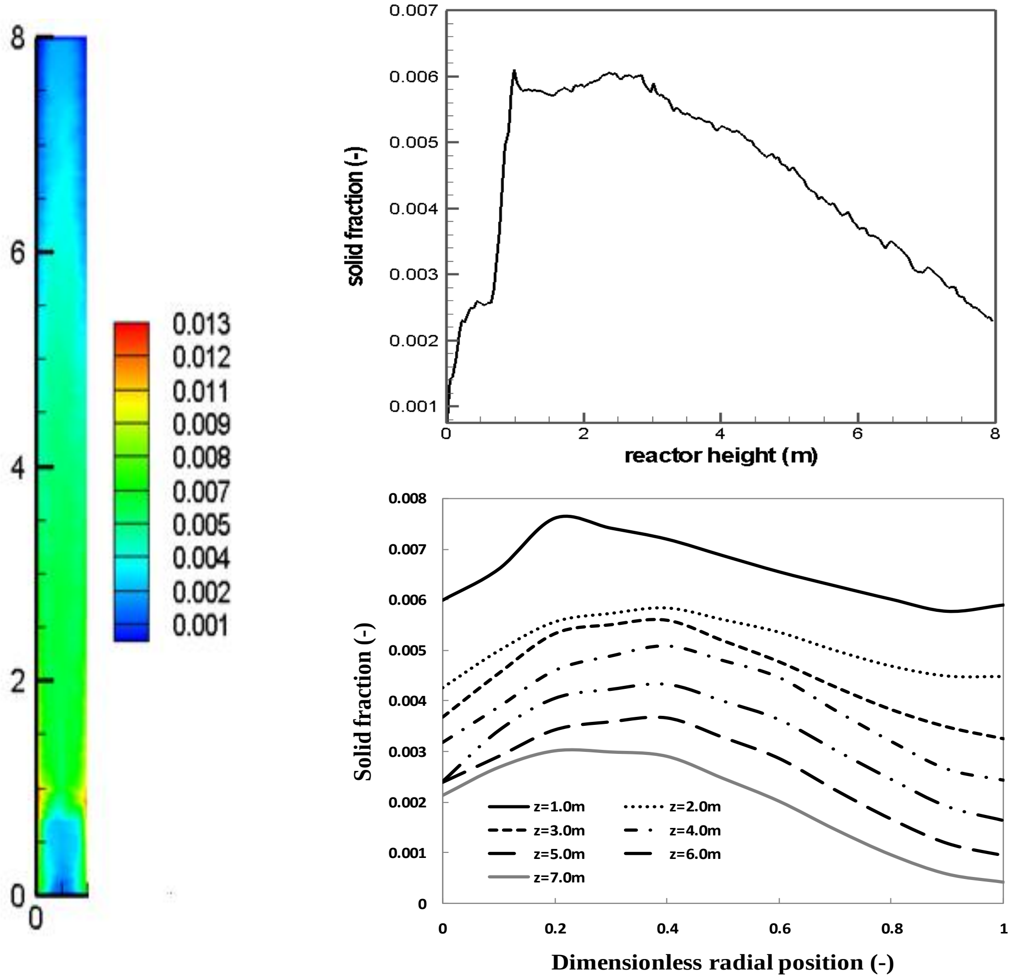

Figure 5-2: Contour of solid fraction inside the reactor (left), solid fraction along the centre-line of the reactor (right-top) and solid fraction in radial directional at different locations on reactor height (right-bottom).

The mole fraction of CO_2 is reduced from 10% at inlet to about 6.5% at outlet, in other words 37.43% $\left(= 100 \times \left(Y_{CO_{2in}} - Y_{CO_{2out}}\left(\frac{Y_{N_{2in}}}{Y_{N_{2out}}}\right)\right)\Big/ Y_{CO_{2in}}\right)$ of CO_2 has been captured in this carbonation reactor. Further reduction in CO_2 concentration can still be achieved by increasing the solid/gas ratio, but the inlet gas velocity must be adjusted to use the maximum possible residence time of the particles before they leave the reactor (Figure 5.4 (right)).

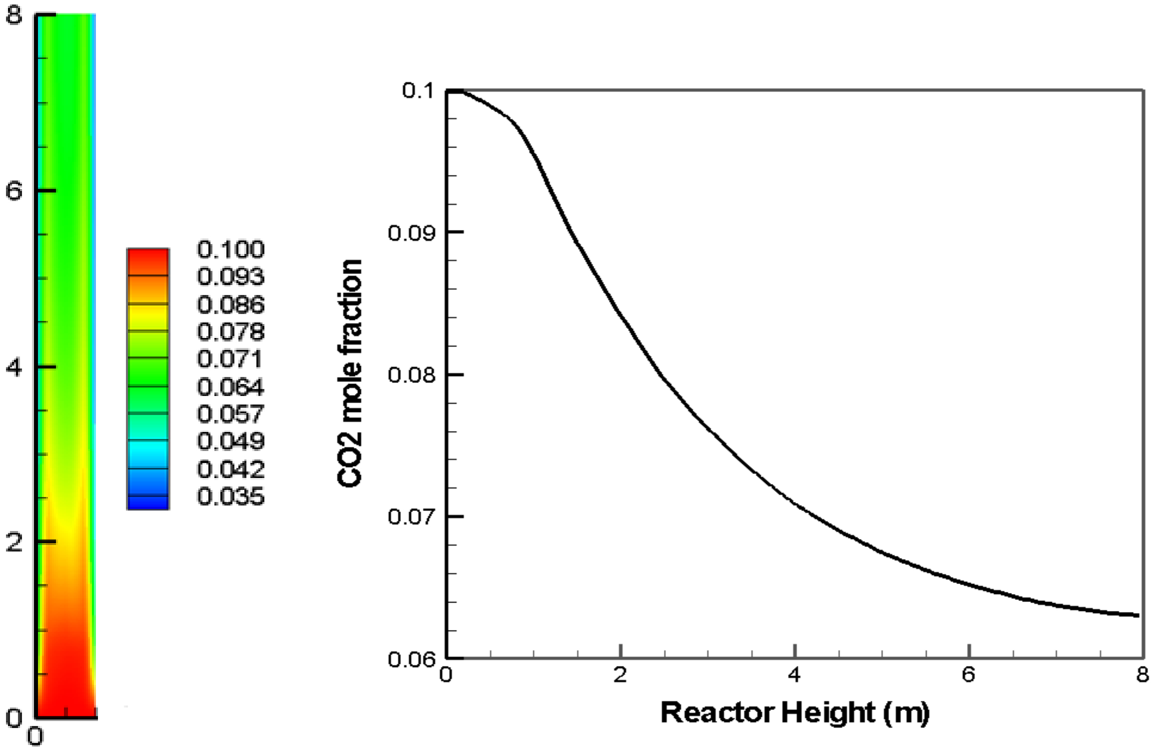

Figure 5-3: Contour of CO_2 mole fraction (left) and CO_2 profile along the reactor height.

The result signifies a sharp reduction of CO_2 (in 1-3m of the reactor height) which is the dense region. Following to this, the value of CO_2 decrees slowly associated with the lean region. The results also predict that over the 6m of the reactor length there is no significant change CO_2. Since the fresh particles entered into the domain between the reactor inlet and dense region which are positioned in near the centre-line, hence such particles move forward and for that reason the dense region contains highly active particles in centre compared with wall-side. Although the wall side contains more volume fraction in dense region but the activity of particles in centre is higher which results to react CO_2 with CaO at rapid reaction stage therefore reduction in CO_2 value in the centre would be higher than the core-annulus region (note that this region is not exactly the wall region but it is closer to wall rather than the centre) as shown in Figure 5.4 (left).

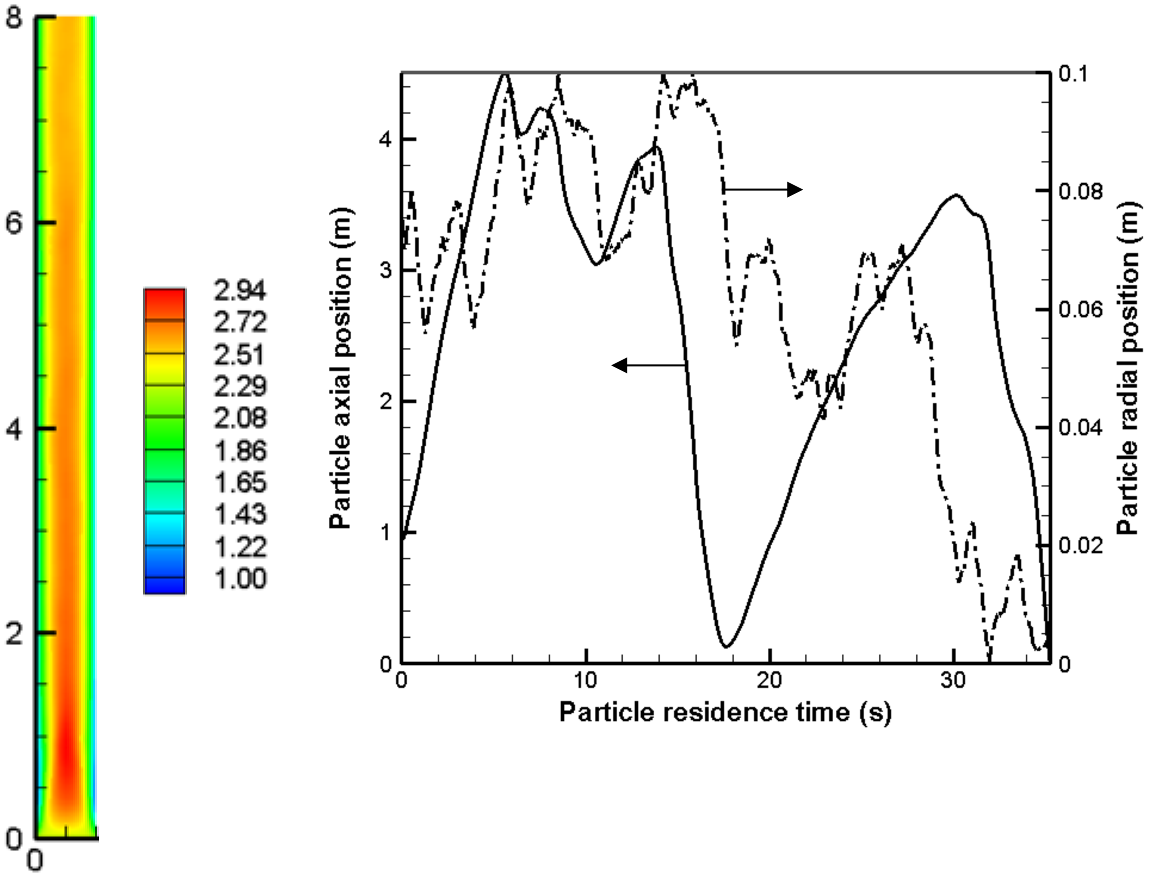

Figure 5-4: gas velocity contour (left) and particle (diameter = $200\mu m$) position in axial and radial direction (right).

Figure 5.5(right) shows the particle position during the residence time inside the reactor. The particles go into the reactor and the initial position for each particle is situated in a random location between 0.7 to 1.0m from the reactor inlet (bottom) and a radial random location. Initially the particle goes forward to the reactor exit but when it approaches to the lower gas velocity near the wall region (Figure 5.5(left)) the particle drops down until it is pushed forward close to the centre region of the reactor. This will continue and by progressing the residence time the particle became heavier and heavier therefore it cannot travel up anymore even at centre region of the reactor. The figure shows the particle is returned back from the near bottom of the reactor at about 18sec of the residence time and the particle was at centre of the reactor at this moment. Finally it drops down at about 35sec of the residence time and it left the reactor from the wall region at bottom of the reactor with 56% of conversion to $CaCO_3$. Although the figure 5-6 does not specify where the particle has left the reactor but this profile shows the particle conversion during its residence time inside the reactor. It means that after 35sec it is no longer inside of the reactor and it is shown in figure 5-5 (right) that it leaves the reactor from the bottom.

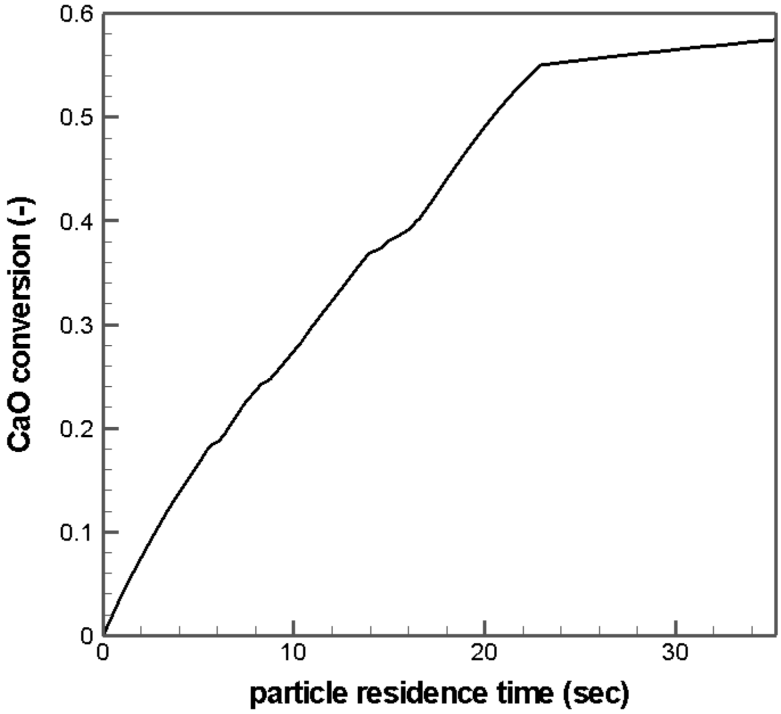

Figure 5-5: Particle conversion during the residence time inside the reactor.

Figure (5.6) shows the particle (CaO) conversion during the residence time inside the reactor. It shows a sharp conversion rate for the fast chemical reaction controlled stage of carbonation reaction. Following this stage, there is a second stage which is regarded as diffusion controlled mechanism. The simulation predicts a non uniform conversion rate at first stage of rapid reaction. Since the carbonation reaction is a function of CO_2 concentration therefore at lower concentrations the reaction rate would be lower. It shows that within the residence time (between 14 to 16 sec) the conversion rate drops. Figure 3(right) indicates that at this time period the particle is in the near-wall at dense region which contains lower CO_2 concentration in that region.

5.3.1 Expanded reactor

In simulation results which are described so far, the initial particle size is uniform. But in a real carbonation reactor in the industry it is not possible to provide uniform particle size for inlet solid particles. The main challenge in using non-uniform particle size would be the residence time of particles. The smaller particles will leave the domain straight away from the reactor exit at the top and the larger particles will do so from the bottom of the reactor due to their larger gravitation force against the drag force.

In order to overcome this issue, an expanded reactor is suggested with capability of handling all particles to have more residence time before leaving the reactor. In such scenario, the reactor is expanded somewhere along the reactor height and the gas flow still enters the reactor from the bottom and leaves the domain from the top reactor exit. By expanding the reactor the large particles will be pushed forward at expansion area and due to the lower gas velocity far from the expansion area they will not approach the reactor exit at top therefore they all be accommodated near the expansion region and a bit further up. For the small particles, they will act in the region from expansion section up to the reactor exit at the top just like a normal reactor for a uniform particle size. The intermediate size of particles also would be accommodated above the expansion region and mostly at middle of the upper zone.

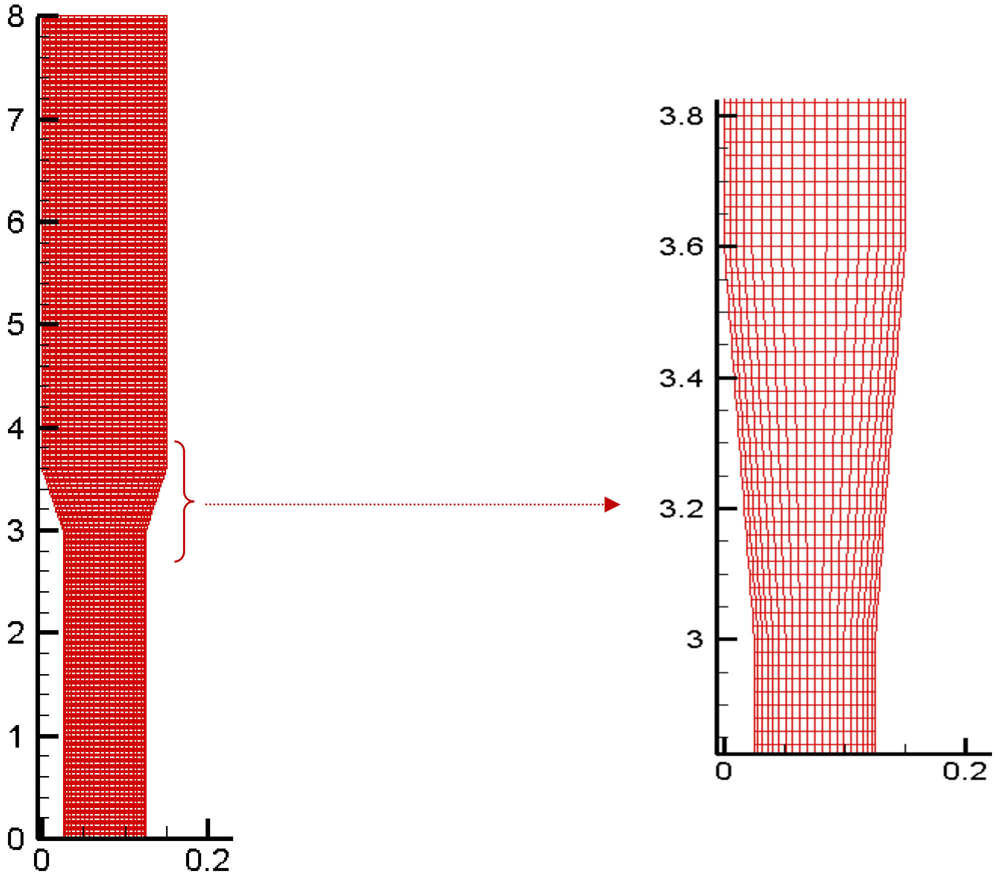

Figure 5-6: Geometry and mesh generation for expanded reactor

In order to investigate the behaviour of an expanded reactor, a set of uniform size of particles are utilized in this simulation and then the bed was expanded by 50% in cross sectional ratio therefore the width of the bed following the expansion is 15cm and the lower bed remains at 10cm in width. In order to handle the dead zone formation in expansion area, the connection between lower and upper bed is linked by a gradual expansion with vertical height of 60cm. Thus compared to the previous simulation with no expansion, in this simulation the geometry consists of 3m of lower region with 10cm in width and following that 60cm gradual expansion to upper bed with 15cm of width and 4.4m in height as shown in Figure 5.7.

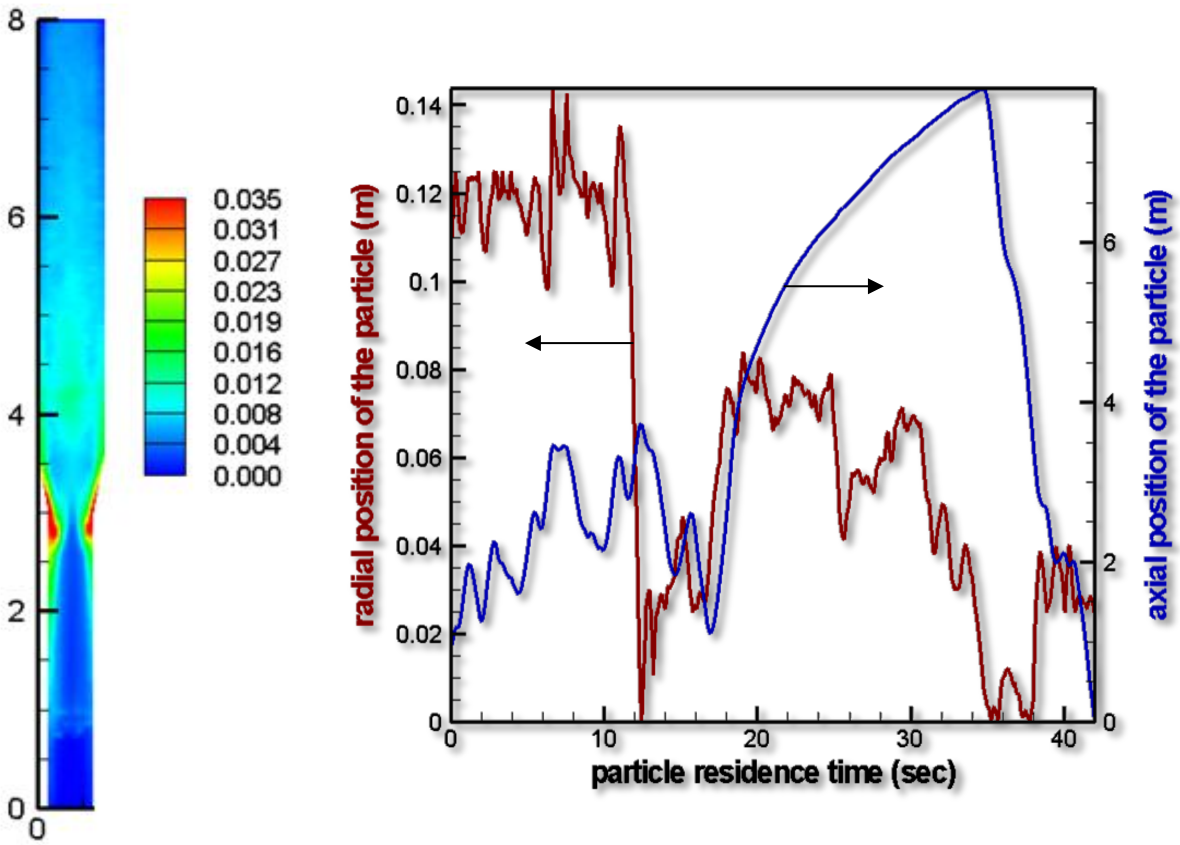

Figure 5-7: Contour of solid fraction (left) in expanded reactor and particle's position during its residence time (right).

Figure 5.8 (left) presents the results obtained for the solid fraction of uniform particles $(200\mu m)$ and inlet gas velocity of 3.8m/s. This gas velocity has been adjusted to get maximum conversion of carbonation reaction at higher residence time of particles inside the reactor. The solid flow rate also has been increased proportionally to keep the same gas/solid flow rate compared to the previous simulation with no expansion in the bed.

The simulation predicts two dense regions: one in expansion area in both left and right near the wall regions and the other one is further up to the expansion area. Due to the high pressure flow field at the expansion region the solid fraction is locally small in that area but just above that there is a dense region. This dense region can be compared with dense region in a straight reactor (a reactor with no expansion).

Figure 5.8(right) shows the particle reposition during the residence time inside the reactor. It demonstrates that the particles principally accommodated around the expansion region. In this case it also goes beyond the dense region further up to the expansion area and this corresponds to the location of the particle which goes through the centre of the domain at high pressure zone (in 20sec of residence time in the figure).

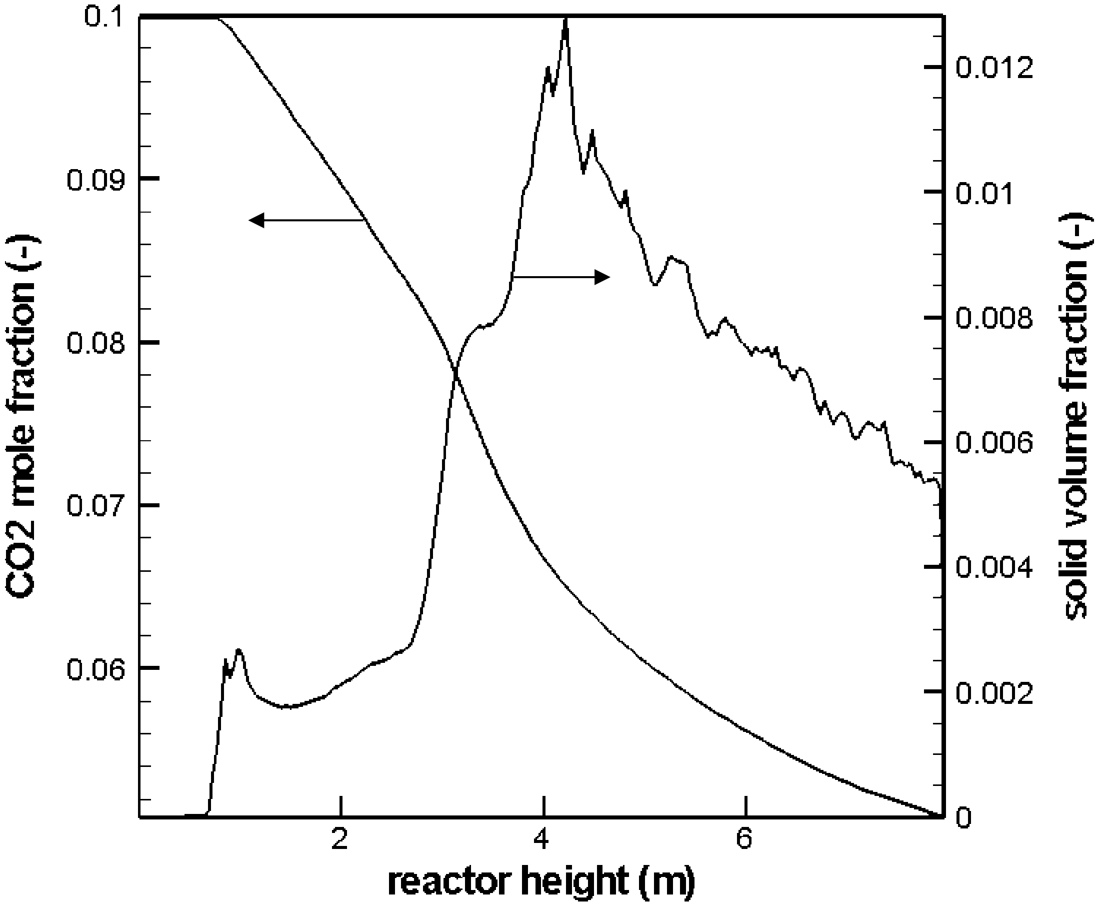

Figure 5-8: CO_2 profile and solid fraction along the centre line of the reactor.

Figure 5.9 illustrates the CO_2 concentration and solid fraction along the centre line of the reactor height. It shows that the maximum solid fraction is located above the expansion area. There is a sharp increment in solid fraction along the gradually expansion region (from 3.0m t0 3.6m) but the maximum solid fraction is in situated in 4.3m of the reactor height.

Figure 5.9 indicates that there is no conversion downward to particle's initial location (0.0 to 0.9m of reactor height) and this is quite a different behaviour when compared to the reactor with no expansion (Figure 5.4) whereas there is some conversion in that region. In expanded reactor due to the flow characteristics at expansion area only particles in the near wall region can travel to the bottom of the reactor while in the standard (no expansion) reactor the particles can also drop down in centre of the domain if the gravity force is dominant.

In this simulation with expanded reactor, the CO_2 mole fraction is reduced from 10% at inlet to about 5.5% in outlet; it means 47.6% of CO_2 has been captured. Compared to the standard reactor the expanded one can capture CO_2 10 percentage point more which is a significant achievement. This is the difference still with uniform particles; it can be more when utilizing non-uniform particles.

5.3.2 Non-Uniform particles

Also a simulation has been carried out to investigate the effect of expanding the bed on carbon capture efficiency utilizing a non-uniform particle size. In this scenario, if we can handle the largest and smallest particles to achieve their maximum residence time then the intermediate sizes would routinely be handled to give them high residence time. The magnitude of residence time can be referred to the values of the uniform size simulation results in view of the evaluation.

In this simulation 3 group of particle size $(100, 150\ and\ 200\mu m)$ with equal flow rates were utilized to explore the performance of the expanded reactor. The gas/solid ratio $(\frac{G_s}{G_g} = 0.076)$ is still the same as the previous simulation for uniform size but the gas velocity reduced from 2.15 m/s to 3.8m/s, because there are smaller particles in this case therefore the velocities has reduced to get maximum ultimate conversion of CO_2 inside the expanded reactor. The results (Figure 5.10) obtained show the similar dense regions but the values are different. There is also a significant difference compared to the case of uniform system, where above the upper dense zone is more dilute in expanded reactor. The reason for this is that the particles with smaller and intermediate sizes are travailing in those areas which lower residence time. The large particles also cannot travel that far from the expansion zone. It also predicts the particles with intermediate size are travelling mostly at all parts of the upper zone while small particles are mostly accommodated in near wall region of the upper zone. From the behaviour of the particles as predicted, it can be deduced that smaller particles have more residence time at near wall region and when they move towards to the center of the reactor they are pushed up to the reactor exit, but still they have more residence time compared to a standard reactor with no expansion.

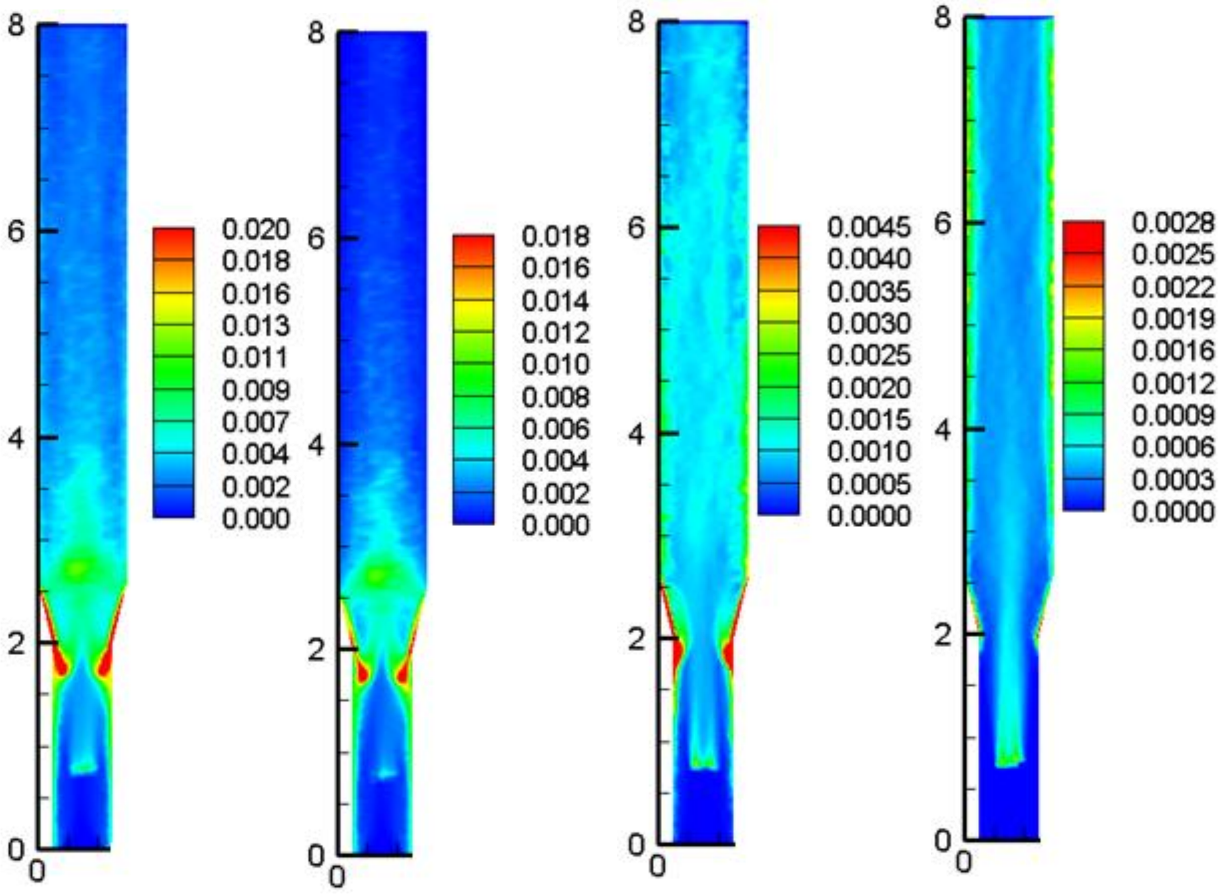

Figure 5-9: solid fractions in expanded reactor (overall, 200, 150 and 100μm: respectively from left to right)

The quantitative values of solid fraction are given along the centre line of the reactor in Figure 5.11. There is one local maximum point which is located near the 1.0m of the reactor height. This is associated to particles' injection position. Another maximum point which is in about 3.0m of the reactor height is the dense region. This dense region is mostly corresponds to large particles. Overall solid fraction profile looks similar to that of large particles because the large particles are accommodated in that dense region.

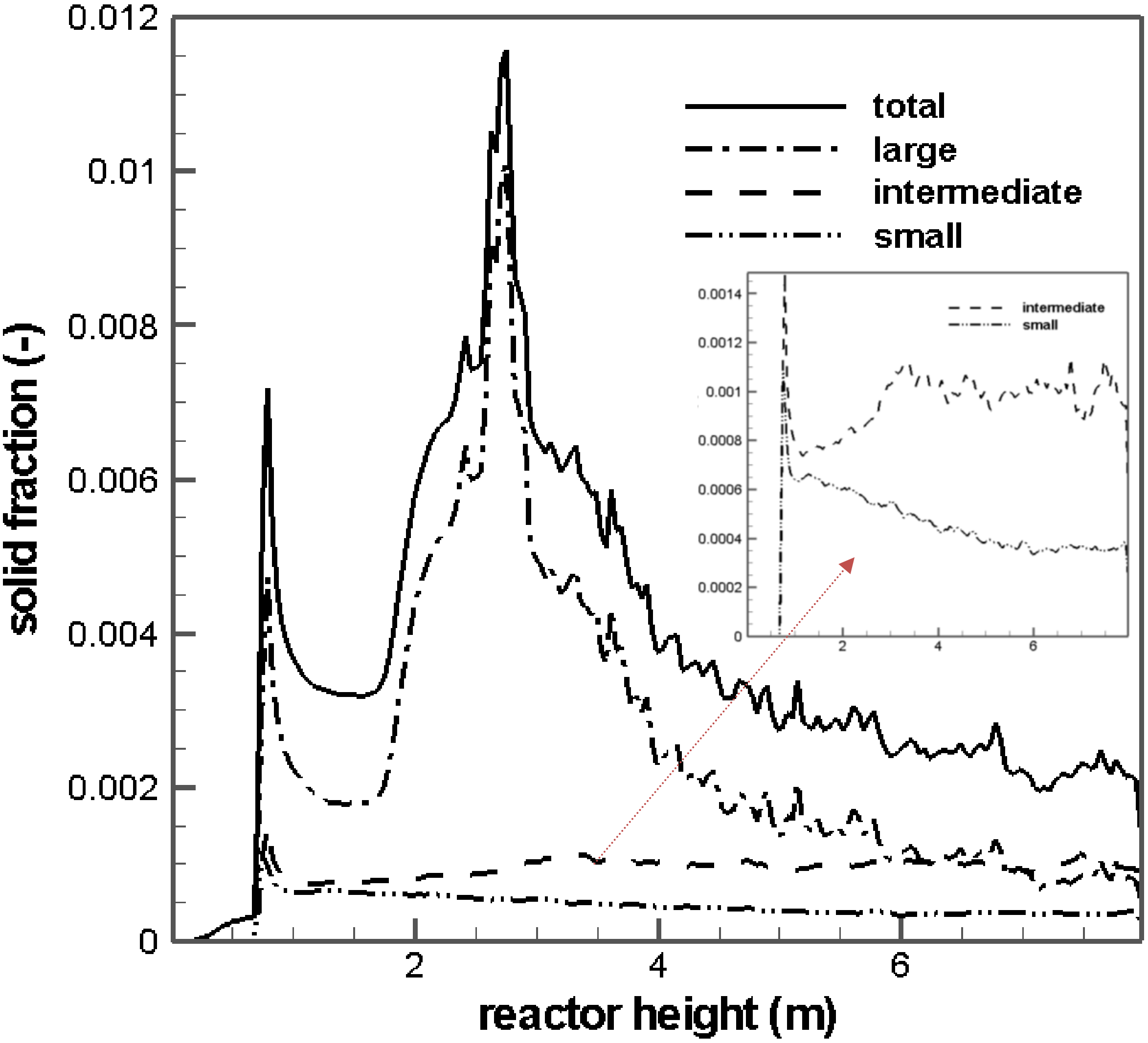

Figure 5-10: solid fraction along the centre line of the reactor for different size of particles.

Unlike the large and small particles, the solid fraction of intermediate particles is increases in the section above the dense region at centre of the domain. The intermediate and small particles are spread in upper expanded region where small particles are mostly in the near wall region.

5.3.3 Gradual expanded reactor

In this case unlike the previous expanded reactor, the reactor expanded gradually from the expansion position up to the reactor exit. This can help to increase more in residence time of intermediate and large particles. The result (Figure 5.12) shows that the height of dense region associated with large particles increased. Due to the hydrodynamic and gas flow field in sudden-expanded reactor, the large particles couldn’t travel further up from the expansion region therefore the residence time of such particles is less compared to the gradual expanded reactor.

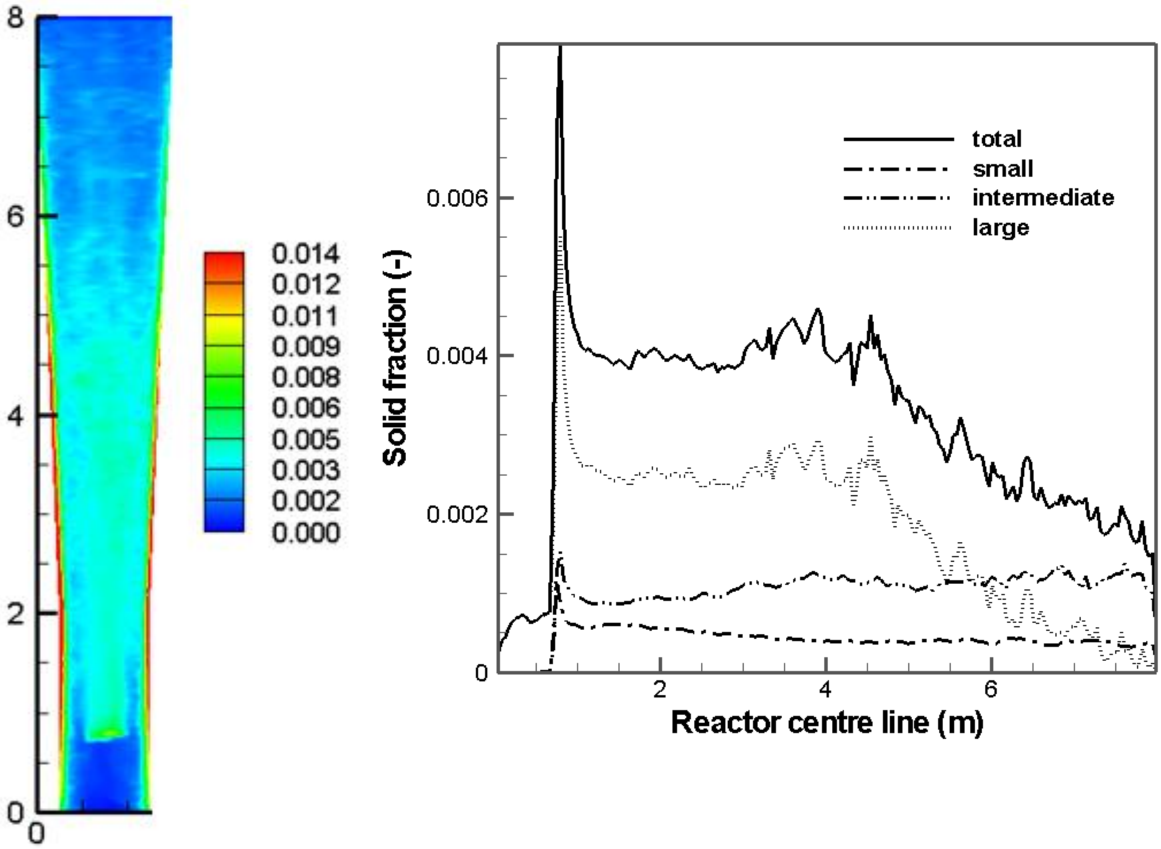

Figure 5-11: solid fraction contour (left) and profiles along the reactor centre-line (right).

In this simulation the inlet velocity reduce from 3.0m/s to 2.5m/s to adjust particle's residence time in maximum, but proportionally the solid flow rate decreased to keep at in same value of previous simulations. This reduction improves the residence time of intermediate particles. The overall CO_2 conversion has improved 5 percentage point compared to the normal expanded reactor. It seems this type of reactor is more appropriate but manufacturing of this kind of reactor might be more expensive.

In next chapter further investigations in a cylindrical reactor carried out to see the effect of the different parameters on reactor performance.

5.4 Conclusions

In this chapter, the results obtained from the numerical simulation of a fluidised bed reactor are presented. The simulation was carried out in a 2-D Cartesian domain in order to minimise computational expense. As can be readily seen in Figures 5-3 to 5-6, results obtained for reactor hydrodynamics and CO_2 concentration seem realistic from both computational and physical point of view.

Particles conversion during their residence time inside the reactor is predicted which shows the effect of fluid domain and CO_2 concentration at different regions of reactor on particles conversion. The effect of geometry expansion on residence time has been investigated. It has been found that the size of geometry has a substantial effect on particles' residence time and consequently improves conversion significantly. Expanded reactor increases the efficiency of the reactor for both uniform and non-uniform particles. This information is an useful idea for rector design.

The 2-D Cartesian model has been considered here due to its low computational expense, but real industrial reactors are cylindrical which is able to avoid dead zones on edge side of the reactor. As a remedy, a full 3-D cylindrical reactor simulation will be carried out in the next chapter.

chapter 6

Cylindrical Reactor

6.1 Introduction

In this chapter simulation of a cylindrical reactor carried out in 3-D to do further investigations on effect of key parameters in reactor performance.

In this chapter the followings are investigated:

- Hydrodynamics of the carbonator
- Effect of number of trajectories on simulation results
- Effect of solid mass loading
- Effect of particle diameter
- Effect of CO_2 concentration on removal efficiency
- Effect of geometry on ultimate conversion of particles (shape and dimension)

Initially A 3-D cylindrical geometry representation of a fluidized bed reactor with 10.0cm in diameter and 8.0m of height was employed in this study. This is the typical size of a fluidized bed riser as well as experimental works from literatures particularly for carbon capture with CaO [147, 120]. The geometry is sectioned into 8 divisions in radial direction, 60 divisions in angular and 400 divisions along the reactor lengths. In order to reduce the computational run-time, a slice of 18 degree is used in rest of the simulations after proving the results of the slice with a full 3-D simulation. Mesh refinement independency has successfully been implemented to obtain the appropriate for numerical solutions.

6.2 Boundary conditions

A 3-D simulation of a cylindrical fluidized bed has been carried out to evaluate and confirm the simulation results of small slices (a segment of 18 degree) for further investigations. Table 6.1 shows the boundary conditions used in this simulation. Appendix

A.5 represents the data input file into the PHYSICA code. It shows the all the material property, boundary and initial conditions which are set into the model for numerical solution. A reactor with 0.1m of diameter and 8.0m in height with uniform gas inlet velocity of 2.15m/s was used in initial investigations of the model. Basically, the height of fast fluidized bed reactors or risers is on the order of 10m and diameters are on the order of a few centimetres to 20 centimetres [148, 149, 150]. Considering this fact about the fast fluidized bed reactors and also the features of such reactors in CO_2 capture with solid sorbents [43, 120], the geometry of the reactor in this simulation has been selected.

Table 6.1 boundary conditions and simulation parameters

Description	**Value**
Particles	
Particle density(kg.m^{-3})	**3340**
Particle diameter(μm)	$\mathbf{100-400}$
Particles sphericity	**1.0**
Fluxes	
Gs: Solid mass flux (kg.m^{-2}.s^{-1})	**0.064-1.0**
Gg: Gas inlet mass flux (kg.m^{-2}.s^{-1})	**0.84-1.3**
Initial Parameters	
CO_2 mole fraction	**0.1-0.2**
Gas initial temperature($^{\circ}$C)	**650**
Geometry	
Diameter of the reactor (m)	**0.1-0.15**
Height of the reactor (m)	**8.0**
Operating Conditions	
Carbonator Temperature ($^{\circ}$C)	**650-660**
Gas inlet velocity (m/s)	**2.15-3.3**
Outlet pressure (kPa)	**101.03**

It should be noted that that at steady-state simulation in this way (particle tracking) the parameter of minimum fluidization velocity does not appear in equations of modelling. Because this type of simulation, unlike the transient simulation, does not take into the account the effect of the static bed.

6.3 Results and discussion.

A fluidized bed carbonator reactor can remove approximately 90% of CO_2 content of combustion exhaust gases. Based on the simulation results, the concentration of CO_2 reduced from 10% at inlet to 1.2 % at outlet, in other words, 89% of CO_2 has been captured with a single fluidized bed reactor.

The full 3-D simulation carried out at low solid inventory $\left(0.064\frac{kg}{m^2 s}\right)$y with a total of 2880 trajectories. This solid flux is calculated based on carbonation reaction to capture about 50% of CO_2 from a flue gas with 10% of CO_2 mole fraction at inlet flow. Gas inlet flow adjusted at 2.15m/s to fluidize CaO particles with 0.2mm of diameter.

6.3.1 Hydrodynamic of carbonator

Figure 6.1(left) shows velocity profile of a slice (18 degree with 5 cells in angular direction) of the reactor and Figure 6.3(middle) represents the result of a full 3-D simulation. There is a good agreement between two simulations. The dispersed solid is dilute in this system thus there is no superior effect of particles on continuous phase in view of the momentum exchange. When mass loading inside the reactor is increased the result shows a significant effect of particles on gas phase (Figure 6.1(right)). At higher mass loadings the gas velocity increased in the near wall regions (blue colour disappears in wall-sides at higher mass loading (Figure 6.1-right)) and also the width of the central plug flow becomes slender. Because of higher solid existence in particle injection area which is located down to the dense region above the reactor inlet, gas velocity looks like a uniform velocity which is slightly similar to fluid velocity in fixed bed reactors.

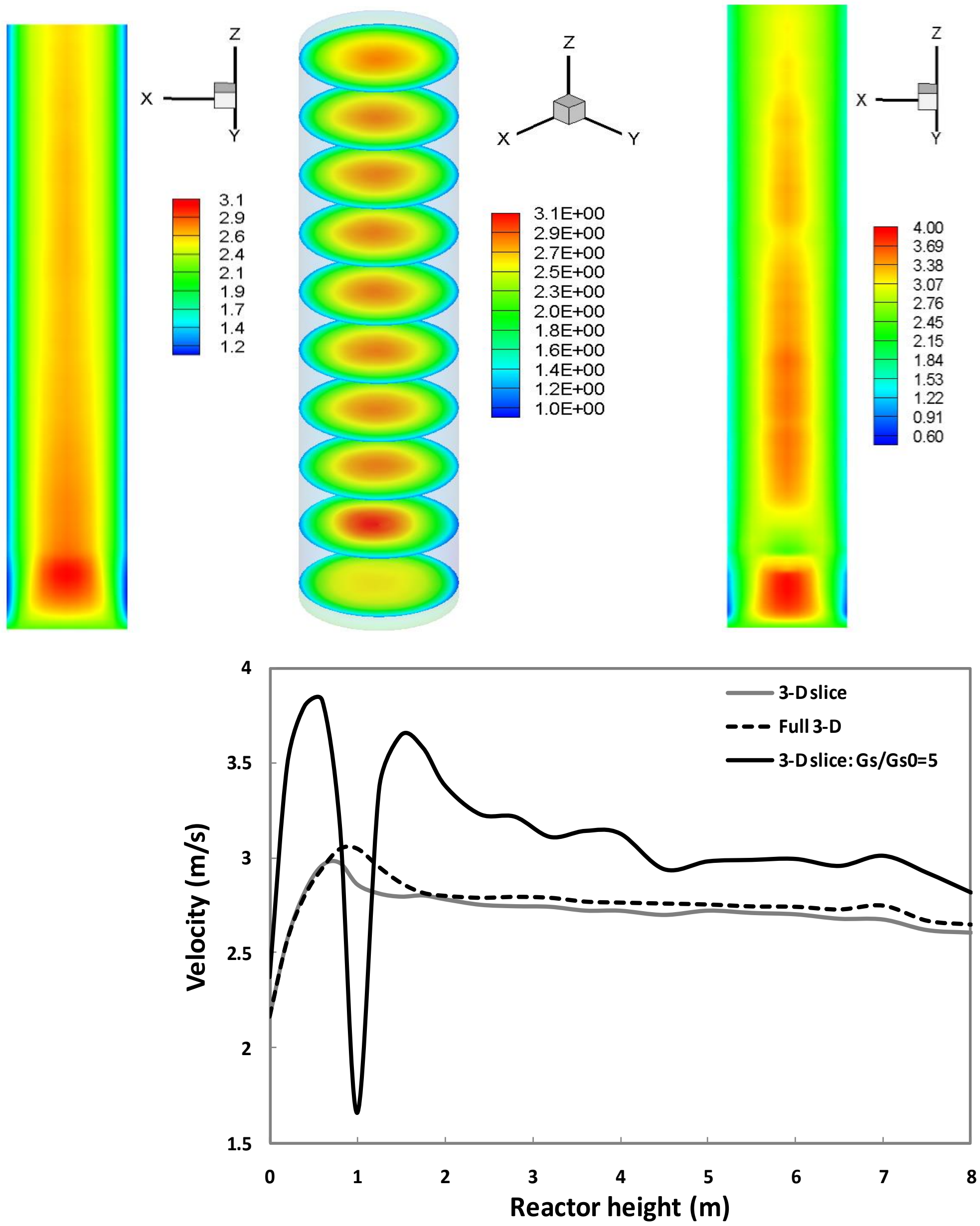

Figure 6-1: Gas phase velocity counter: slice of a cylindrical reactor (top-left) full 3-D simulation (top-middle), in a slice with 5 times higher solid mass loading in cylindrical slice (top-right) and comparison of velocity profile in reactor centre-line (bottom).

The comparison between 3-D slice and full 3-D shows a good agreement between these two simulations which means 3-D slice can be trusted as a full 3-D for further simulations. Figure 6.1 (bottom) also shows heavy changes on gas velocity at dense zone at higher mass loading. It also indicates two local maximum points which are regarded to the particle injection area and following that the dense region. In more dilute cases (3-d slice and full 3-D) there is no such significant effect of particle injection area as it strongly appears in higher mass loading case (3-D slice with Gs/Gs0=5).

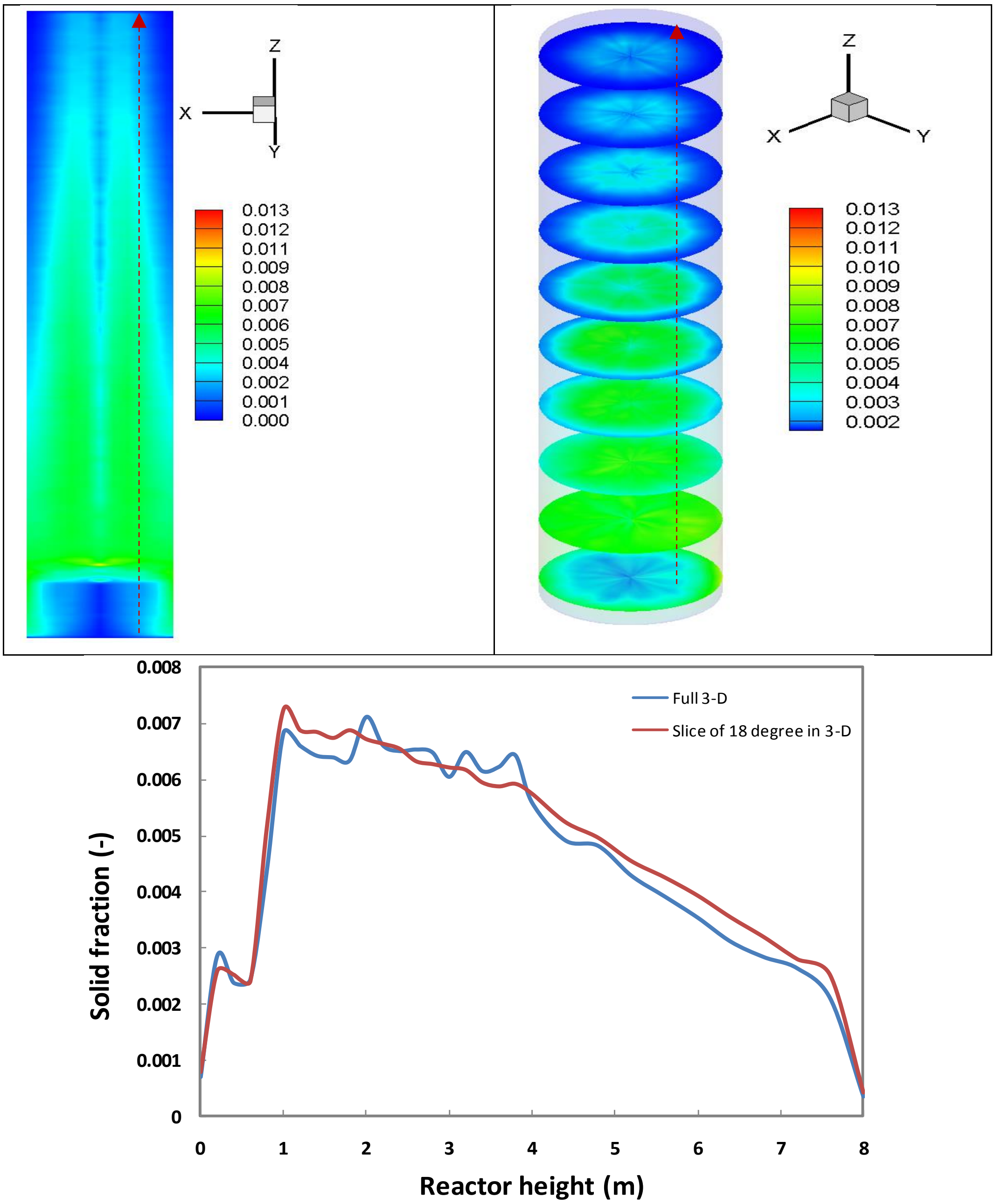

Figure 6-2: solid volume fraction (%) inside the reactor: At cross sectional surface in a 3-D slice (a segment of 18 degree) (top-left), a full 3-D simulation (top-right) and comparsion of solid fraction between slice 3-D and full 3-D along the reactor height and radial midpoint (bottom).

Figure 6.2 shows solid volume fractions inside the reactor in 3-D and 3-D slice. It shows good agreement between two simulations, as both of them shows an annulus shape of solid holdup at upper middle of the reactor and a slightly dense region in lower section of the reactor. Both of them indicate a low solid concentration in centre of the reactor, which is due to higher gas velocity in that region which makes particles residence time lower in centre. Following the dense region is a lean region which is compatible with a typical fast fluidized bed reactor's behaviour [107].

Figure 6.2 (bottom) shows that both of the full 3-D and a slice of 3-D simulation are similar with a little difference in predicting of solid fraction. This deference can be regarded to handling of particles in 3-D slice in which the particles those leaving the domain form the sides, they must be returned into the domain. In this case, when a particle leaving the domain from left-side of the domain it must be returned to the right hand side. In the other word, it has been assumed that the mass leaving from onside, an equal mass enters into the domain from the opposite side.

Due to the characteristics of the carbonation reaction and particles structure, the size of particles does not change significantly therefore the reaction product gives some added mass into the porosity of particles and make them heavier (gravity force increases) and they falling down to the bottom of the reactor. Since the trajectory of every individual particle is different with others and also the amount of CO_2 that exposed to that particle at different cells would be different the ultimate conversion and also the conversion at a specific residence time would be different and escape of particles from the bed due to the low conversion rate of the reaction would be unavoidable, but only a few number of particles escaped and the rest deposited on the bottom walls of the.

6.3.2 Trajectory effect

In this simulation the total mass flow rate of solid is divided by the number of trajectories (an integer number) and each trajectory contains a fraction of total mass flow rate. The number of trajectories at any certain mass loading in a fluidized bed reactor can affect the results. The accuracy of the model increases with increase in the number of trajectories, but at the expense of computational time. In order to achieve reasonable results, it is essential to use a minimum number of trajectories with adequate prediction performance criteria. In this simulation, the number of trajectories was initially set to 9 and was then doubled until the results show no more significant variations on effective parameters.

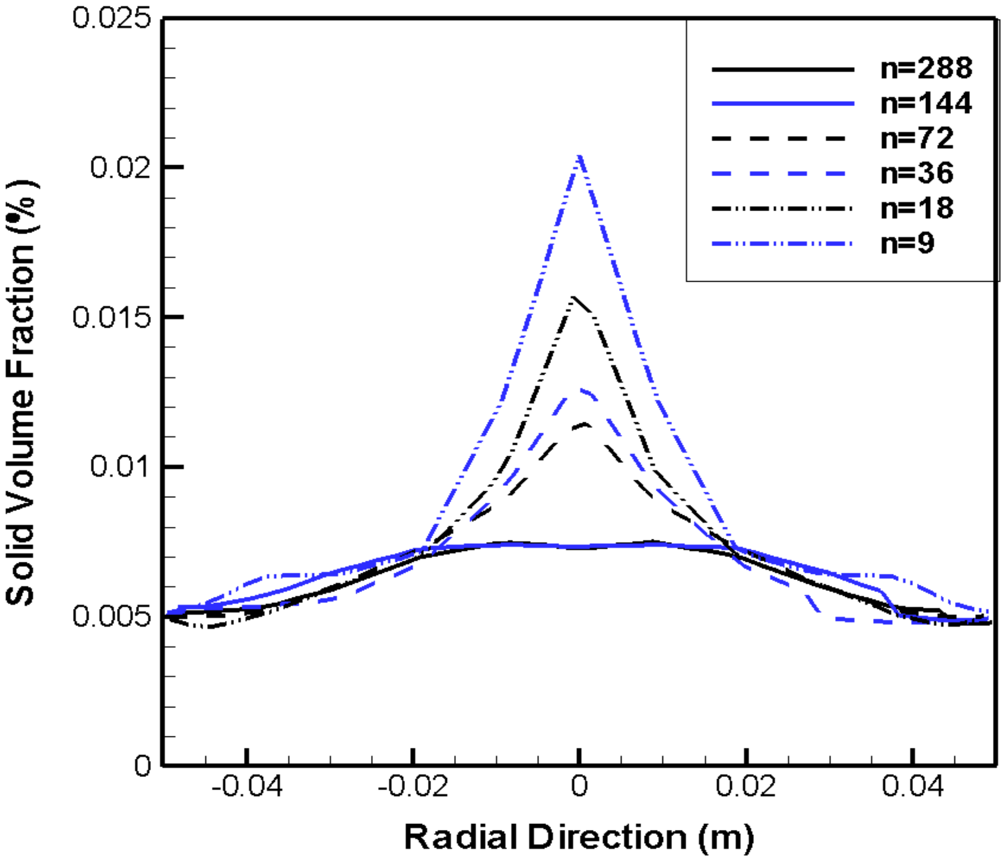

Figure 6-3: solid volume fraction in dense region (on 2.0*m* from the bottom of the reactor) for different number of trajectories.

Figure 6.3 shows the effect of number of trajectories on solid volume fraction in dense region (*z=1.5m*). It can be seen that there was significant difference when the number of trajectories was between 9 and 144, afterwards further increase in the number of trajectories did not really make any difference. Since this result is for a slice of the reactor with 18 degree thus for a full body of the reactor 2880, ($\frac{360}{18} \times 144$), trajectories required to obtain results which are independent on trajectory.

6.3.3 CO_2 removal

Figure 6.4 shows profiles of CO_2 concentration within the computational domain. It is readily seen that there is a significant reduction in CO_2 concentration at lower region of the reactor than the upper region. This can be explained by fast initial stage of the carbonation reaction taking place inside the reactor. Since the particles initially entered from the lower part of the reactor close to the inlet, reactions starts taking place as soon as the particles get exposed to CO_2. Another reason is the high CO_2 concentration at lower section of the reactor which gives a high conversion rate in lower section of the reactor.

The results also show low CO_2 concentration in the near wall regions. This is due to the lower gas velocity and the consequent high residence time which is typical of those regions as it is presented at contour picture. It also shows that based on the operating conditions the second half of the reactor does not have a significant effect on CO_2 concentration.

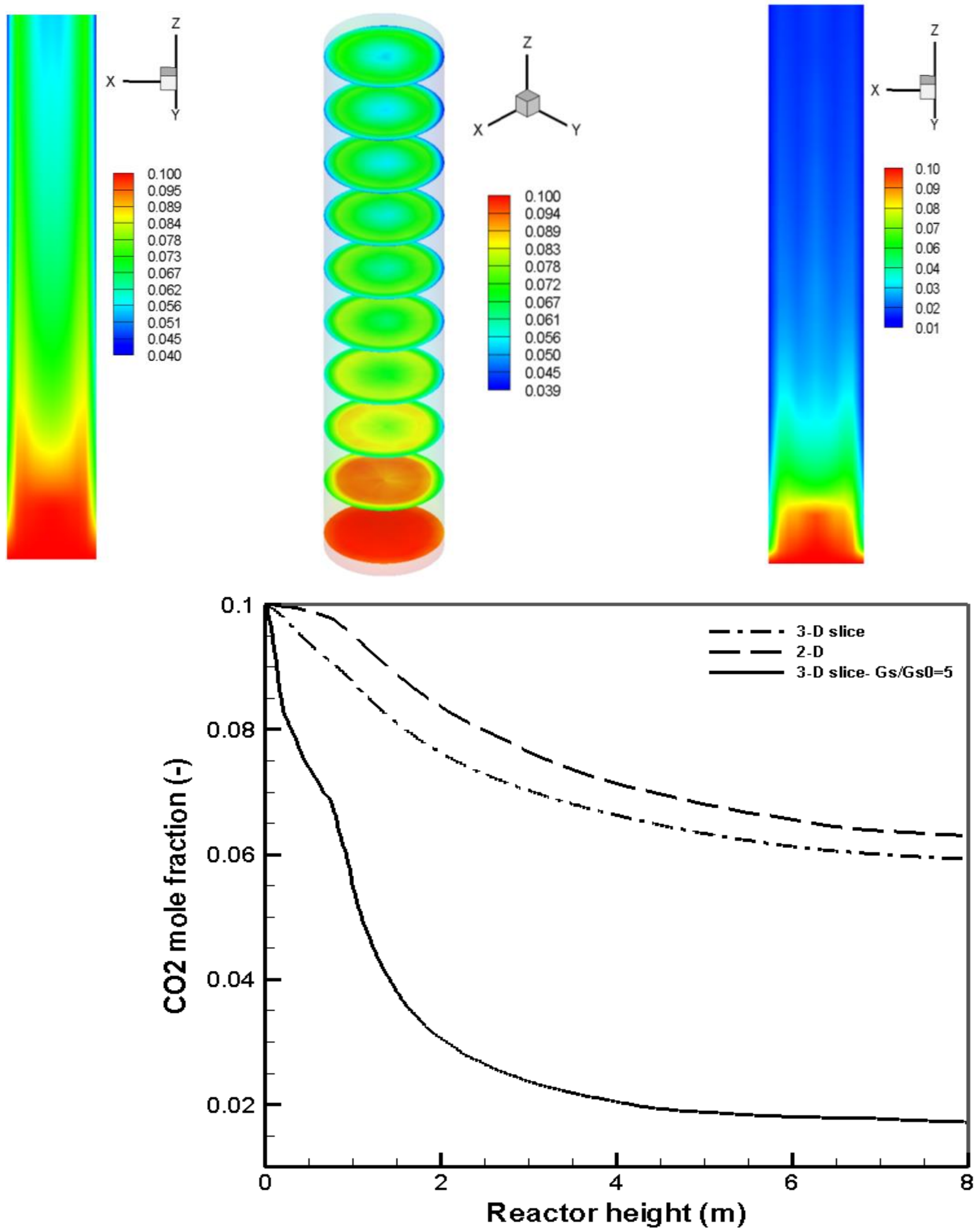

Figure 6-4: Contour of CO_2 mole fraction inside the fluidized bed reactor ($\frac{G_s}{G_{s_0}} = 1$)in 2-D (left), 3-D (middle) and 2-D with $\frac{G_s}{G_{s_0}} = 5$ (right).

Comparing the 2-D and 3-D slice in prediction of CO_2 conversion, the 2-D simulation predicts a bit less conversion and it can be due to the dead-zones in rectangular shaped geometries which results less gas-solid contact. The 3-D slice shows CO_2 mole fraction reduced to 0.02 from 0.1 at the inlet. It means CO_2 has been converted more than 80% in this case.

6.3.4 Effect of initial CO_2 concentration

Figure 6.5 shows the effect of initial CO_2 mole fraction on removal efficiency of the reactor. In this investigation, a similar solid mass flow rate as well as the same gas volume flow rate is used to evaluate the effect of CO_2 on reaction rate and capture efficiency.

The removal percentage increased by increasing the initial CO_2 mole fraction in gas inlet flow, but it must be noted that this increment can happen as long as the particles conversion doesn't exceed the fast initial reaction stage of the CaO carbonation. In other words, at longer particles residence time in which the carbonation reaction is controlled by diffusion rate, increasing the initial CO_2 concentration will reduce the ultimate removal percentage. Because in transition from reaction controlled to diffusion controlled stage, the sintering of particles porosity would be higher in high CO_2 concentration therefore diffusion rate would be slower proportionally.

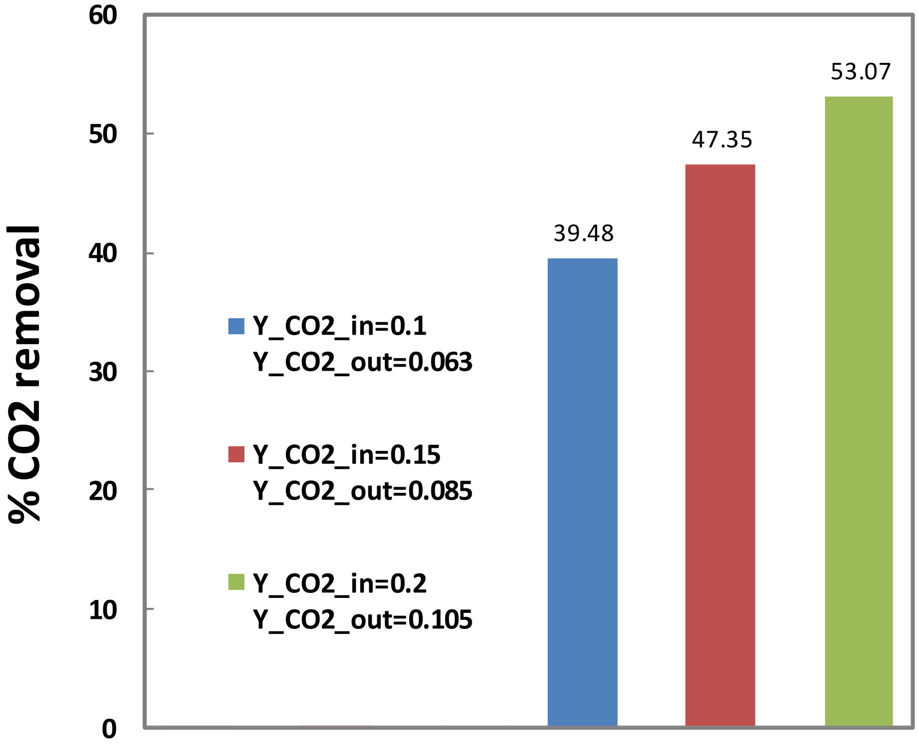

Figure 6-5: Effect of CO_2 content of inlet gas flow on removal percentage.

Increasing the CO_2 also changes the solid fraction at dense zone as well as the solid volume fraction at lean region. At higher CO_2 concentration of inlet gas flow, the dense zone becomes more extensive and this is due to a high reaction rate (carbonation reaction rate depends on CO_2 concentration) where the particles become heavier quickly.

Figure 6.6 shows the effect of CO_2 concentration of inlet flow on height of the dense zone and lean region. It indicates that at the lean region unlike the dense region the solid volume fraction decreased with increasing CO_2 mole fraction at the inlet flow. It seems that at the high reaction rate the reactor performance is highly influenced by the dense region. In other words, at higher reaction rates a bubbling fluidized bed reactor model can describe the behaviour of the reactor.

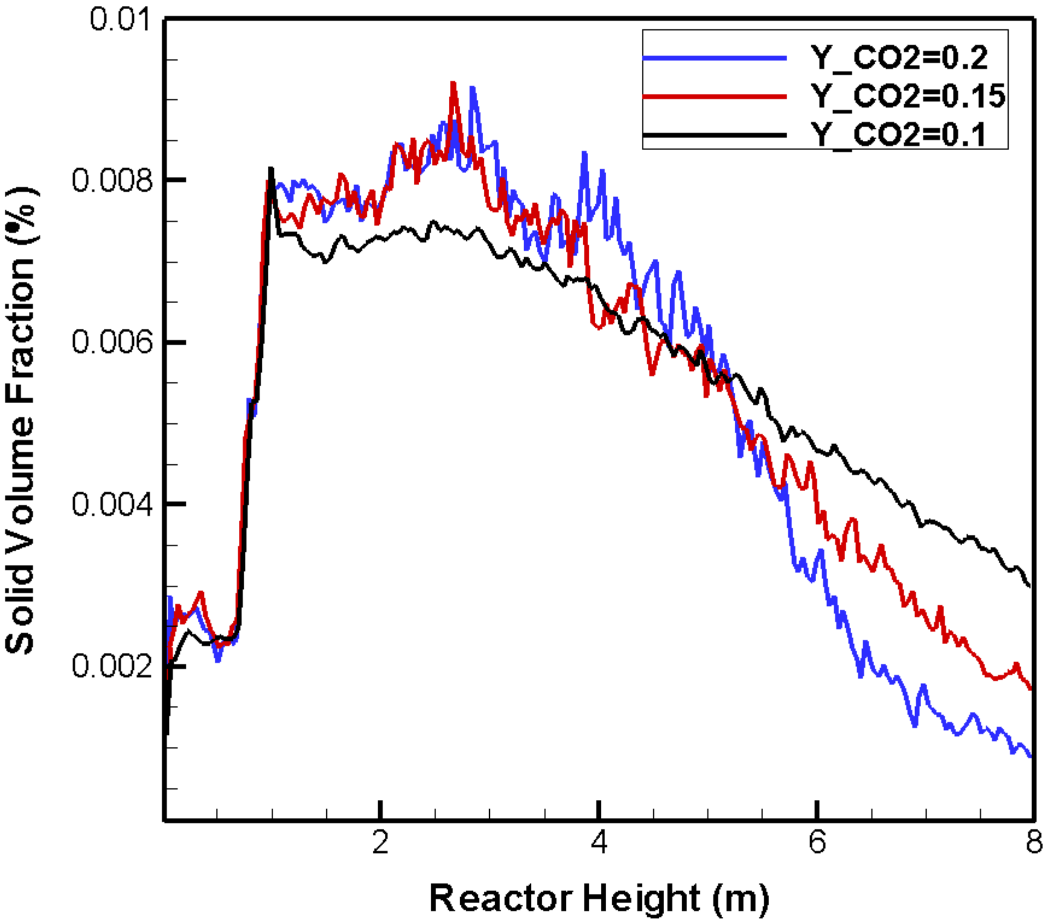

Figure 6-6: Solid volume fraction along the reactor height at three different inlet CO_2 mole fractions.

Although the initial CO_2 concentration in flue gases is constant and cannot be adjusted as an operating conditions to control the reactor performance. The simulation result captured the nature of the solid flow (gas-solid pattern) for any particular removal efficiency with a certain initial CO_2 concentration and the required reactor height which are important design parameters were well described.

6.3.5 Mass loading effect

In order to investigate the effect of solid mass loading effect on performance of the carbonator reactor the mass flux was increased from $\left(G_s = 0.064\,\frac{kg}{m^2 s}\right)$ to $\left(10G_s = 0.64\,\frac{kg}{m^2 s}\right)$ with 10 times increment ratio. It should be noted that during this simulation the static bed has not been considered. Because this simulation is steady-state therefore there is no need to take into the account of the static bed. In this work, tracking of each trajectory is started at a random location near the gas-inlet flow and it has been continued till the trajectory (particles) leave the computational domain.

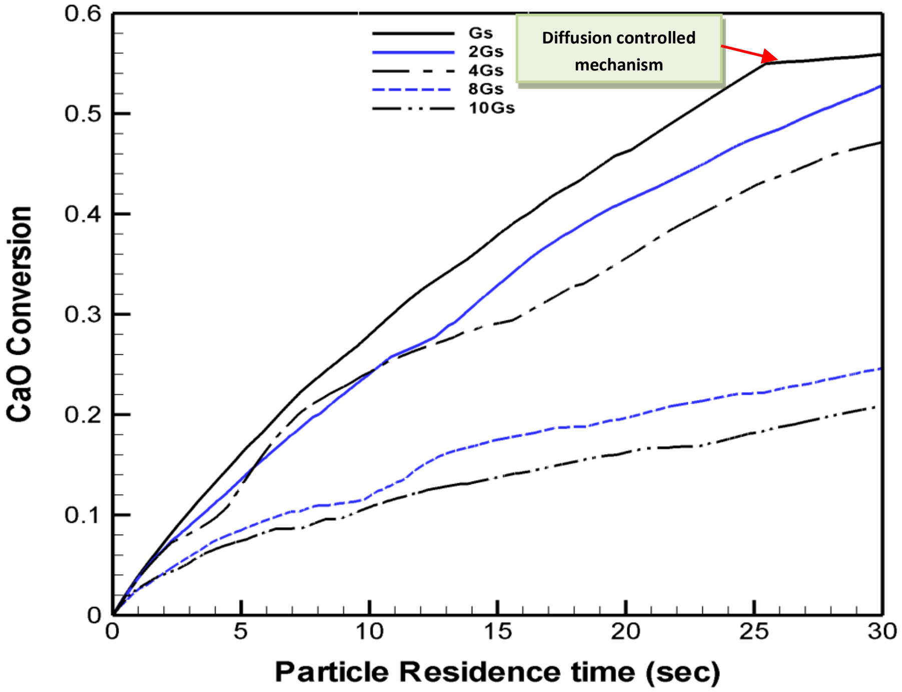

Figure 6-7: Effect of solid flow rate on conversion of CaO particles.

Figure 6.7 shows a particles' conversion curve, for a period of 30 second during their residence inside the reactor. Because at different mass loadings the particles residence time is different therefore the comparison is done in a specific time period while some of them have residence time greater than 30 seconds. The profile for a more dilute bed with solid flux of G_S shows both the reaction controlled and diffusion controlled stages within the first 30 seconds, while the other profiles at higher mass loadings doesn't signify the diffusion controlled stage.

By increasing the solid inventory inside the reactor the CO_2 removal would be increased but not linearly. Due to the dependency of carbonation reaction on CO_2 concentration the CaO conversion of each particle decreases with an increase in the solid flow rate due to the lower CO_2 fraction exposed to solid particles. Figure 6.7 shows the particles conversion at different solid flow rates. It indicates that a 10 times increase in the solid flow rate causes the CaO conversion to decrease from 57% to about 20%.

Figure 6.8 presents the effect of solid flow rate on overall CO_2 mole fraction along the reactor length. Although the particle conversion reduces with increasing the solid inventory, but the entire CO_2 removal increases due to higher solid to gas ratio inside the reactor. The result also shows sharper reduction at initial region of the reactor due to high reactor rate in that region which is due to higher molar ration of CaO to CO_2 and higher residence time of particles in lower region which produces quick reaction and heavier mass of particles.

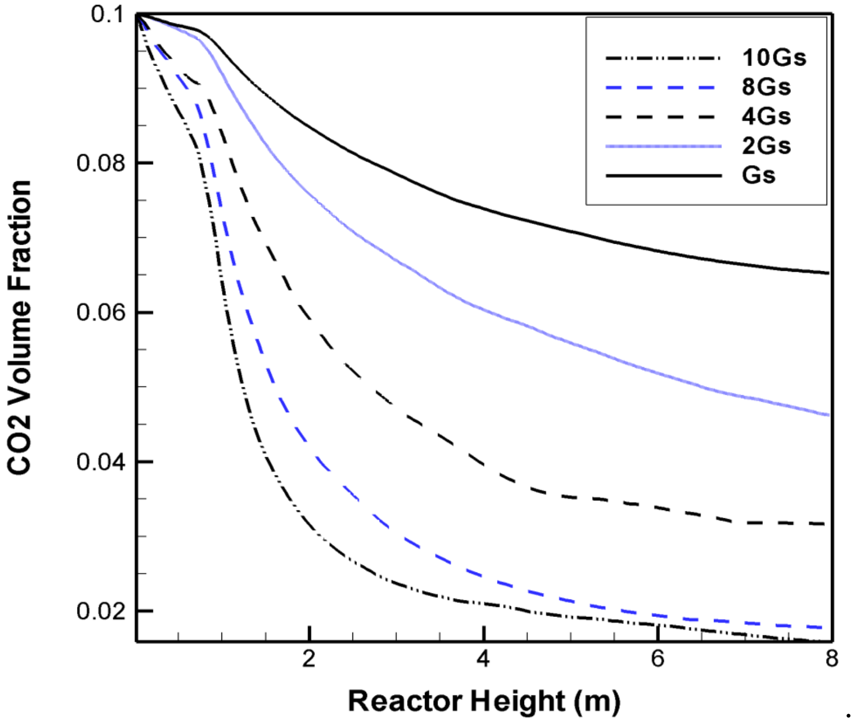

Figure 6-8: Effect of solid flow rate on CO_2 concentration along the reactor height.

Figure 6.8 shows higher rate of CO_2 removal by increasing the solid flux, but the average particles' ultimate conversion is reduced (Figure 6.9). This entails that increment of 10times in solid flow rate doesn't results in 10times more CO_2 removal. This is an important matter in reactor design to take into account the relation between the solid inventory, particles' conversion and CO_2 efficiency. The simulation results can suggest the proper solid flow rate to obtain a desired CO_2 capture which can reduce the operating cost.

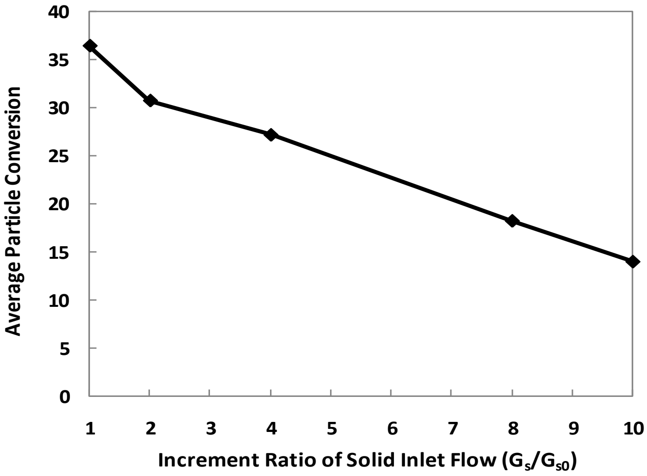

Figure 6-9: Effect of solid flow rate on particles' average ultimate conversion.

6.3.6 Effect of particle diameter

Figure 6.10 shows the effect of particles' diameter on carbonation reaction. It indicates that at small diameters the average ultimate conversion of CaO particles is higher comparing to the bigger particles in same solid/gas ratio. When the particles' diameter is increased, the required velocity in the bed increased to fluidize the particles; this produces a proportional increase in flow rate and solid inlet flux to maintain a constant solid-gas rate in all four simulations. Small particles provide higher surface area therefore the reaction rate would be increased. Apart from the higher surface area provided by small particles, the residence time of small particles are also higher than the bigger particles and it results in higher conversion rate within the domain.

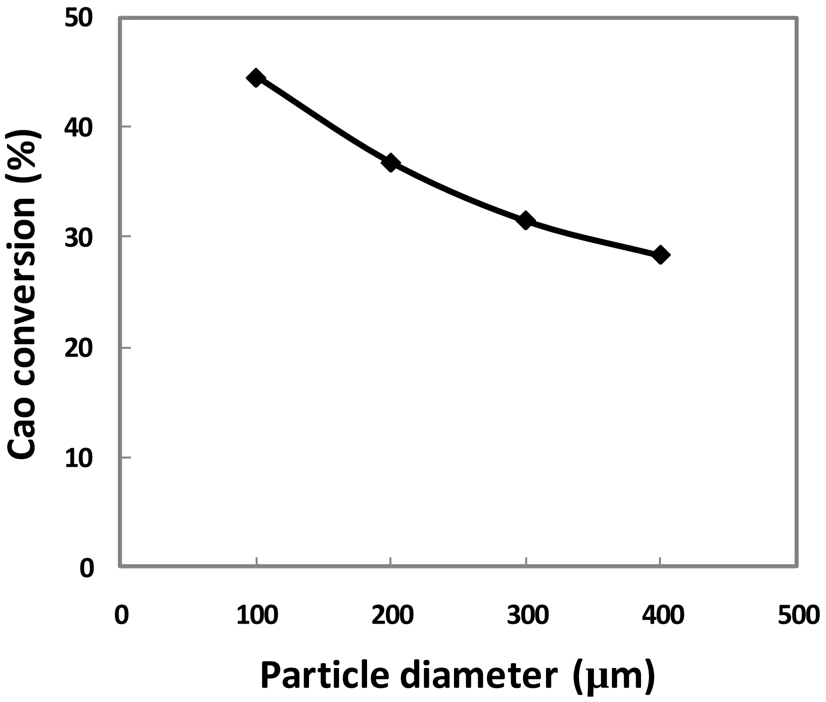

Figure 6-10: Eeffect of particles' diamter in coversion during their residence time inside the reactor.

The effect of particle diameter on CO_2 is presented in Figure 6.11. It indicates that with increase in the diameter from 0.1mm to 0.4mm the CO_2 removal percentage has changed from 89% to 68 % . it seems using small particles are much more efficient. This simulation is caried out at solid flow rate of $5G_s$ (see table 6.1) for particles' diameter of 0.2mm, for the other particle size it has baeen adjused based on the gas flow rate.

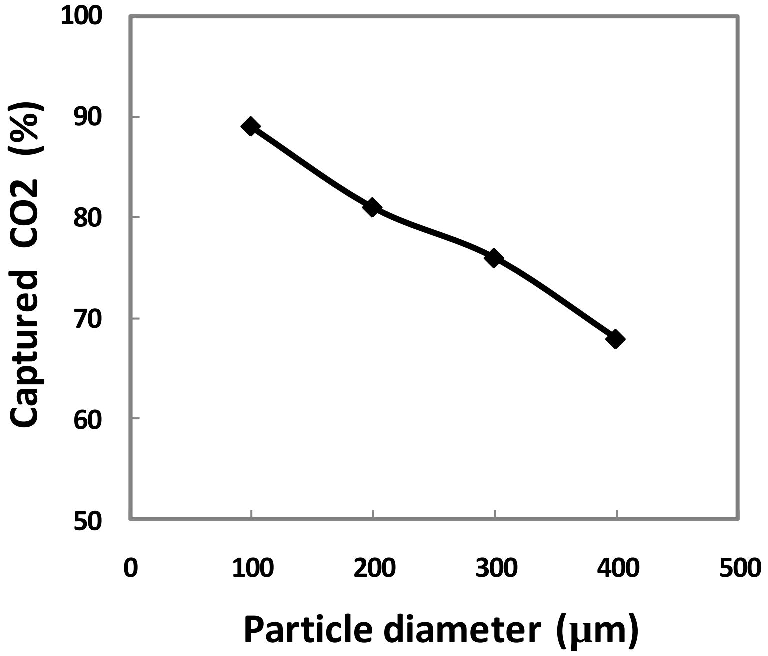

Figure 6-11: Particle diameter effect on CO_2 removal.

6.3.7 Geometry Effect

Operating a fluidized bed reactor with a uniform particle size is not possible in an industrial process. Further, each particle size requires appropriate gas velocity to keep them in fluidization point. In a range of particle size, the velocity would be set based on the particles' size distribution but still some part of the particles cannot be handle; some cannot be fluidized thus leaving the reactor from the bottom section in a very speedy manner (short residence time). In order to overcome to this issue, a reactor can be divided into different sections with different gas velocities.

In this work the reactor has been expanded from different positions from the reactor inlet. The diameter ratio of expanded section to the reactor inlet is set to 1.50. Particles with diameter of 0.15mm and 0.2mm and same flux were used to investigate the effect of reactor expansion on CO_2 capture efficiency.

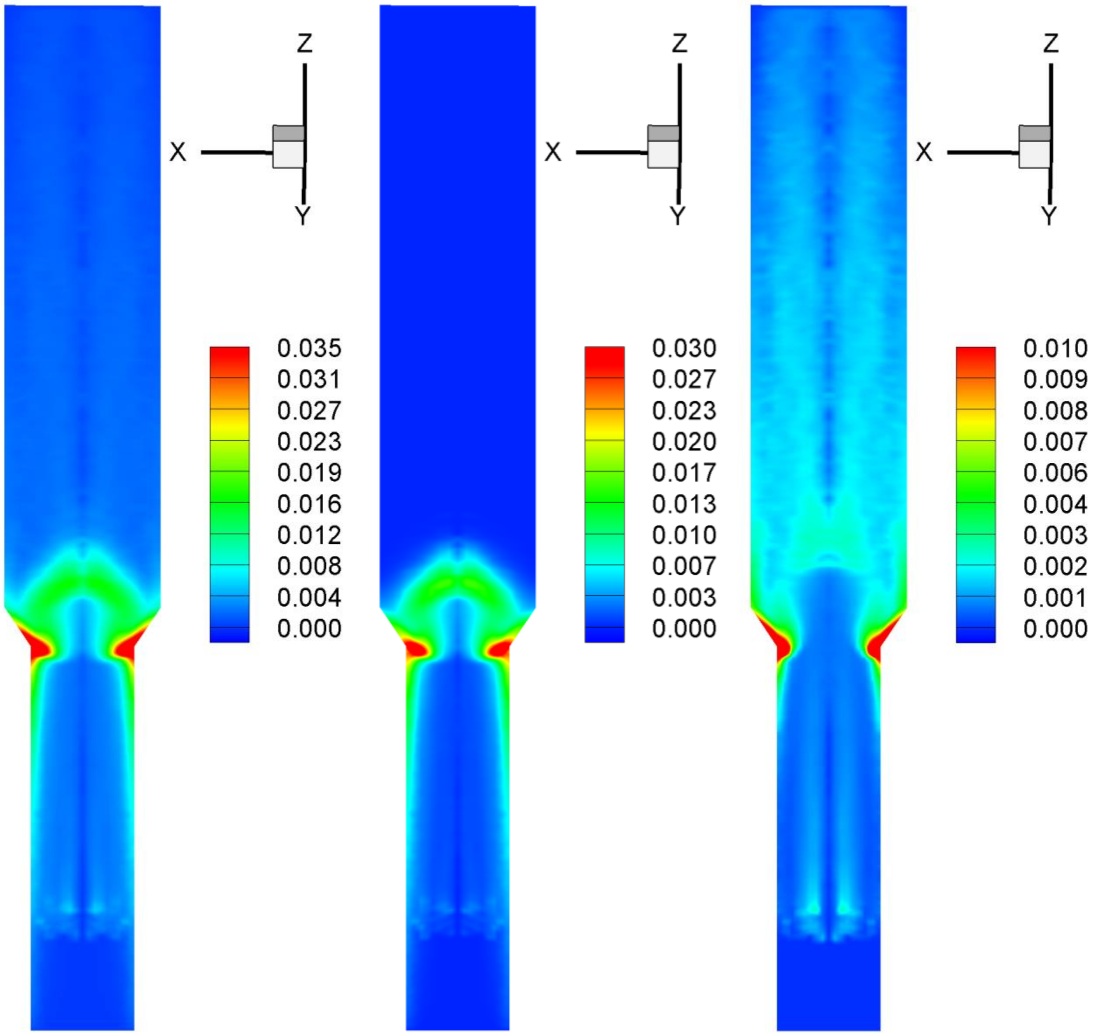

Figure 6-12: Solid volume fraction in an expanded reactor with two group of particles size (0.15mm and 0.2mm). (left: total volume fraction in the bed, middle: large particles, right: small particles).

Figure 6.12 shows the solid fraction of two groups of particles in a expanded reactor. It indicates that bigger particles are accommodated at expansion area while the small particles filled the upper region of the reactor. The sectioning increased the bed conversion comparing to a straight reactor with same solid/gas flow rate where the small particles leaving the domain shortly after inflowing to the reactor.

For a different range of particle sizes the expansion area can be adjusted to obtain the maximum conversion. It cans also be divided into different expansion zones depending on range of particle sizes.

Figure 6.13 indicates the effect of the expansion position on overall particle conversion of the reactor. It shows that increase in expansion location from 2.0m produces a corresponding increase in conversion until a certain limit when conversion begins to drop with further increase in expansion position. The maximum conversion is achieved between 3.0m to 4.0m. The reason for this is that at very low expansion locations, the large particles are not properly converted, and at higher positions the small particles leave the domain very quickly.

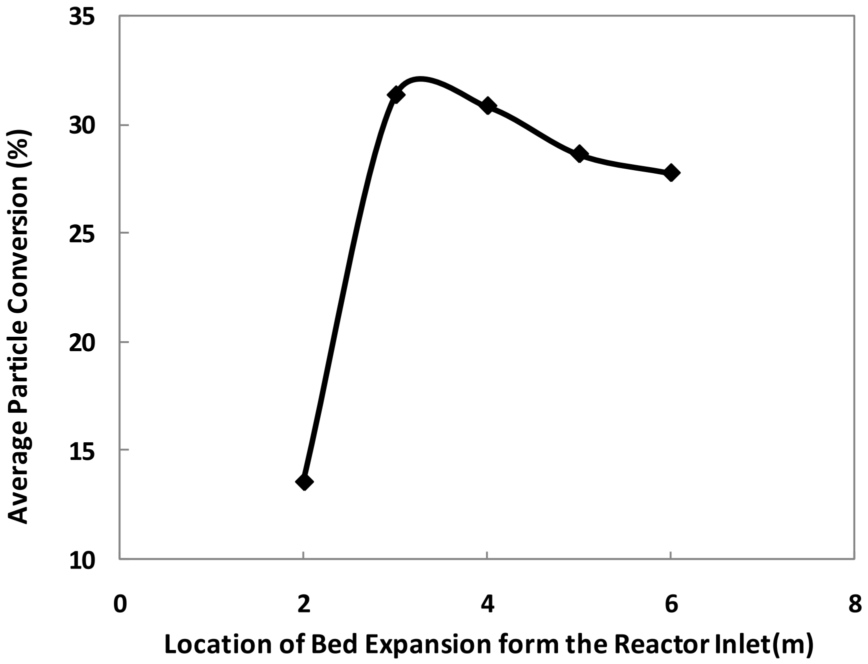

Figure 6-13: Effect of expansion position on over CO_2 conversion of the bed.

6.3.8 Application of 1-D model and Validation

The results of CFD simulation can be used to determine the required input data from hydrodynamics of the reactor for 1-D model. Although the 1-D model requires some parameters from CFD simulation results but it would be much faster in some cases compared to CFD simulations which takes so much time to complete calculations. 1-D model can be used to determine the required reactor length, effect of inlet CO_2 concentration, and carbonation reaction rate as well as particle properties such as CaO active fraction in the bed.

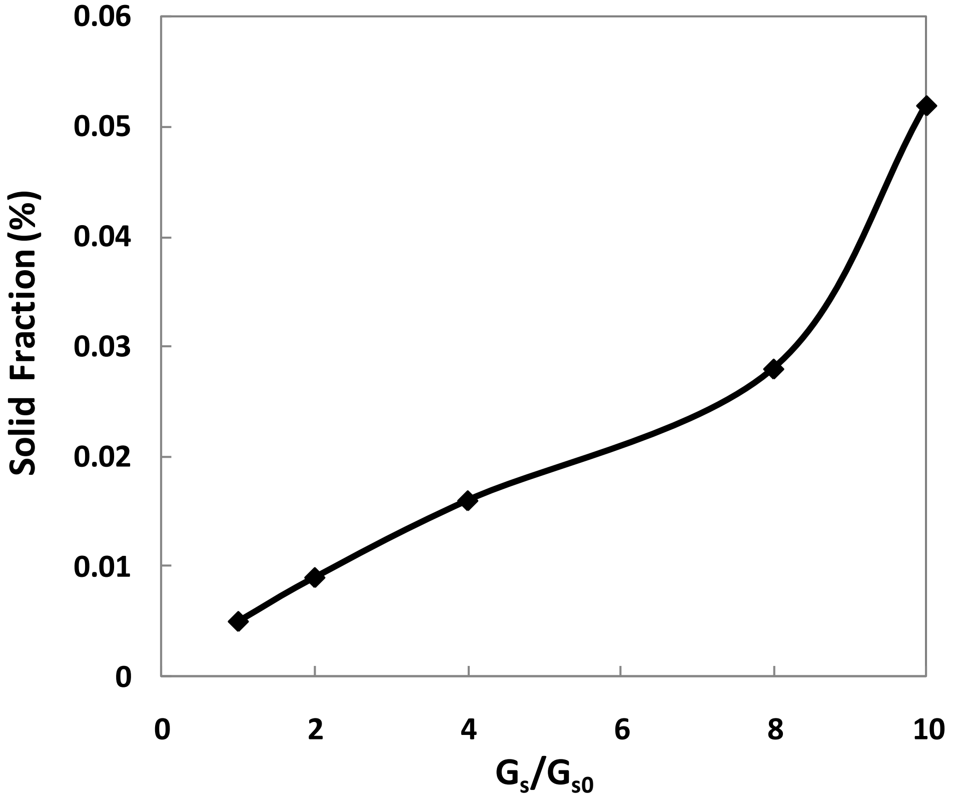

Figure 6-14: Solid volume fraction of lean region at different solid/gas ratios.

Since there is no significant dense region at very dilute operating condition of the fluidized bed reactor, therefore1-D model can be utilized to the lean region to predict the CO_2 concentration, by increasing the ratio of solid to gas the dense region appears in lower section of the reactor. From the result presented in Figure 6.6, it can be deduced that the dense region is developing from 0.5m ($4G_s$) to about 1m (at $10G_s$). Figure 6.14 shows the average solid fraction at lean region which is key input data into the 1-D model. The variation of solid volume fraction at higher solid inventories is bigger because with increase in the solid loading in the bed the dense region moves forward thus the solid fraction ratio of dense to lean decreases.

Using the same operating conditions which are applied in CFD simulation (Figure 6.8 in the mass loading effect section) and also using the solid fraction of the bed from the results as input data for the 1-D model, the Figure 6.15 has been achieved for comparing the CFD result with 1-D model. It shows a good agreement with CFD results in Figure 6.8. There is a little over-prediction of CO_2 when compared with CFD results and this can be due to the dense region which has not been considered in 1-D model. There is a small dense region in CFD results although they are not so pronounced, but they can have a substantial effect on the reaction rate in that region. The results of 1-D model is validated against the experimental data for a given data in chapter 3, therefore good agreement of 1-D model and CFD simulation is the same as agreement of experimental data and CFD model.

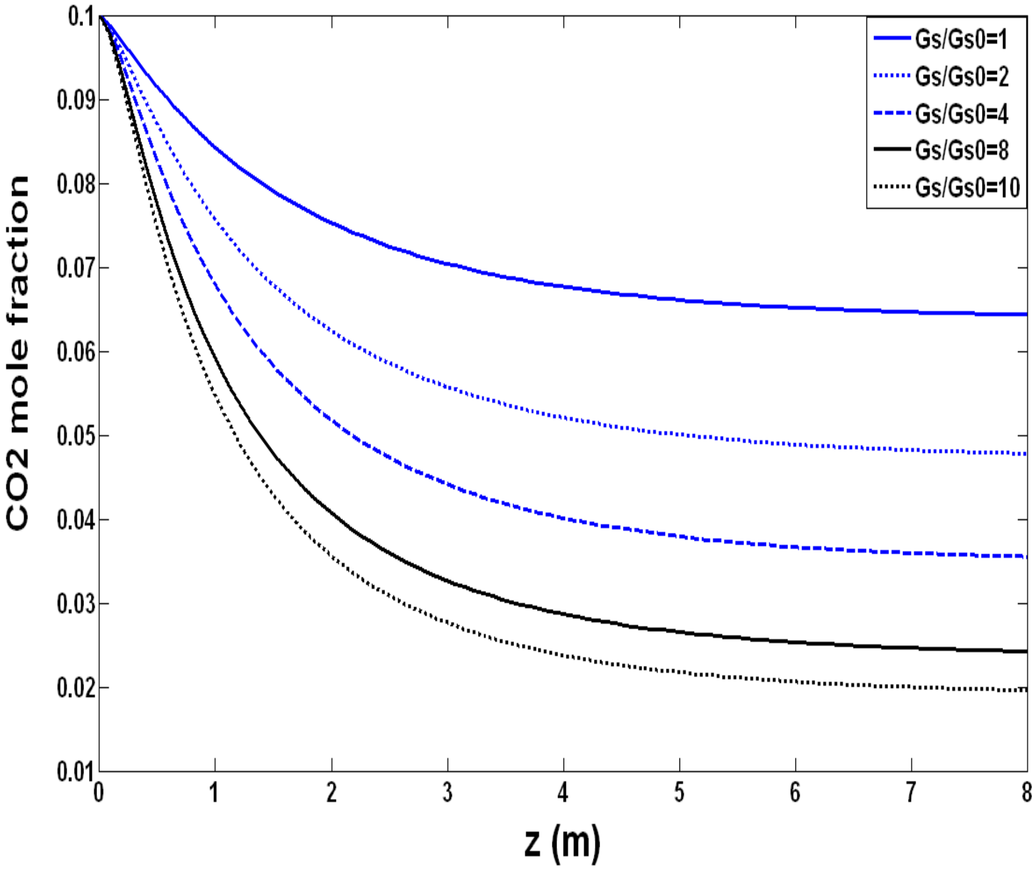

Figure 6-15: Predictive CO_2 mole fraction in 1-D model using the parameters of CFD results.

Figure 6.16 presents the comparison of CO_2 capture in 1-D model and CFD simulation results. It shows that at well diluted operating conditions, the results are in very good agreement. With increasing the solid flow rate the 1-D model provides under predictions in comparison with CFD simulation results. It seems that at high values of solid flow rate the estimation of average volume fraction corresponding to each zone would be difficult and needs more accuracy of data set in to the 1-D model to get more accurate results.

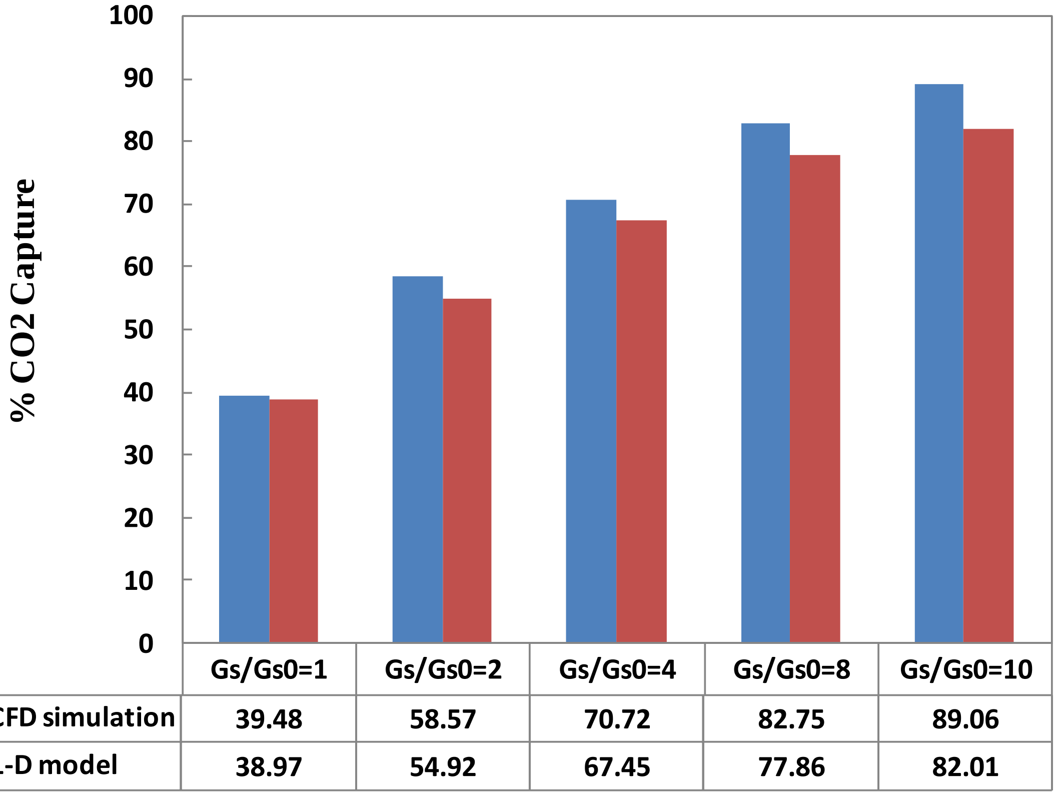

	Gs/Gs0=1	Gs/Gs0=2	Gs/Gs0=4	Gs/Gs0=8	Gs/Gs0=10
🟦 CFD simulation	39.48	58.57	70.72	82.75	89.06
🟥 1-D model	38.97	54.92	67.45	77.86	82.01

Figure 6-16: CO_2 capture in different solid flow rates ($G_{s0} = 0.064 \frac{kg}{m^2 s}$) predicted by CFD simulation and 1-D model.

It also indicates that about 90% of CO_2 can be captured in a single fluidized bed reactor with fresh solid sorbent. In a circulating fluidized bed reactor with make-up flow, it can still be achieved 90% of CO_2 capture but it needs more solid flow rate (circulating the solid) and also more energy required to process this volume of solid. Depending on the cost of the process associated with particle preparation (transport, grinding, sieving, etc.) and operating cost corresponding to the solid circulation, the value of make-up flow must be optimized to reduce the total cost of the process. The make-up flow can change from a maximum value (at zero circulation rate) to a minimum value (maximum circulation rate) which can be adjusted based on the minimum cost of the whole capture process.

6.4 Conclusions

A fluidized bed reactor has been modelled using an Eulerian/Lagrangian CFD model that considers particle tracking and heterogeneous reaction associated with the carbonation reaction between CaO and CO_2. The study highlights the importance of several factors in a fluidized bed reactor that are essential to a successful design.

The gas-solid contact has been studied with regard to the hydrodynamics of particle fluidization and mass transfer due to the carbonation reaction. The results indicate that different solid zones exist inside the reactor corresponding to different particle seizes. The simulation can correctly predict the reactor dimensions based on the ultimate conversion required. The particle residence time is another important parameter in the design and this model demonstrated the capability to give enough detail of the residence time and collection of particles depending on size. However, the evidence given by the model is that such a design is possible and gives a practical means of removing CO_2 emissions from large sources using existing technology.

The geometry of the reactor plays an important role in carbon capture efficiency. This effect is more pronounced when the range of the particle size is wide. A proper reactor length as well as the expansion area and the amount of the expansion also can be predicted for reactor design purpose.

chapter 7

Conclusions and Future Work

7.1 Conclusions

CO_2 capture and storage has been reviewed in view of its importance and a variety of alternative technologies were also presented. Fluidization system and governing equations are presented. Post-combustion capture with solid sorbent from power plants' flue gases has been studied particularly in this work.

Modelling and CFD simulation of a fluidized bed reactor have been carried out to enhance the understating of gas-solid behaviour, reactor hydrodynamic and possibility of a steady state operating system in industrial scale. Eulerian/Lagrangian CFD model is used in this simulation. Numerical solution with CFD technique in a FORTRAN based in-house code has been utilised to explore the reactor performance. This involves particle tracking with heterogeneous gas-solid reaction to estimate the ultimate residence time and conversion of every individual particle in trajectories inside the reactor. In particular, an enhancement of particle's residence time has been sought by the modification of the reaction domain, and has been found to play a key role in CO_2 conversion.

- A 1-D Kunii-Levenspiel model is adapted into a fluidized bed reactor for carbon capture with CaO particles. Both CFD and 1-D models were utilised in the investigation in a fashion that avoids unnecessary repetitions of CFD simulation thereby reducing computational expense. Hydrodynamic parameters (such as solid volume fraction) from CFD simulation have been used as input data to 1-D model to get profiles of gas concentration. This model is validated against the available data from the literature and the agreement was acceptable as shown in the result section.

- Hydrodynamics of a fluidized bed in 2-D Cartesian, 3-D and effect of key parameters were also investigated in this work. It has been established that appropriate operating condition as well as shape of the geometry lead to a high efficiency of CO_2 capture in a fast fluidized bed reactor. The model was also successful in predicting the proper reactor geometry of fluidized bed reactor required to obtain a specified ultimate CO_2 removal.

- It has been demonstrated in this study that using a single fluidized bed with fresh sorbent can remove almost 90% of gas flow CO_2 content. Well-reacted particles deposits readily on the walls of the reactor to be collected and removed from the system. Particles can reach to up to 65% of conversion during the residing inside the reactor.

- It has also been demonstrated that using an expanded reactor can give high conversion rate of solid sorbent when the reactor is operating with non-uniform size of particles. These key factors are essential in design of appropriate reactors for power plants with fossil fuel combustion which emits a high level of CO_2 to the atmosphere. The regulation of expansion is based on the size distribution and variety in the system. In some cases multi-extension may be require to get maximum conversion in a fluidized bed reactor.

7.2 Recommendations for future work

- Using a fluidized bed reactor operating at maximum conversion of solid sorbents is essential. For this purpose and considering the sintering of particle's surface due to an initial fast carbonation reaction it can be concluded that controlling the rate of reaction at initial stages can help to use the maximum capacity of particle's porosity. In order to use the maximum capacity of a particle, the gas should diffuse easily inside the particle with no blockage on the surface of particle to allow the gas flow in to the centre of the particle. This can be practicable if the initial fast reaction can be slowed down to allow the gas to diffuse inside the particle before the sintering. Since the reaction during carbonation is a function of CO_2 concentration of the carrier gas, operating at low CO_2 concentration initially and differentially increasing of CO_2 concentration exposed to the particle can be a suitable approach to gain a maximum possible conversion. Investigation of this approach in a future work is strongly recommended. It is difficult to establish such equipments, but as a solution the feeding particles into the reactor can be contacted with reactor outlet gas flow before entering into the reactor. In this case the height of the feeder needs to be higher enough (depending on the particle size to provide some residence time for particles in a counter-current flow contactor (feeding particles with carbonator reactor outlet gas flow). In this scenario at feeding section the most active CaO particles (in top of the feeder) would be in contact with a gas phase with lowest CO_2 fraction and by moving further down in the feeder contactor the differential increment at CO_2 fraction and reduction at CaO activity proceeds till to the end of the feeder (solid inlet of the carbonator reactor).

- Further inter-particle collision is expected to be important in systems involving high volumes of solid circulation such as circulating fluidized bed. For such reaction scenarios, a four-way coupling is required to handle the inter-particles collision. Thus, it is strongly recommended here that future works should consider a full fledge four-way coupling as opposed to two-way coupling considered in this present study.
- Establishing an experimental rig to confirm the simulation results regarding the bed expansion is also recommended. CFD simulation results and experimental study can be utilized also to set up a pilot plant of a fluidized bed reactor in future.

References

[1] J. Hansen, M. Sato, R. Ruedy, K. Lo, D.W. Lea, and M. Medina-Elizade. “Global Temperature Change”, Proceedings of the National Academy of Science 103, no. 39 (2006).

[2] IPCC, 2005 – B. Metz, O. Davidson, H.d. Coninck, M. Loos and L. Meyer (Eds.) Cambridge University Press, UK. pp 431.

[3] B.R. Stanmore and P. Gilot, “Review—Calcination and carbonation of limestone during thermal cycling for CO_2 sequestration”, Fuel Processing Technology 86 (2005) 1707– 1743.

[4] C.K. Yi, S.H. Jo, Y. Seo, J.B. Lee, C.K. Ryu, “Continuous operation of the potassium-based dry sorbent CO_2 capture process with two fluidized-bed reactors”, greenhouse gas control 1 (2007) 31 – 36.

[5] IEA (2010), Energy Technology Perspectives: scenarios and strategies to 2050, France.

[6] POSTnote, The Parliamentary Office of Science & Technology, Carbon capture and storage, 2005, No:238.

[7] IPCC, 2007- M.L. Parry, O.F. Canziani, J.P. Palutikof, , P.J. Linden, C.E. Hanson, Cambridge University Press, Cambridge.

[8] A.B. Rao, E.S. Rubin, D.W. Keith1, M.G. Morgan, ‘Evaluation of potential cost reductions from improved amine-based CO_2 capture systems’, Energy Policy 34 (2006) 3765–3772.

[9]W.J.J. Huijgen, R.N.J. Comans, G.J. Witkamp. 'Cost evaluation of CO_2 sequestration by aqueous mineral carbonation', Energy Conversion and Management 48 (2007) 1923–1935.

[10] M. Alonso, N.Rodríguez, G.Grasa, J.C.Abanades, 'Modelling of a fluidized bed carbonator reactor to capture CO_2 from a combustion flue gas', Chemical Engineering Science 64 (2009) 883 – 891.

[11] J. Oexmann and A. Kather, 'Post-combustion CO_2 capture in coal-fired power plants: comparison of integrated chemical absorption processes with piperazine promoted potassium carbonate and MEA', Energy Procedia 1 (2009) 799–806.

[12]Y. Yongping, Z. Rongrong, D. Liqiang, M. Kavosh, K. atchigolla, J. Oakey, 'Integration and evaluation of a power plant with a CaO-based CO_2 capture system', International Journal of Greenhouse Gas Control 4 (2010) 603–612.

[13] T. Kuramochi, A.Faaij, A. Ramı´rez, W. Turkenburg , 'Prospects for cost-effective post-combustion CO_2 capture from industrial CHPs', International Journal of Greenhouse Gas Control 4 (2010) 511–524.

[14] E.J. Anthony. Solid looping cycles: A new technology for coal conversion, Industrial Engineering Chemical Research, 47 (2008) 1747-1754.

[15] J. Ströhle, A. Galloy, B. Epple, 'Feasibility Study on the Carbonate Looping Process for Post-Combustion CO_2 Capture from Coal-Fired Power Plants', Energy Procedia 1 (2009) 1313–1320.

[16] J.C. Abanades. The maximum capture efficiency of CO_2 using carbonation/calcination cycle of CaO/CaCO3', Chem. Eng. J. 90 (2002) 303–306.

[17] T. Shimizu, T. Hirama, H. Hosoda, K. Kitano, M. Inagaki and Tejima, 'A twin fluidized-bed reactor for removal of CO_2 from combustion process', Trans IChemE, Vol 77, Part A, January 1999.

[18] J. Wang, E.J. Anthony, J.C. Abanades, 2004: Clean and efficient use of petroleum coke for combustion and power generation. Fuel, 83, 1341-1348.

[19] D. Alvarez, J.C. Abanades, "Pore-size and shape effects on the re-carbonation performance of calcium oxide submitted to repeated calcinations /recarbonation cycles", Energy and Fuels, 19(2005), 270–278.

[20] G.S. Grasa, J.C. Abanades, M. Alonso., B. Gonzalez, Reactivity of highly cycled particles of CaO in a carbonation/calcination loop, Chem. Eng. J. 137 (2008) 561-567.

[21] L.M. Romeo, Y. Lara, P. Lisbona, J.M. Escosa, 'Optimizing make-up flow in a CO_2 capture system using CaO', Chemical Engineering Journal 147 (2009) 252–258.

[22] Q. Zhou, D. Peng, Z. Peng, G. Liu, X. Li, "Agglomeration of gibbsite particles from carbonation process of sodium aluminate solution", Hydrometallurgy 99 (2009) 163–169.

[23] H. Knuutila, H.F. Svendsen, M. Anttila, 'CO_2 capture from coal-fired power plants based on sodium carbonate slurry; a systems feasibility and sensitivity study', international journal o f greenhouse gas control 3 (2009) 143 – 151.

[24] K. Wang, X. Guo, P. Zhao, F. Wang, C. Zheng, 'High temperature capture of CO_2 on lithium-based sorbents from rice husk ash', Journal of Hazardous Materials 189 (2011) 301–307.

[25] L.M. Romeo, Y. Lara, P. Lisbona, A. Martinez, 'Economical assessment of competitive enhanced limestones for CO_2 capture cycles in power plants', Fuel Process Technol, 90 (2009), 803–11.

[26] A. MacKenzie A, D.L. Granatstein, E.J. Anthony, J.C. Abanades, “Economics of CO_2 capture using the calcium cycle with a pressurized fluidized bed combustor”, Energy Fuel 2007;21:920–6.

[27] C. Salvador, D. Lu, E.J. Anthony, J.C. Abanades, ‘Enhancement of CaO for CO_2 capture in an FBC environment’, Chem. Eng. J. 96 (1–3) (2003) 187–195.

[28] J.C. Abanades, E.J. Anthony, D.Y. Lu, C. Salvador, D. Alvarez, ‘Capture of CO_2 from combustion gases in a fluidized bed of CaO’, AIChE J. 50 (2004) 1614–1622.

[29] J.C. Abanades, E.J. Anthony, J. Wang, J.E.Oakey, ‘Fluidized bed combustion systems integrating CO_2 capture with CaO’, Environ. Sci. Technol. 39 (2005) 2861–2866.

[30] G. Grasa, R. Murillo, M. Alonso, J.C. Abanades, ‘Application of the Random Pore Model to the Carbonation Cyclic Reaction’, AIChE Journal, 2009 Vol. 55, No. 5.

[31] N.H. Florin and A.T. Harris “Preparation and Characterization of a Tailored Carbon Dioxide Sorbent for Enhanced Hydrogen Synthesis in Biomass Gasifiers”, Ind. Eng. Chem. Res., 2008, 47 (7), pp 2191–2202.

[32] V. Manovic, E.J. Anthony, D. Loncarevic, ‘CO_2 looping cycles with CaO-based sorbent pretreated in CO_2 at high temperature’, Chemical Engineering Science 64 (2009) 3236 – 3245.

[33] R. Barker, 1973. Reversibility of the reaction CaCO3 = CaO + CO_2. Journal of Applied Chemistry and Biotechnology 23(10): 733-742.

[34] M. Aihara, T. Nagai, J. Matsushita, Y. Negishi, H. Ohya, “Development of porous solid reactant for thermal-energy storage and temperature upgrade using arbonation/decarbonation reaction”, Applied Energy, 69, (2001), 225-238.

[35] J. Mastin, A. Aranda, J. Meyer, 'New synthesis method for CaO-based syntheticsorbents with enhanced properties for high-temperature CO_2 –capture', 10th International Conference on Greenhouse Gas Control Technologies. Volume 4, 2011, Pages 1184-119.

[36] N. Florin and P. Fennell, 'SyntheticCaO-based sorbent for CO_2 capture,' 10th International Conference on Greenhouse Gas Control Technologies. Volume 4, 2011, Pages 830-838.

[37] D. Gidaspow, Multiphase Flow and Fluidization Continuum and Kinetic Theory Descriptions, Academic Press, New York, 1994.

[38] G. Grasa, J.C. Abanades, "CO_2 capture capacity of CaO in Long Series of Carbonation/Calcination Cycles", Industrial and Engineering Chemistry Research, 45 (26), (2006), 8846-8851.

[39] F. Fang, Z.S. Li, N.S. Cai, 'Experiment and Modelling of CO_2 Capture from Flue Gases at High Temperature in a Fluidized Bed Reactor with Ca-Based Sorbents', Energy & Fuels (2009), 23, 207–216.

[40] IEA (2000), Energy Technology and Climate Change: A Call to Action, OECD and IEA, Paris.

[41] N. Rodriguez, M. Alonso, G. Grasa, J.C. Abanades, "Heat requirements in a calciner of CaCO3 integrated in a CO_2 capture using CaO," Chem. Eng. Jl, 138:1-3, 148, (2008).

[42] I. Martínez, G. Grasa, R. Murillo, B. Arias and J. C. Abanades, "Kinetics of Calcination of Partially Carbonated Particles in a Ca-Looping System for CO_2 Capture", Energy Fuels, 2012, 26 (2), pp 1432–1440.

[43] A. Charitos, N. Rodríguez, C. Hawthorne, M. Alonso, M. Zieba, B. Arias, G. Kopanakis, G. Scheffknecht, J.C. Abanades, "Experimental Validation of the Calcium

Looping CO_2 Capture Process with Two Circulating Fluidized Bed Carbonator Reactors", Ind. Eng. Chem. Res., 2011, 50 (16), pp 9685–9695.

[44] IPCC, 2001- J. T. Houghton, Y. Ding, D. J. Griggs, M. Noguer, P. J. van der Linden, X. Dai, K. Maskell and C. A. Johnson. Cambridge University Press, Cambridge, UK, and New York, USA.

[45] A. Chakma, A.K. Mehrotra, B. Nielsen, Comparison of chemical solvents for mitigating CO_2 emissions from coal-fired power-plants, Heat Recovery Syst 1995; 15:231–240.

[46] B. Metz, O Davidson, P. Bosch, R. Dave, L.A. Meyer. Contribution of Working Group III to the Fourth Assessment Report of the Intergovernmental Panel on Climate Change. Cambridge Univ. Press, UK and New York (USA), 2007.

[47] P. D. Cobden, P.V. Beurden, H.Th.J. Reijers, G.D. Elzinga, S.C.A. Kluiters, J. W. Dijkstra, D. Jansen, R.W. van den Brink. 'Sorption-enhanced hydrogen production for pre-combustion CO_2 capture: Thermodynamic analysis and experimental results' greenhouse ga s control 1(2007) 170 – 179.

[48] P. Linga, R. Kumar, P. Englezos, 'The clathrate hydrate process for post and pre-combustion capture of carbon dioxide', Journal of Hazardous Materials 149 (2007) 625–629.

[49] A.B. Rao, E.S. Rubin, "A technical, economic, and environmental assessment of amine-based CO_2 capture technology for power plant greenhouse gas control", Environmental Science and Technology 36, (2002) 4467–4475.

[50] W.J.J. Huijgen, G.J. Ruijg, R.N.J. Comans, G.J. Witkamp, 'Energy consumption and net CO_2 sequestration of aqueous mineral carbonation', Industrial Eng Chem Res 2006;45(26):9184–94.

[51] G. Léonard and G. Heyen, 'Modeling post-combustion CO_2 capture with amine solvents', Computer Aided Chemical Engineering Volume 29, 2011, Pages 1768-1772.H. Enwald, E. Peirano, A.E. Almstedt, Eulerian two-phase flow theory applied to fluidization, Int. J. Multiph. Flow 22 (1996) 21– 66.

[52] U. Desideri, A. Paolucci, 'Performance modelling of a carbon dioxide removal system for power plants', Energy Conversion & Management 40 (1999) 1899±1915.

[53] D. Singh, E. Croiset, P.L. Douglas, M.A. Douglas, 'Techno-economic study of CO_2 capture from an existing coal-fired power plant: MEA scrubbing vs. O_2/CO_2 recycle combustion', Energy Conversion and Management 44 (2003) 3073–3091.

[54] W.J.J. Huijgen, "Carbon dioxide sequestration by mineral carbonation, Thesis, Energy research Centre of the Netherlands", The Netherlands, (2007), ISBN: 90-8504-573-8.

[55] N.A. Røkke, Ø. Langørgen, 'Enabling pre-combustion plants – the DECARBit project', Energy Procedia 1 (2009) 1435–1442.

[56] H. Audus, O. Kaarstad, G. Skinner. 'CO_2 Capture by Pre-combustion Decarbonisation of Natural Gas Series', Interlaken,Switzerland 1998.

[57] C. Powell, G. Qiao, "Polymeric CO_2/N_2 gas separation membranes for the capture of carbon dioxide from power plant flue gases", J.Membr.Sci.279, 1–49 (2006).

[58] R. Bredesen, T.A. Peters, "Membranes in Energy Systems with CO_2 Capture, in Membranes for Energy Conversion", Volume 2 (eds K.-V. Peinemann and S. Pereira Nunes), Wiley-VCH Verlag GmbH & Co. KGaA, Weinheim, Germany. doi: 10.1002/9783527622146.ch7 (2008).

[59] C.A. Scholes, K.H. Smith, S.E. Kentish, G.W. Stevens, 'CO_2 capture from pre-combustion processes srategies for membrane gas separation', International Journal of Greenhouse Gas Control 4 (2010) 739–755.

[60] M. Kanniche, R. Gros-Bonnivard, P. Jaud, J. Valle-Marcos, J.M. Amann, C. Bouallou, 'Pre-combustion, post-combustion and oxy-combustion in thermal power plant for CO_2 capture', Applied Thermal Engineering 30 (2010) 53–62.

[61] Vattenfal- Carbon capture and storage. URL: http://www.vattenfall.com

[62] A.P. Simpson, A.J. Simon, 'Second law comparison of oxy-fuel combustion and post-combustion carbon dioxide separation', Energy Conversion and Management 48 (2007) 3034–3045.

[63] N. Zhang, N. Lior, 'Two novel oxy-fuel power cycles integrated with natural gas reforming and CO_2 capture' Energy, 2006.

[64] W. Chunbo, J. Lufei, T. Yewen, E.J. Anthony, 'Carbonation of fly ash in oxy-fuel CFB combustion' Fuel xxx (2007).

[65] B.M. Abraham, J.G. Asbury, E.P. Lynch, A.P.S. Teotia. Coal-oxygen process provides carbon dioxide for enhanced recovery. Oil Gas J1982;80(11):68–70.

[66] T. Kiga, S. Takano, N. Kimura, K. Omata, M. Okawa, T. Mori. Characteristics of pulverised-coal combustion in the system of oxygen/recycled flue gas combustion. Energy Conversion and Management 38, 134 (1997).

[67] B.J.P. Buhre, L.K. Elliott, C.D. Sheng, T.F.W. Gupta. Oxy-fuel combustion technology for coal-fired power generation. Prog Energy Combust 2005;31:283–307.

[68] H. Li, J. Yan. Preliminary study on CO_2 processing in CO_2 capture from oxy-fuel combustion. ASME paper GT2007-27845; 2007.

[69] W. San, H. Jericha B. Bauer, E. Goettlich. “Qualitative and quantitative comparison of two promising oxy-fuel power cycles for CO_2 capture”. ASME paper GT2007-27375; 2007.

[70] P.Glarborg, L.L.B. Bentzen. Chemical effects of a high CO_2 concentration in oxy-fuel combustion of methane. Energy & Fuels 22, 291–296 (2008).

[71] E.S. Hecht, C.R. Shaddix, A. Molina, B.S. Haynes, ‘ Effect of CO_2 gasification reaction on oxy-combustion of pulverized coal char’, In: 33rd Symposium (International) on Combustion, pp. 1699–1706 (2010).

[72] S.K. Park, T.S. Kim, J.L. Sohn, Y.D. Lee, ‘An integrated power generation system combining solid oxide fuel cell and oxy-fuel combustion for high performance and CO_2 capture’, Applied Energy 88 (2011) 1187–1196.

[73] M.B. Toftegaard , J. Brix, P.A. Jensen , P. Glarborg, A.D. Jensen, ‘Oxy-fuel combustion of solid fuels’,Progressin Energy and Combustion Science 36 (2010) 581e625.

[74] K. Chrissafisa, C. Dagounaki, K.M. Paraskevopoulos, ‘The effects of procedural variables on the maximum capture efficiency of CO_2 using a carbonation/calcination cycle of carbonate rocks’, Thermochimica Acta 428 (2005) 193–198.

[75] M. Vasilije, “Steam Reactivation of Spent CaO-Based Sorbent for Multiple CO_2 Capture Cycles”; Anthony, Edward J. Environmental Science & Technology vol. 41 issue 4 February 15, 2007. p. 1420-1425.

[76] Z. Chen, C. J. Lim, J.R. Grace, ‘Study of limestone particle impact attrition, Chemical Engineering Science 62 (2007) 867 – 877.

[77] D. A. Green, B.S. Turk, R.P. Gupta, A. Lopez-Ortiz, D.P. Harrison, Y. Liang, ‘ Carbon Dioxide Capture from Flue Gas Using Dry, Regenerable Sorbents’, Reporting

Period: April 1, 2001 to June 30, 2001, DOE Cooperative Agreement No.: DE-FC26-00NT40923.

[78] W.K. O'Connor, D,C. Dahlin, P.C. Turner, and R. Walters, 'carbon dioxide sequestration by ex-suit mineral carbonation', American Society of Mechanical Engineers, Washington, D.C., 1999.

[79] W.J.J. Huijgen, G.J. Ruijg, R.N.J. Comans, G.J. Witkamp, 'Aqueous mineral carbonation as a possible CO_2 sequestration process', the 8th international conference on GreenHouse Gas control Technologies (GHGT-8), Trondheim, Norway, 2005, ECN-RX--06-069.

[80] F.S. Zeman, K. S. Lackner, "Capturing carbon dioxide directly from the atmosphere", World Resources Review, 16 (2004) 62–68.

[81] N. V., G´alvez M.E., Steinfeld A., "Kinetic analysis of the carbonation reactions for the capture of CO_2 from air via the Ca(OH)2–$CaCO_3$–CaO solar thermochemical cycle", Chemical Engineering Journal 129 (2007) 75–83.

[82] S. Freguia, G. T. Rochelle, 'Modelling of CO_2 capture by aqueous mono-ethanolamine', Aiche J 2003, 49, (7), 1676-1686.

[83] P. Moresa, N. Scennaa, S. Mussati, 'Post-combustion CO_2 capture process: Equilibrium stage mathematical model of the chemical absorption of CO_2 into monoethanolamine (MEA) aqueous solution', chemical engineering research and design 89 (2011) 1587–1599.

[84] L. Zhao, E. Riensche, R. Menzer, L. Blum, D. Stolten, 'A parametric study of CO_2/N_2 gas separation membrane processes for post-combustion capture', Journal of Membrane Science 325 (2008) 284–294.

[85] H.F. Nicholas, B. John and S.F. Paul, “ynthetic CaO-Based Sorbent for CO_2 Capture from Large-Point Sources”, Energy Fuels, 2010, 24 (8), pp 4598–4604.

[86] S. Chi and G. Rochelle, “Oxidative Degradation of Monoethanolamine”, First International Conference on CO_2 Sequestration, Washington, DC, US. 2001.

[87] T. Supap, R. Idem, P. Tontiwachwuthikul, C. Saiwan, “The roles of O2 and SO2 in the degradation of monoethanolamine during CO_2 absorption from industrial flue gas streams”, EIC Climate Change Technology, IEEE, (2006) 1-6.

[88] G.T. Rochelle, G.S. Goff, J.T. Cullinane, S. Freguia, “Research Results for CO2 Capture from Flue Gas by Aqueous Absorption/Stripping”, The University of Texas at Austin, Austin, Texas USA, presented at the Laurance Reid Gas Conditioning Conference, Norman, Oklahoma USA, February (2002) 25-27.

[89] H.P.Mangalapally, R. Notz, N. Asprion, G. Sieder, H. Garcia, H. Hasse, “Pilot plant study of four new solvents for post combustion carbon dioxide capture by reactive absorption and comparison to MEA.”, International Journal of Greenhouse Gas Control vol. 8 May, 2012. p. 205-216.

[90] T.C. Merkel, H. Lin, X. Wei and R. Baker, “Power plant post-combustion carbon dioxide capture: An opportunity for membranes”, Journal of Membrane Science 359 (2010) 126–139.

[91] X. Li, M.F. Bertos, C.D. Hills, P.J. Carey, S. Simon, ‘Accelerated carbonation of municipal solid waste incineration fly ashes’, Waste Management 27 (2007) 1200–1206.

[92] P. Valentina, P. Alessandra, B. Renato, “Gas–solid carbonation kinetics of Air Pollution Control residues for CO_2 storage. ”, Chemical Engineering Journal vol. 148 issue 2-3 May 15, 2009. p. 270-278

[93] P.J. Gunning, C.D. Hills, and P.J. Carey, “Accelerated carbonation treatment of industrial wastes”, Waste Management, 30 (6), (2010), pp. 1081-1090. ISSN 0956-053X.

[94] M.F. Bertos, S.J.R. Simons, C.D. Hills, P.J. Carey, ‘A review of accelerated carbonation technology in the treatment of cement-based materials and sequestration of CO_2’, Journal of Hazardous Materials B112 (2004) 193–205.

[95] Q. Chen, Y. Ke, L. Zhang, M. Tyrer, C.D. Hills, G. Xue, ‘Application of accelerated carbonation with a combination of Na2CO3 and CO_2 in cement-based solidification/stabilization of heavy metal-bearing sediment’, Journal of Hazardous Materials 166 (2009) 421–427.

[96] H. Gupta and L.S. Fan, “Carbonation-Calcination Cycle Using High Reactivity Calcium Oxide for Carbon Dioxide Separation from Flue Gas”, Ind. Eng. Chem. Res. 2002, 41, 4035-4042.

[97] A. Silaban, D.P. Harrison,. High temperature capture of carbon dioxide: characteristics of the reversible reaction between CaO(s) and CO2(g). Chemical Engineering Communications 137, 177–190 (1995).

[98] A. Charitos, C. Hawthorne, A.R. Bidwe, S. Sivalingam, A. Schuster, H. Spliethoff, G. Scheffknecht, ‘Parametric investigation of the calcium looping process for CO_2 capture in a 10kWth dual fluidized bed’, International Journal of Greenhouse Gas Control (IJGGC-296 (2010)).

[99] J. David, “Economic Evaluation of Leading Technology Options for Sequestration of Carbon Dioxide,” M.S. Thesis, Technology and Policy Program, MIT, Cambridge, MA (2000).

[100] K.S. Lackner, C.H. Wendt, D.P. Butt, E.L. Joyce, D.H. Sharp. Carbon Dioxide Disposal in Carbonate Minerals. Energy 20, (1995), 1153–1170.

[101] J. Ding and D. Gidaspow, A bubbling fluidization model using kinetic theory of granular flow, A.I.Ch.E. Journal 36 (1990), pp. 523–538.

[102] S. Benyahia, H. Arastoopour, T.M. Knowlton and H. Massah, Simulation of particles and gas flow behavior in the riser section of a circulating fluidized bed using the kinetic theory approach for the particulate phase, Powder Technology 112 (1–2) (2000), pp. 24–33

[103] A. Neri, D. Gidaspow, "Riser hydrodynamics: simulation using kinetic theory. Particle Technology and Fluidization", AIChE Journal. 46(2000), 52– 67.

[104] Y. Zeng, X. Wan, Z. Qian, F. Wei and Y. Jin, "Numerical simulation of the gas-particle turbulent flow in riser reactor based on k-ε-k_p-ε_p-T two-fluid model," Chem. Eng. Sci, 56, (2001,) 6813-6822.

[105] D.J. Patil, A.V. Annaland and J.A.M. Kuipers, Critical comparison of hydrodynamic models for gas–solid fluidized beds—part II: freely bubbling gas–solid fluidized beds, Chemical Engineering Science 60 (1) (2005), pp. 73–84.

[106] Ergun, S., Orning, A.A. "Fluid Flow Through Packed Columns", Chemical Engineering Progress. 48 89-94 (1952).

[107] D. Kunii, and O. Levenspiel, "Fluidization Engineering", 2nd edition, Butterworth-Heinemann, Boston, 1991.

[108] M. Ishii,. Thermo-Fluid Dynamic Theory of Two Phase Flow. Eyrelles Publisher, Paris, (1975) pp: 275.

[109] Y.V. Ranade, 'Computational flow modelling for chemical reactor engineering', ISBN 0-12-576960-1 (2001).

[110] D.K. Lee. An apparent kinetic model for the carbonation of calcium oxide by carbon dioxide, Chemical Engineering Journal 100 (2004) 71–77.

[111] V. Manovic, E.J. Anthony, “Thermal activation of CaO-based sorbent and self-reactivation during CO_2 capture looping cycles”, Environ. Sci. Technol, 42(2008)4170–4174.

[112] V. Manovic, E.J. Anthony, “Improvement of CaO-based sorbent performance for CO_2 looping cycles”, Thermal Science 2009 Volume 13, Issue 1, Pages: 89-104.

[113] A. Sánchez-Biezma, J.C. Ballesteros, L. Diaz, E. de Zárraga, F.J. Álvarez, J. López, B. Arias, G. Grasa, J.C. Abanades, “Postcombustion CO_2 capture with CaO. Status of the technology and next steps towards large scale demonstration”, Energy Procedia 4 (2011) 852–859.

[114] S.K. Bhatia, D.D. Perlmutter, The effect of product layer on the kinetics of the CO_2-lime reaction, AIChE J. 29 (1983) 79.

[115] O. Levenspiel, Chemical Reaction Engineering, John Wiley & Sons, New York, 1999.

[116] F. Zeman, “Effect of steam hydration on performance of lime sorbent for CO_2 capture, international journal of greenhouse gas control”, 2 (2008) 203 – 209.

[117] R.C. Darton, R.D. LaNauze, J.F. Davidson, D. Harrison. “Bubble growth due to coalescence in fluidised beds”. Transactions of the Institution of Chemical Engineers 55, (1977)274–280.

[118] J. F. Davidson and D.L. Keairns. “Fluidization”. Proceedings of the Second Engineering Foundation Conference, Cambridge: Cambridge University Press, 1978.

[119] E.Turnbull, J.F. Davidson. “Fluidized combustion of char and volatiles from coal”. AIChE J. 30, 881–889 (1984).

[120] A. Lasheras, J. Strohle, A. Galloy, B. Epple, “Carbonate looping process simulation using a 1D fluidized bed model for the carbonator”, International Journal of Greenhouse Gas Control 5 (2011) 686–693.

[121] F. Fang, Z.S. Li, N.S. Cai. “CO_2 capture from flue gases using a fluidized bed reactor with limestone”, Korean J. Chem. Eng., 26(5), 1414-1421 (2009).

[122] C.T. Crowe, “On models for turbulence modulation in fluid-particle flows”, International Journal of Multiphase Flow 26 (2000) 719-727.

[123] J.A.M. Kuipers, K.J. Duin, F.P.H. Beckum, W.P.M. Swaaij, “ A numerical model of gas-fluidized bed”, Chemical Engineering Science 47 (1992), 1913–1924.

[124] T.B. Anderson and R. Jackson, “A fluid mechanical description of fluidized beds. Equations of motion”, Industrial and Engineering Chemistry Fundamentals 6 (1967), 527–539.

[125] D. McBride, N. Croft and M. Cross, ‘Finite volume method for the solution of flow on distorted meshes’, International Journal of Numerical Methods for Heat & Fluid Flow, Vol. 17 Iss: 2 pp. 213 – 239 (2007).

[126] J. Boussinesq, `Theorie de L'Ecoulement Toubillant', Mem. Acad. Sci., 23(46) (1877).

[127] W. Rodi, Turbulence Models and their Application in Hydraulics. Delft International Institute for Hydraulic Research (1980).

[128] D. Tritton,. Physical Fluid Dynamics. Clarendon Press, Oxford (1988).

[129] B.E. Launder and D.B. Spalding, `The Numerical Computation of Turbulent Flows', Computer Methods in Applied Mechanics and Engineering, 3, 269-289 (1974).

[130] M. Nallasamy, "Turbulence Models and Their Application to the Prediction of Internal Flows: A Review", Computers and Fluids, 15(2), 151-194 (1987).

[131] J.S. Shirolkar, C.F.M. Coimbra and M. Queiroz McQuay, "Fundamentals Aspects of Modelling Turbulent Particle Dispersion in Dilute Flows", Prog. Energy Combusti. Sci., Vol. 22, 1996, pp. 363-399.

[132] A.D. Gosman, E. Ioannides. "Aspects of computer simulation of liquid-fueled combustors", 19th Aerospace Sci. Meeting, St. Louis, MO. (1981) Paper AIAA-81-0323,.

[133] C.P. Chen and P.E. Wood, "Turbulence Closure Model for Dilute Gasparticle Flows", Can. J. Chem. Eng. 63, 349–360 (1985).

[134] G.G. Stokes (1851), "On the effect of the internal friction of fluids on the motion of pendulums", Trans. Cambridge Phil. (1851) Soc., 9, 8.

[135] G. Gouesbet, A. Berlemont, A. Picart, "Dispersion of discrete particles by continuous turbulent motions", Extensive discussion of the Tchen's theory, using a two-parameter family of lagrangian correlation functions, Phys. Fluids, 27(4), (1984), 827.

[136] C.M. Tchen, "Mean value and correlation problems connected with the motion of small particles suspended in a turbulent fluid", PhD thesis, Delft University of Technology, The Netherlands (1947).

[137] M.R. Maxey, J.J. Riley, "Equation of motion for a small rigid sphere in a non uniform flow", Phys. Fluids, 26(4), (1983), 883.

[138] L. Schiller, Z. Naumann, "A Drag Coefficient Correlation," Verein Deutscher Ingenieure 77, (1935), 318.

[139] PHYSICA code, the university of Greenwich, URL: http://staffweb.cms.gre.ac.uk/~physica/

[140] B. González, M. Alonso, J.C. Abanades, ‘Sorbent attrition in a carbonation/calcination pilot plant for capturing CO_2 from flue gases ‘,Fuel 89 (2010) 2918–2924.

[141] P. Sun, J.R. Grace, C.J. Lim, E. J. Anthony, ‘Adiscrete-pore-size-distribution-based gas–solid model and its application to the CaO + CO_2 reaction’, Chemical Engineering Science 63 (2008) 57 – 70.

[142] S. Elgobashi, “Particle-Laden Turbulent Flows: Direct Numerical Simulation and Closure Models”, Appl. Sci. Res., 48,3-4, (1991) 301-304.

[143] D. B. Spalding, `A Novel Finite Difference Formulation for Differential Expressions Involving both First and Second Derivatives', International Journal for Numerical Methods in Engineering, 4, 551-559 (1972).

[144] R. Courant, E. Isaacson and M. Rees, `On the Solution of Nonlinear Hyperbolic Differential Equations by Finite Difference', Communications in Pure and Applied Mathematics, 5, 243-255 (1952).

[145] S.V. Patankar, Numerical Heat Transfer and Fluid Flow. McGraw-Hill, New York (1980).

[146] G. S. Djambazov, "Zonal Method for Simultaneous Definition of Block-Structured Geometry and Mesh", Journal of Algorithms & Computational Technology, Volume 6, Number 1, pp. 203-218, March 2012, ISSN 1748-3018, doi: 10.1260/1748-3018.6.1.203

[147] E. Abbasi, H. Arastoopour, “CFD Simulation of CO_2 Sorption in a Circulating Fluidized Bed Using Deactivation Kinetic Model”, Proceeding of the Tenth International

Conference on Circulating Fluidized Beds and Fluidization Technology, CFB-10, edited by T. M. Knowlton, ECI, New York (2011): 736-743.

[148] Y. Zhao, Y. Ding, C. Wu, Yi Cheng, “Numerical simulation of hydrodynamics in downers using a CFD–DEM coupled approach”, Powder Technology 199 (2010) 2–12.

[149] S. Bhusarapu, M.H. Al-Dahhan, M.P. Duduković, “Solids flow mapping in a gas–solid riser: Mean holdup and velocity fields”, Powder Technology 163 (2006) 98–123.

[150] M. Tartan, D. Gidaspow, “Measurement of granular temperature and stresses in risers”, AIChE J., 50: 1760–1775 (2004). doi: 10.1002/aic.10192.

Appendices

Appendix A.1

Particle velocity and momentum

##

Particle momentum equation is solved to update particles new velocities as well as the source terms of momentum which are used in two ways coupling to see the effect of particles motion on gas phase.

##

```
C----------------------------------------------------------------------
C     Calculate slip velocity, Reynolds number and drag coefficient.
C  Arguments
C::A  IN  Dprt     - Particle diameter.
C::A  IN  denprt   - Particle density.
C::A  IN  denfl    - Fluid density.
C::A  IN  visfl    - Fluid laminar viscosity.
C::A  IN  ufl      - Fluid x component of velocity.
C::A  IN  vfl      - Fluid y component of velocity.
C::A  IN  wfl      - Fluid z component of velocity.
C::A  IN  gx       - x component of gravity.
C::A  IN  gy       - y component of gravity.
C::A  IN  gz       - z component of gravity.
C::A  IN  dt       - current particle time step.
C::A  I&O uprt     - Particle x component of velocity.
```

```
C::A  I&O vprt     - Particle y component of velocity.
C::A  I&O wprt     - Particle z component of velocity.
C::A  OUT uslip    - x component of slip velocity.
C::A  OUT vslip    - y component of slip velocity.
C::A  OUT wslip    - z component of slip velocity.
C::A  OUT velslip  - modulus of slip velocity.
C::A  OUT Re       - Local Reynolds number for the current motion.
C::A  OUT Cd       - Local drag coefficient for the current motion.
C::A  OUT Fdx      - x component of drag force.
C::A  OUT Fdy      - y component of drag force.
C::A  OUT Fdz      - z component of drag force.
C::A  OUT sourcex  - x-momentum source on the gas in the given timestep.
C::A  OUT sourcey  - y-momentum source on the gas in the given timestep.
C::A  OUT sourcez  - z-momentum source on the gas in the given timestep.
C-------------------------------------------------------------------
      pi = 3.14159
      A = 0.25*pi*Dprt**2
      uold = uprt
      vold = vprt
      wold = wprt
      uslip = uold - ufl
      vslip = vold - vfl
      wslip = wold - wfl
      velslip = Sqrt(uslip**2 + vslip**2 + wslip**2)
      velslip = MAX (velslip, 1.0E-8)
      Re = velslip*Dprt*denfl/visfl
      Re = MAX (Re, 1.0E-3)
      Cd = (24./Re)*(1.+0.15*Re**0.687) + 0.42/(1.+42.5e3/Re**1.16)
```

```
C------------------------------------------------------------------
C     Solve particle momentum equation in the integral form.
C------------------------------------------------------------------

      tao = (4.0*denprt*Dprt**2)/(3.0*(denfl*visfl)*Cd*Re)
      norm_dt = dt/tao
      norm_dt = MIN (norm_dt, 50.0)
      aux = 1.0/exp(norm_dt)
      gx=0.0
      gz=0.0
      unew = ufl-(ufl-uold)*aux+gx*tao*(1.0-aux)
      vnew = vfl-(vfl-vold)*aux+gy*tao*(1.0-aux)
      wnew = wfl-(wfl-wold)*aux+gz*tao*(1.0-aux)
      IF (U_SOLV) THEN
        IF ((unew .LT. 1.0E-8) .AND. (unew .GE. -1.0E-8)) unew = 1.0E-8
      ENDIF
      IF (V_SOLV) THEN
        IF ((vnew .LT. 1.0E-8) .AND. (vnew .GE. -1.0E-8)) vnew = 1.0E-8
      ENDIF
      IF (W_SOLV) THEN
        IF ((wnew .LT. 1.0E-8) .AND. (wnew .GE. -1.0E-8)) wnew = 1.0E-8
      ENDIF

C--------------------------------------------------------------------------
C     Update new particle velocity components, calculate drag force components.
C--------------------------------------------------------------------------

      uprt = unew
```

```
vprt = vnew
wprt = wnew

uslip = uprt - ufl
vslip = vprt - vfl
wslip = wprt - wfl
velslip = sqrt(uslip**2+vslip**2+wslip**2)
Re = velslip*Dprt*denfl/visfl
Cd = (24./Re)*(1.+0.15*Re**0.687) + 0.42/(1.+42.5e3/Re**1.16)
Fd  = 0.5*Cd*denfl*(velslip**2)*A
Fdx = -(uslip/velslip) * Fd
Fdy = -(vslip/velslip) * Fd
Fdz = -(wslip/velslip) * Fd
sourcex = (uold-uprt)+gx*dt
sourcey = (vold-vprt)+gy*dt
sourcez = (wold-wprt)+gz*dt
END
```

Appendix A.2

Stochastic turbulence model

##

Stochastic turbulence model used to consider particles fluctuations. A Non-uniform fluctuation distribution is carried out in this work. A uniform distribution gives incorrect results which the particles are diverted to left hand side!

##

```
C-----Stochastic turbolence model for particles.
      IF (TURB_MOD) THEN
        crossing_time = crossing_time+dt
        IF (crossing_time .GT. interaction_time) THEN
         C_mu_C_d = 0.09
         eddy_size = (C_mu_C_d**(3./4.))*(gasTKN**(3./2.))/gasTDN
         gauss_rand = gasdev(idum)
         IF (U_SOLV .AND. V_SOLV .AND. W_SOLV) THEN
          stand_dev = sqrt(2./3.*gasTKN)
        fluct = gauss_rand*stand_dev
            gauss_rand = gasdev(idum)
            fluct1 = gauss_rand*stand_dev
            gauss_rand = gasdev(idum)
            fluct2 = gauss_rand*stand_dev
            gauss_rand = gasdev(idum)
            fluct3 = gauss_rand*stand_dev
c         eddy_life = eddy_size/sqrt(3*(fluct**2))
```

```
                  eddy_life = eddy_size/sqrt((fluct1**2+fluct2**2+fluct3**2))
              ELSE
                  gauss_rand = gasdev(idum)
                stand_dev = sqrt(gasTKN)
               fluct1 = gauss_rand*stand_dev
                  gauss_rand = gasdev(idum)
                  fluct2 = gauss_rand*stand_dev
c               eddy_life = eddy_size/sqrt(2*(fluct**2))
                  eddy_life = eddy_size/sqrt(fluct1**2+fluct2**2)
c                 fluct=sqrt(fluct1**2+fluct2**2)
              ENDIF
                IF (U_SOLV) up = up+fluct1
                IF (V_SOLV) vp = vp+fluct2
                IF (W_SOLV) wp = wp+fluct3
                transit_time = eddy_size/
   @                  sqrt((up-upart)**2+(vp-vpart)**2+(wp-wpart)**2)
              interaction_time = MIN(eddy_life, transit_time)
                crossing_time = 0.0
             ELSE
                IF (U_SOLV) up = up+fluct1
                IF (V_SOLV) vp = vp+fluct2
                IF (W_SOLV) wp = wp+fluct3
            ENDIF
           ENDIF
C-----end.
```

Appendix A.3

Particle reposition

##

In this section, the particles displacement is handled to return back the out-bound particles in to the domain. Depending on the particles position and velocities they can be return to an appropriate location to fulfil the situation of a full 3-D simulation in a slice of a cylinder.

##

```
C-----------------------------------------------------------------------
C::R  SUBROUTINE move_particle
C     Copyright Multi-Physics Software Limited    1990, 1993, 1996, 1999
C     Use restricted as to rights of licence
C  Log:
C::L   Written by :   Nick Croft    6th January 1999; Modified by Mazaher Molaei March 2012
C  Description:
C::D  Calculate the new position of a particle.
C  Called by:
C::B  Nothing
C  Calls to:
C::T  copy_vector
C  Arguments:
C::A  I&O  Pos     -  Position of the particle.
C::A  IN   Upart   -  U-Velocity of particle.
C::A  IN   Vpart   -  V-Velocity of particle.
C::A  IN   Wpart   -  W-Velocity of particle.
```

```
C::A  IN   Uparto  -  U-Velocity of particle at start of motion.
C::A  IN   Vparto  -  V-Velocity of particle at start of motion.
C::A  IN   Wparto  -  W-Velocity of particle at start of motion.
C::A  IN   Dt      -  Particle motion time step.
C::A  OUT  Umove   -  Actual u velocity used in the motion.
C::A  OUT  Vmove   -  Actual v velocity used in the motion.
C::A  OUT  Wmove   -  Actual w velocity used in the motion.
C-------------------------------------------------------------------
      SUBROUTINE move_particle
     @        ( Pos,    Upart,  Vpart,  Wpart,  Uparto, Vparto,
     @          Wparto, Dt,     Umove,  Vmove,  Wmove )

      INCLUDE '../inc/geom.fh'

      REAL    Upart,  Vpart,  Wpart,  Uparto, Vparto, Wparto, Dt, ytan, tettan, ytn, tetcos, lytn, yposo
      REAL    Umove,  Vmove,  Wmove,  Pos(1:DIMENS)

C Local Variables
      REAL    oldpos(1:3), xpos, ypos, tempu, alpha, r

      CALL copy_vector ( DIMENS, Pos, oldpos )
      Umove = 0.5*(Upart+Uparto)
      Vmove = 0.5*(Vpart+Vparto)
      Wmove = 0.5*(Wpart+Wparto)
      IF ( SWIRL ) THEN
        xpos = Pos(1) + Umove*Dt
        ypos = Dt*Vmove
```

```
  Pos(1) = SQRT(xpos*xpos+ypos*ypos)
  IF ( xpos .LT. 0.0 ) THEN
    xpos = -xpos
    Upart = - Upart
    alpha  = ATAN(ypos/xpos)
  ELSE IF ( xpos .GT. 0.0 ) THEN
    alpha  = ATAN(ypos/xpos)
  ELSE
    alpha = 0.0
  END IF
  tempu = Upart*COS(alpha) + Vpart*SIN(alpha)
  Vpart = Vpart*COS(alpha) - Upart*SIN(alpha)
  Upart = tempu
  umove = (Pos(1) - oldpos(1)) / Dt
  vmove = 0.0
ELSE

     xpos=pos(1)+ Umove*Dt
     ypos=pos(2)+ Vmove*Dt
     zpos=pos(3)+ Wmove*Dt
     yposo = Dt*Vmove
     alpha  = ATAN(yposo/xpos)
    IF (U_SOLV .AND. V_SOLV .AND. W_SOLV) THEN
     r=0.05
     tettan=TAN(teta/2)
     tetcos=COS(teta/2)
     xmx=r*tetcos
     ytn=xpos*tettan
```

```
        lytn=-ytn
              IF ( xpos .lt. 0.0 ) THEN
                    xpos=-xpos
                    Upart=-Upart
              END IF
        IF ( xpos .gt. 0.0.and.xpos.lt.xmx ) THEN
              IF ( ypos .gt. ytn.or.ypos.lt.lytn ) THEN
              ypos=-ypos
            Upart = Upart*COS(alpha) + Vpart*SIN(alpha)
          Vpart = Vpart*COS(alpha) - Upart*SIN(alpha)
              END IF
        END IF
        Pos(1) = Pos(1) + Umove*Dt
        Pos(2) = Pos(2) + Vmove*Dt
        Pos(3) = Pos(3) + Wmove*Dt
       ELSE
        Pos(1) = Pos(1) + Umove*Dt
        Pos(2) = Pos(2) + Vmove*Dt
       END IF
       END IF

    END
```

Appendix A.4

Mass source terms

##

In this section the carbonation reaction calculations carried out to determine the mass and energy source terms as well as the conversion of particles.

###

```
c--------------Chemical Reaction----Mass and Heat Source Terms------------------------------
        xumax=0.875
        kreact=0.74
        rho_cao=3.34
        rho_caco3=2.71
        rho_ratio=rho_cao/rho_caco3
        mw_ratio=100.09/56.0778
        diam_fact=1.
        cellno_old=cellno
        mass_init=3340*(3.14*(pdia)**3)/6
        pco2=Ra(co2_p+cellno-1)*(Ra(PN_p+cellno-1)+1.01e5)
        cco2=0.001*pco2/(Ra(TN_P+cellno-1)*8.314)
        eco2=0.001*1500/(Ra(TN_P+cellno-1)*8.314)
        aco2=(cco2-eco2)*Ra(ELEVOL_P+cellno-1)*44.0

        IF(cco2.gt.eco2)THEN
        ks=(5.59e-6)*exp((-2.13e3)/(8.314*Ra(TN_P+cellno-1)))
        tau=ks*(cco2-eco2)*prt_time*(4.2e6)/(0.53)
        ddif=(3.37e-6)*exp((-1.63e3)/(8.314*Ra(TN_P+cellno-1)))
        ddif=ddif*cco2*56/3340.0
        bta=(2*ks*3340.0*0.53)/(56.0*ddif*4.2e6)
```

```
        r_conv=1-exp((1-(tau*0.76+1)**2)/1.52)
        tdif=(4.2e6/0.53)*sqrt(ddif*prt_time/2)
        d_conv=1-exp((1-(1+1.52*tdif)**2)/1.52)
        x=part_conv(i)
        pref=ks*(4.2e6)*cco2*(1-x)
        psy1=sqrt(1-1.52*alog(1-x))
        psy2=0.53*(1+(bta/1.52)*(psy1-1))
        dx=(pref*psy1/psy2)*dt
        tt1=exp((-1.63e3)/(8.314*Ra(TN_P+cellno-1)))*3.37e-6
        eta=106
                IF(part_conv(i).LT.0.55)THEN
                        part_conv(i)=part_conv(i)+dx
                ELSE
                        part_conv(i)=part_conv(i)+dx*exp(-(part_conv(i))/0.55-1)

                END IF
        rol_conv=r_conv
        dol_conv=d_conv
        Ra(X_CONV_P+cellno-1)=part_conv(i)
        del_xconv=part_conv(i)-part_oldconv(i)
        volcel=1.0/Ra(ELEVOL_P+cellno-1)
        massgas=massgas-(dx*trk_fl_rate*44.01)/(56.08)
        heatgas=heatgas+dx*(trk_fl_rate*1000/56.07)*168
        part_oldconv(i)=part_conv(i)
        rho_fact=1+part_conv(i)*44.0/56.0
        msco2=massgas/(res_time*volcel)
         END IF

c------END--------------------------------------------------------------
```

Appendix A.5

INFORM file for particle tracking and CO_2 capture

```
############################################################################
INFORM file includes steady state continuous flow with k-e standard model, transient
particle tracking model with total tracking path-lines of “npart”, interaction between gas
phase and dispersed particles are taken in account with momentum (mom_src_x,
mom_src_y, mom_src_z), mass (co2_frc) and heat (heat_src) source terms.
############################################################################

GEOMETRY_MODULE
  MESH  cy3D.mbl
  GRAVITY_Z  -9.81
END
REAL MU,CMU,K,EPS,V
V=3.3
MU=8.85E-5
CMU=0.09
K=(3/2)*(0.1*V)^2
EPS=0.005*(K^2)*CMU/MU

GENERIC_MODULE
  STEADY_STATE_RUN
  MAX_SWEEPS  5998
  USER_INTERVAL_SAVE  ON
END
```

```
PARSER_MODULE
PRINT_CONSTANT_VALUES      ON
END

MONITOR_MODULE
  BLOCK_FORMAT    ON
  OUTPUT_INTERVAL  10
  MONITOR_LOCATION .025 0.0 2.0
  WRITE_TO_FILE test_out.txt
END

GENERAL_EQUATION_MODULE
 PRINT_SOURCES ON
END
MESH_MODULE
  CHECK_ORTHOGONALITY  ON
END

MATERIAL_PROPERTY_MODULE
REAL  rho_gas, rho_part
rho_gas = 0.3906
  DENSITY
    MATERIAL  1   CONSTANT rho_gas
  END

  VISCOSITY
    MATERIAL  1  CONSTANT  8.858E-05
  END
```

```
  THERMAL_CONDUCTIVITY
    MATERIAL  1 CONSTANT   0.0595
  END

  SPECIFIC_HEAT
    MATERIAL  1 CONSTANT   1194.7
  END

  THERMAL_EXPANSION_COEFFICIENT
    MATERIAL  1 CONSTANT   3.661E-3
  END
END

 HEAT_TRANSFER_MODULE
      SOLVE_TEMPERATURE
         RESIDUAL_REFERENCE 1.0E+03
         INITIAL_VALUES ALL 923.0
         BOUNDARY_CONDITIONS
            PATCH 1 FIXED_VALUE    VALUE  923.0
         END
         USER_SOURCE_TERMS
                    heat_src 0
            END
      END
   END


FLUID_FLOW_MODULE
```

```
  MOMENTUM_FALSE_TIMESTEP  0.001
  BOUND_FACE_PRESSURE  ON
  BUOYANCY
    BOUSSINESQ_APPROXIMATION  OFF
    REFERENCE_DENSITY  0.0
  END

 SOLVE_U-MOMENTUM
      INITIAL_VALUES  ALL  0.0
      BOUNDARY_CONDITIONS
        PATCH  1  FIXED_VALUE    VALUE  0.
        PATCH  4  WALL COEFF 1. VALUE  0.
            PATCH  2  IN_OUT  VALUE  0.0
      END
#       FALSE_TIMESTEP 0.001
            USER_SOURCE_TERMS
        mom_src_x 0
      END
   END

 SOLVE_V-MOMENTUM
      INITIAL_VALUES  ALL  0.0
      BOUNDARY_CONDITIONS
       PATCH  1  FIXED_VALUE    VALUE  0.0
       PATCH  4  WALL COEFF 1. VALUE  0.
       PATCH  2  IN_OUT  VALUE  0.0
      END
#       FALSE_TIMESTEP 0.001
```

```
          USER_SOURCE_TERMS
      mom_src_y 0
    END
  END

 SOLVE_W-MOMENTUM
    INITIAL_VALUES  ALL  2.45
    BOUNDARY_CONDITIONS
     PATCH  1  FIXED_VALUE    VALUE  V
     PATCH  4  WALL COEFF 1. VALUE  0.
     PATCH  2  IN_OUT  VALUE  0.0
    END
#      FALSE_TIMESTEP 0.001
          USER_SOURCE_TERMS
      mom_src_z 0
    END
  END

  SOLVE_PRESSURE
   INITIAL_VALUES  ALL  0.0
   UNDER_RELAXATION  0.7
   BOUNDARY_CONDITIONS
    PATCH  2  FIXED_VALUE  VALUE  0.0
   END
   RESIDUAL_REFERENCE  10.
#    FALSE_TIMESTEP  0.05
  END
END
```

```
TURBULENCE_MODULE
 KE_MODEL
  SOLVE_KINETIC_ENERGY
    INITIAL_VALUES ALL  K
#    UNDER_RELAXATION 0.5
    BOUNDARY_CONDITIONS
      PATCH  1  FIXED_VALUE  VALUE  K
      PATCH  2  IN_OUT  VALUE  K
      PATCH  4  WALL COEFF 1. VALUE  0.
    END
    FALSE_TIMESTEP  0.0002
  END
#                              !  enut = 0.09 * k^2 / eps
  SOLVE_DISSIPATION_RATE
    INITIAL_VALUES ALL  EPS
#    UNDER_RELAXATION 0.5
    BOUNDARY_CONDITIONS
      PATCH  1  FIXED_VALUE  VALUE  EPS
      PATCH  2  IN_OUT  VALUE  EPS
      PATCH  4  WALL COEFF 1. VALUE  0.
    END
   FALSE_TIMESTEP  0.0002
  END
  SAVE_GENERATION_RATE   NEVER
 END
END
```

```
  SCALAR_MODULE
     SOLVE_co2
       INITIAL_VALUES ALL 0.1
       SAVE_VARIABLE TRANSIENT
#        UNDER_RELAXATION        0.1
       DIFFUSION_TERM       OFF
       TRANSIENT_COEFFICIENT
          MATERIAL 1  CONSTANT  0.5806
#           MATERIAL  1  USER_ROUTINE  IDEALGAS   1    44.0
       END
       CONVECTION_COEFFICIENT
          MATERIAL 1  CONSTANT  0.5806
#           MATERIAL  1  USER_ROUTINE  IDEALGAS   1    44.0
       END
        BOUNDARY_CONDITIONS
         PATCH  1  FIXED_VALUE  VALUE  0.1
             PATCH  2   IN_OUT     VALUE  0.0
#            PATCH  4  FIXED_VALUE  VALUE  0.0

      END
       FALSE_TIMESTEP  0.01
       USER_SOURCE_TERMS
              co2_frc 0
       END
     END
   END

   GENERAL_EQUATION_MODULE
```

```
  PRINT_SOURCES ON
  END

POST-PROCESSING_MODULE
  TECPLOT_FORMAT
  TIME_STEP_FREQUENCY  50
  END
END

INTEGER npart
npart=2880
USER_MODULE
  PARTICLE_TRACKING
    FIRST_TRACKING              2000
    TRACKING_FREQUENCY          20
    SOURCE_RELAXATION           0.1
    DROPLET_RELAXATION          0.7

    NUMBER_OF_PARTICLES         npart
    PARTICLE_DENSITY            3340
    MASS_FLOW_RATE              1.36e-3
    DIAMETER_MEAN               0.0002
    GAS_CP                      520.0
    GAS_CV                 312.0
    U_SOLVER               ON
    V_SOLVER               ON
    W_SOLVER               ON
    TURBULENCE_MODEL       ON
```

```
    PRINT_PATH                  ON
    TRACK_WITHIN_ITERATION_LOOP    ON
    CRITICAL_TIME                          100.0
    MAXIMUM_TIME_STEP               0.01
    MINIMUM_TIME_STEP               1.0e-5
    STAGNATION_VELOCITY            1.e-4
    TIME_STEPS_PER_ELEMENT      15
    RESTITUTION_COEFFICIENT     0.99
    SAVE_DIAMETERS                      TRANSIENT
    SAVE_VOLUME_FRACTIONS     TRANSIENT
  END
END
STOP
```

Appendix B

Shape function for particle tracking

B.1 Deciding when a point is inside a polyhedron

Consider any plane (face) which has normal $\vec{n}$ and $\vec{r}_1$is a point on the plane. Which side of the plane contains a point $\vec{r}_p$ can be determined by calculating [139]:

$$d = \vec{n}.\left(\vec{r}_p - \vec{r}_1\right) \tag{1}$$

If d is positive then the point is on the side of the plane to which the normal points, if it is zero the point is on the plane and if it is negative then it is on the opposite side of the plane to normal. For a convex polyhedron with planar faces then a point is inside the polyhedron if :

$$min\left(\vec{n}_f.\left(\vec{r}_p - \vec{r}_f\right)\right) < 0$$

Where the minimum is taken over all faces, f, of the polyhedron and $\vec{r}_f$ is any point on the plane.

B.2 Which face has a particle left a convex polyhedron through?

Again only planar faced polyhedra will be considered. This algorithm requires a movement vector for the particle. This may be a movement calculated during the tracking of a particle or may be constructed by taking the vector from the polyhedron centre to the particle position. Any point on a plane can be expressed as:

$$\vec{r}_1 + \alpha\vec{t}_1 + \overrightarrow{\beta t}_2 \tag{2}$$

where $\vec{t}_i$ are two independent tangents to the plane. The moving particle can be expressed as:

$$\left(\vec{r}_p - \vec{r}_m\right) + \lambda\vec{r}_m \tag{3}$$

where $\vec{r}_m$ is the movement vector. When the particle crosses the plane these two equations (Eq. 2 and Eq. 3) are equal. The terms in the tangents can be dropped by taking the dot product with the plane normal. After rearranging an equation for λ can be obtained:

$$\lambda = \left(\vec{r}_1 - \vec{r}_p + \vec{r}_m\right).\vec{n}/(\vec{r}_m.\vec{n}) \tag{4}$$

This check can be repeated for each face of the polyhedron and the face through which the particle left has the minimum λ value provided both the numerator and the denominator in the above equation are positive.

B.3 Calculation of shape function values for a tetrahedron

To estimate the values of the continuum within an element shape functions are used. The basis of this is the calculation of the shape function values associated with the sub-tetrahedron which contains the particle. To calculate the shape function values associated with a position it is useful to realise that for any tetrahedron corner the shape function value is the ratio of the normal height of the position above the opposite face divided by the normal height of the corner. For corner C_j with position $\vec{r}_j$ the opposite face contains the other three corners of the tetrahedron. The height of any point, $\vec{r}_p$, above this face is given by [139]:

$$\vec{\hat{n}}_j.\left(\vec{r}_p - \vec{r}_k\right) \tag{5}$$

where $\vec{r}_k$ is any point on the face and $\vec{\hat{n}}_j$ is the unit normal to the face opposite corner $C_j$with the normal pointing towards C_j. One normal to the plane can be calculated by:

$$\vec{n}_j = (\vec{r}_l - \vec{r}_k) \times (\vec{r}_m - \vec{r}_k) \tag{6}$$

where the subscripts l, m and k represent the three corners of the face. As the requirement is to find a ratio is does not matter that this is not a unit vector and it may be pointing in the wrong direction. The shape function value, N_j, associated with C_j is

$$N_j = \frac{\vec{n}.(\vec{r}_p - \vec{r}_k)}{\vec{n}.(\vec{r}_j - \vec{r}_k)} \tag{7}$$